

1 **Understanding the Role of Contrails and Contrail Cirrus in Climate Change: A Global**
2 **Perspective**

3

4 Dharmendra Kumar Singh, Swarnali Sanyal, Donald J. Wuebbles

5 Department of Climate, Meteorology & Atmospheric Sciences (CliMAS), University of Illinois
6 Urbana-Champaign, Urbana, IL 61802, Illinois, USA

7

8 *Correspondence to:* Dharmendra Kumar Singh (dksingh8@illinois.edu)

9

10 **Abstract**

11 Globally, emissions from aviation affect Earth's climate via complex processes. Contrail cirrus and
12 carbon dioxide emissions are the largest factors contributing to aviation's radiative forcing on
13 climate. Contrail cirrus, like natural cirrus clouds, impacts Earth's climate. Even with the extensive
14 ongoing research, the relative importance of the climate effects of contrails compared to other
15 aviation effects on climate still has major uncertainties requiring further research. Contrail cirrus
16 encompasses linear contrails and the associated cirrus clouds; these are characterized by ice
17 particle properties, e.g., size, concentration, mixing, extinction, ice water content, optical depth,
18 geometrical depth, and cloud coverage. The climate impact of contrails may intensify due to
19 projected increases in air traffic. The radiative forcing from global contrail cirrus has the potential
20 to triple and could reach as much as 160 mW m⁻² by 2050. This projection is based on anticipated
21 growth in air traffic and a potential shift to higher altitudes. The future climate impact of contrail
22 cirrus is influenced by factors like the magnitude and geographical spread in air traffic,
23 advancements in fuel efficiency, the effects of the use of alternative fuels, and the effects of the
24 changing climate on the background atmosphere. This study reviews the microphysical processes
25 affecting contrail formation and the aging of contrails and contrail-cirrus. Furthermore, the study
26 explores global observational datasets for contrails, current analyses, and future projections and
27 will aid in evaluating the effectiveness and trade-offs associated with various mitigation strategies.
28 The research highlights gaps in knowledge and uncertainties while outlining research priorities for
29 the future.

30

31 **Keywords:** Aviation, contrails, contrail cirrus, radiative forcing, climate model, climate change

32

33

34

35

36

37

38

39

40

41

42 **1 Introduction**

43 The increase in the atmospheric carbon dioxide (CO₂) concentration has had the most substantial
44 impact on human-induced climate change over recent decades (IPCC, 2021). Emissions from
45 aviation are a minor but significant contributor to these changes in climate, especially because of
46 emissions of CO₂ and the effects of contrail formation from emitted water vapor (H₂O). Aviation
47 expansion is outpacing economic growth, with projections indicating that over the next two
48 decades, the demand for aviation could grow to about 3 times its present level (Wuebbles et al.,
49 2007), with the International Civil Aviation Organization having previously projected a 4.3%
50 annual growth to 2050 (ICAO 2012). Recent analyses by Boeing and Airbus suggest slightly lower
51 rates of increase of 3.6-3.8% (Boeing, 2022; Airbus, 2023). These analyses suggest that aviation
52 could become an even more important contributor to climate change in the future. Taking both
53 CO₂ and non-CO₂ effects into account, The global aviation industry comprises about 3.5-4% of
54 the current human-made (anthropogenic) activities forcing on climate (Lee et al., 2020; Klöwer et
55 al., 2021; Grewe et al., 2021).

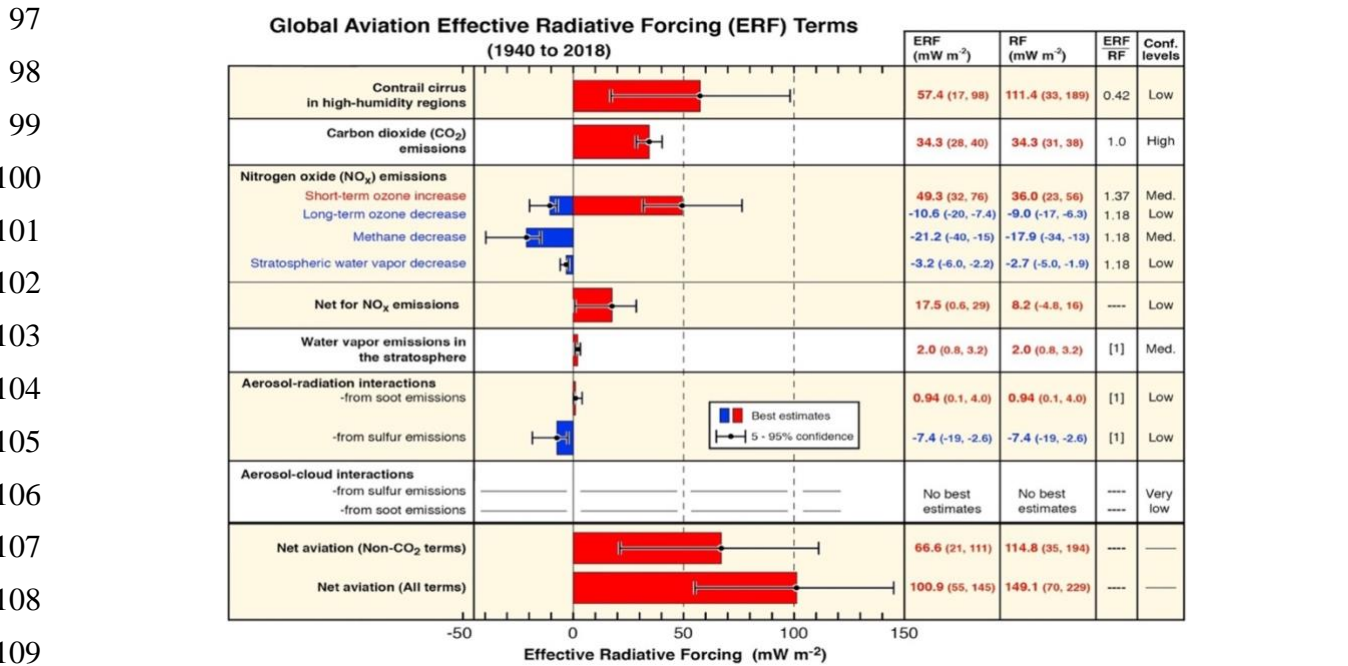
56 Aviation-induced cirrus is one of the most significant radiative forcing contributors from the
57 aviation sector. (IPCC, 1999; Lee et al., 2009, 2021; Brasseur et al., 2016). However, considerable
58 ambiguities persist, stemming from various origins, such as our incomplete understanding of cirrus
59 cloud characteristics, their geographical distribution, and their life span. (Kärcher 2018; Burkhardt
60 et al., 2018; Schumann and Heymsfield 2017). With current aircraft largely burning fossil fuel,
61 CO₂ emissions are the other major forcing. Additionally, NO_x (oxides of nitrogen) emission also
62 has a notable impact through the production of tropospheric ozone, but this is partially
63 counteracted by chemical feedback effects on concentrations of atmospheric methane (CH₄). Fig.
64 1 (Lee et al., 2021) provides the most current assessment of the climate-forcing effects resulting
65 from different aviation emissions on a global scale, spanning from 1940 to 2018; these effects are
66 shown in terms of radiative forcing (RF) and effective radiative forcing (ERF). Radiative forcing
67 in the context of contrails is due to the net radiative energy flux at the top of the atmosphere (TOA)
68 caused by the presence of contrails in the atmosphere (Fuglestedt et al., 2010). A positive
69 radiative forcing (RF) signifies an increase in atmospheric warming, as depicted by the red bars in
70 Figure 1. ERF, on the other hand, adjusts the RF by accounting for rapid responses occurring
71 within the Earth's climate system. While RF and ERF provide valuable insights, it's important to
72 acknowledge that these are global metrics. Contrails primarily affect the upper troposphere and
73 are short-lived, leading to potentially larger regional effects, particularly in densely populated
74 areas with high air traffic.

75 In the scientific literature, contrail cirrus is defined as encompassing both linear contrails and the
76 resulting formation of cirrus clouds. Figure 2 provides an overview of aviation exhaust plume
77 emissions and factors influencing contrail formation. The characteristics of contrail cirrus include
78 average ice particle sizes and concentrations, extinction, ice water content, optical depth,
79 geometrical depth, and contrail coverage. Integral contrail properties involve parameters such as
80 contrail cirrus volume, total number of ice particles, overall ice water content, and total extinction
81 (area integral of extinction) per contrail length.

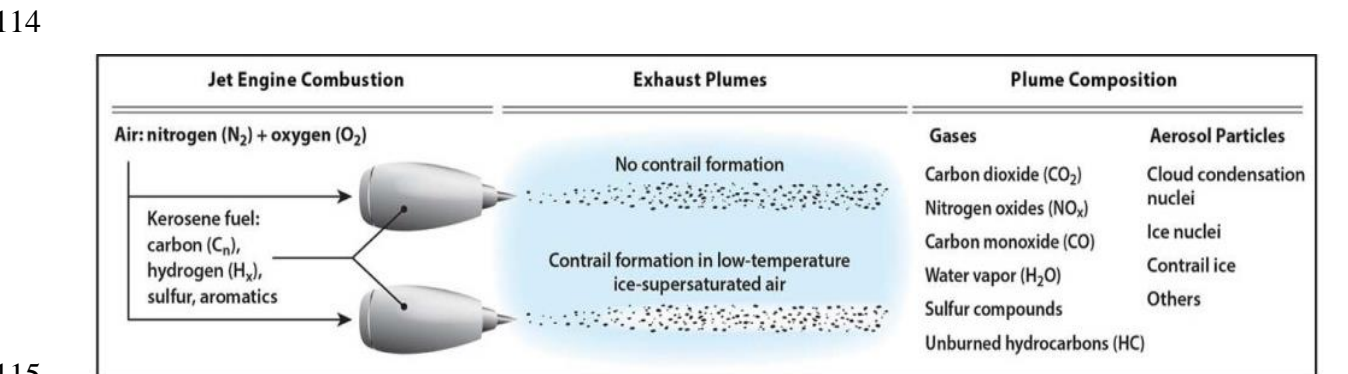
82 While significant progress has been made in recent years to incorporate contrail effects into global
83 climate models, as evidenced by the pioneering work of Burkhardt and Kärcher (2011) and the
84 continued advancements by others, like Bock and Burkhardt (2016), Bier and Burkhardt (2022),
85 Chen and Gettelman (2013), and Schumann et al. (2015), uncertainties remain in how well these
86 models capture the long-term influence of contrails on cirrus clouds. These uncertainties arise from

87 limitations in our understanding of how contrails age and spread (Bickel et al., 2020), the properties
 88 of the tiny ice crystals that make them up, and the behavior of contrails in regions with high ice
 89 content. Further research is crucial to address these uncertainties and improve the accuracy and
 90 reliability of contrail modeling for future climate projections.

91 The generation of persistent contrails depends on coming across ice-supersaturated conditions
 92 along a flight path, and these conditions show variability in both space and time within the
 93 troposphere and tropopause region (Irvine et al., 2013; Lamquin et al., 2012; Bier et al., 2017).
 94 Estimating the RF from contrail cirrus requires knowledge of complex microphysical processes,
 95 radiative transfer, and the interaction of contrails with background cloudiness (Burkhardt et al.,
 96 2010).



110 **Figure 1.** Current best evaluation of the climate forcing between 1940 and 2018 from commercial
 111 aviation for different types of emissions. ERF accounts for short-term feedback in the climate
 112 system not accounted for in the traditional RF evaluation. Adapted with permission from Lee et
 113 al. (2021).



116 **Figure 2.** Schematic overview of exhaust plumes (contrail formation in low temperature) and their
 117 composition. Adapted with permission from Lee et al. (2021).

118 This review article aims to provide a comprehensive overview of our understanding of contrails,
119 encompassing their formation, progression, and the consequent repercussions on Earth's climate
120 system. In the process, the microphysical processes underlying contrail formation are explored
121 along with their representation in the simulation of contrails in current climate-chemistry models
122 of the global atmosphere. Furthermore, we address the uncertainties surrounding this topic and
123 identify areas requiring further research in the future.

124 **2 Microphysics of Contrail Formation, Aging, And Transition to Contrail Cirrus**

125 Microphysical processes play a pivotal role in the formation of contrails and their evolution in the
126 atmosphere. This section is aimed at discussing these processes, their effects on the lifetime of
127 contrails, and the possible transition of contrails to contrail cirrus in the upper troposphere.

128 **2.1 The Physics of Contrail Formation and Aging**

129 The fundamental principles for determining the formation of contrails were independently
130 developed by E. Schmidt in 1941 and H. Appleman in 1953. Contrails appear when the hot and
131 moist exhaust from aircraft quickly mixes with the cold and humid surrounding air, causing the
132 humidity in the exhaust gases to exceed the saturation point for liquid water (Appleman, 1953;
133 Schmidt, 1941; Schumann, 1996). A schematic representation of the Schmidt-Appleman criterion
134 for contrail formation is shown in Figure 3. In this diagram, the two solid curves depict saturation
135 levels concerning liquid water (upper curve) and ice (lower curve). The phase trajectory of the
136 mixture, consisting of exhaust gases and ambient air, follows a straight line from the upper right
137 to the lower left in the e-T diagram, where 'e' represents the partial pressure of water vapor in the
138 mixture, and 'T' represents its absolute temperature (as denoted by the dashed lines). The path that
139 lines up with the water saturation curve (dotted) specifies the highest temperatures at which
140 contrail formation can take place. When the trajectory terminates in an ice-supersaturated state,
141 the persisting contrails have the potential to disperse and transform into contrail cirrus.

142 In cases where the conditions do not meet the criteria, the contrail formed will have a brief lifespan,
143 lasting only a few minutes. The mixing process is presumed to occur isobarically, resulting in a
144 straight-line mixing (phase) trajectory on an e-T diagram. The Schmidt-Appleman criterion
145 (SAC), which is primarily based on thermodynamics, establishes the threshold temperature for
146 contrail formation. This threshold is determined by several factors, such as ambient air pressure,
147 humidity, the amount of water and heat released by the aircraft per unit of fuel, and the overall
148 efficiency of the aircraft engine's propulsion system. (Jensen et al., 1998; Schumann, 1996).
149 Accurate assessments of contrails necessitate precise data on ambient meteorological conditions.
150 The persistence of contrails is contingent on meeting a specific humidity threshold, as defined
151 below.

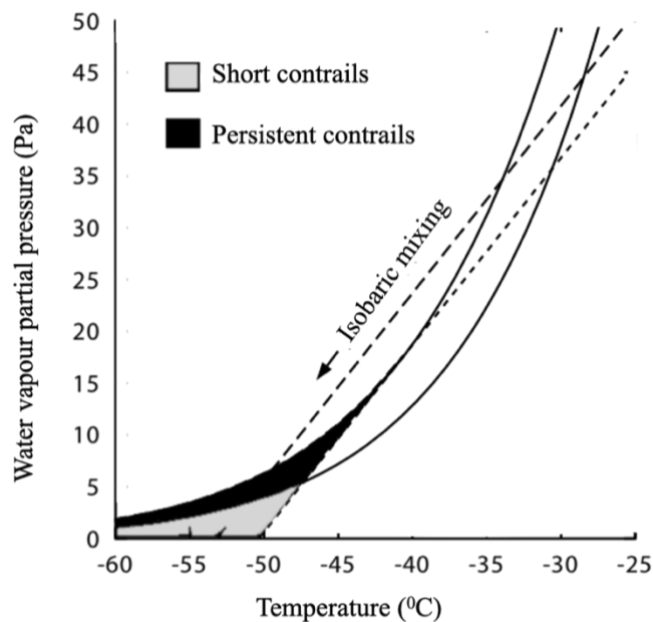
152 The persistence of contrails hinges on the atmospheric-specific humidity. Temperature and vertical
153 motions within the atmosphere play key roles in determining this humidity. Additionally, the
154 optical characteristics and lifespan of contrails are key aspects of contrail formation and are
155 influenced by various meteorological factors. These factors include turbulence, vertical motions,
156 wind shear, and the presence of ambient cirrus clouds. The size and duration of the ice-
157 supersaturated region, the availability of water vapor for ice crystal growth, and consequently, the
158 sedimentation of these ice crystals within the contrail are also essential considerations (Bock and
159 Burkhardt, 2016). Crucially, the radiative forcing (RF) and the ensuing climate impacts depend on
160 a multitude of meteorological parameters. Additionally, factors such as the albedo and the

161 brightness temperature of the atmosphere in the absence of contrails play a significant role, as
162 outlined by Schumann et al. (2012).

163 Upon reaching the ambient temperature through the process of mixing with the surrounding air,
164 contrails undergo changes in size depending on the ambient humidity. When the ambient relative
165 humidity remains supersaturated concerning ice ($RH_{ice} > 100\%$), contrails experience growth in
166 ice water content and can remain detectable for up to 5 hours or even longer, as highlighted in
167 various studies (Gierens and Vázquez-Navarro, 2018; Schumann and Heymsfield, 2017; Bier et
168 al., 2017). This extended persistence contrasts with the mean lifetime of contrails, typically noted
169 to be around 2-3 hours (Schumann et al., 2015; Vázquez-Navarro et al., 2015; Tesche et al.,
170 2016; Sausen et al., 1998). Contrails, under such conditions, have the potential to disperse and
171 transform into thin cirrus layers. On the other hand, when the ambient relative humidity is not
172 supersaturated concerning ice, contrail ice particles sublime and dissipate. The timescale of this
173 sublimation and dissipation process is contingent on the sizes of the contrail ice particles and the
174 ambient air RH_{ice} (Schumann, 2012).

175 Combinations of satellite information and ground-based lidar measurements, such as in the Atlas
176 et al. (2006) case study, showed a lifetime of more than 2 hours and a mean optical thickness
177 (integrated extinction coefficient over a vertical column of unit cross section) of 0.35. Duda et al.
178 (2004) studied the development of contrail clusters over the Great Lakes and derived optical
179 thickness (optical depth, τ) from 0.1 to 0.6 for contrails that lasted several hours (Kärcher et al.,
180 2009). Graf et al. (2012) studied the cirrus cover cycle and observed timescales between 2.3 to
181 4.1 hours for contrail cirrus and 1.4 to 2.4 hours for linear contrails.

182



192

193 **Figure 3.** Phase diagram with mixing lines for aircraft exhaust Adapted from Gierens et al. (2008)
194 (Licensed under CC BY 4.0).

195 The critical factor influencing this contrasting behavior lies in the concept of ice supersaturation.
196 Ice supersaturation refers to conditions where the ambient humidity exceeds the saturation point

197 for ice, even at temperatures below freezing. These conditions are essential for the persistence and
198 growth of contrails. While the initial formation process might occur at varying humidity levels,
199 studies like Ovarlez et al. (2002) highlight the presence of ice supersaturation within cirrus clouds,
200 which can significantly impact contrail persistence. Jensen et al. (2001) revealed a surprisingly
201 high frequency of ice supersaturation in the upper troposphere, even in the absence of visible ice
202 clouds. This finding highlights the importance of considering ice supersaturation for accurate
203 assessments of contrail persistence and its potential transformation into cirrus clouds.

204 Upon reaching the ambient temperature through the process of mixing with the surrounding air,
205 contrails undergo changes in size depending on the ambient humidity. When the ambient relative
206 humidity remains supersaturated concerning ice ($RH_{ice} > 100\%$), contrails experience growth in
207 ice water content and can remain detectable for up to 5 hours or even longer. The microphysical
208 properties of contrails, including ice crystal size distribution and habit, significantly influence their
209 radiative effects and persistence. These properties are determined by the initial conditions during
210 contrail formation and subsequent processes. Ice crystal shapes in contrails are primarily randomly
211 oriented, small ice crystals, with a possibility of some horizontally oriented plates existing as well.
212 This finding is supported by Iwabuchi et al. (2012) who analyzed contrails using a combination of
213 MODIS and CALIPSO satellite data. Their study showed that contrails have larger backscattering
214 coefficients than neighboring cirrus clouds, indicative of smaller ice crystals. The analysis also
215 suggested a tendency for stronger depolarization when ice crystals are small, with a mean linear
216 depolarization ratio (LDR) of approximately 0.4-0.45 for young contrails and contrail cores
217 (Iwabuchi et al., 2012).

218 There has been ongoing uncertainty regarding whether persistent contrails exclusively form in
219 cloud-free supersaturated areas or if they can also develop within existing cirrus clouds (Burkhardt
220 et al. 2008). Subsequent modeling work (Tesche et al. 2016) suggested that persistent contrails
221 indeed have the potential to form within cirrus clouds. While the formation of contrails is
222 commonly observed in clear skies, they also emerge in conditions where the sky is covered with
223 thin or even subvisible cirrus clouds (Immler et al. 2008).

224 The temperature threshold for contrail formation, known as the SAC threshold, is slightly higher
225 in cirrus clouds compared to clear air (Gierens, 2012). This difference is attributed to the additional
226 humidity introduced by the ice water content (IWC) from cirrus clouds (Verma and Burkhardt
227 2022). In situ measurements have indicated high ice supersaturation both inside and outside cirrus
228 clouds (Comstock et al. 2004). Moreover, observational evidence suggests that contrails embedded
229 within cirrus clouds are not significantly thinner than contrails forming in clear air (Poellot et al.
230 1999).

231 A reliable estimation of the radiative effects stemming from contrail cirrus relies heavily on their
232 optical properties, which are intricately linked to their microphysical properties and age, as well
233 as their geographical distribution. The microphysical characteristics of contrail cirrus at various
234 plume ages, as observed in diverse airborne campaigns, have been systematically compiled and
235 detailed (Schröder et al. 2000; Schumann et al. 2017; Chauvigné et al. 2018). Fresh contrails,
236 typically observed in plumes around 2 minutes old, exhibit distinct features, including an ice
237 crystal number concentration reaching thousands per cubic centimeter and ice crystals measuring
238 up to a few micrometers in diameter. This characterization is consistent with observations (Märkl
239 et al., 2024, Bräuer et al., 2021a; Petzold et al., 1997). Contrails in their initial 2-5 minutes of
240 existence have been frequently measured (Voigt et al., 2011; Gayet et al., 2012). The distinctive
241 feature of these young contrails lies in their notably high ice crystal number concentration of small

242 ice particles, making them easily discernible from natural cirrus formations. However, contrails
243 often coexist with natural cirrus and may be incorporated into thin or subvisible cirrus (Kübbeler
244 et al., 2011; Gierens, 2012; Unterstrasser et al., 2017). This coexistence poses a challenge in
245 distinguishing between aged contrails and natural cirrus, complicating efforts to clarify the
246 contribution of contrail cirrus to the radiative balance. Contrail cirrus is characterized by a low ice
247 water content (IWC) ranging from 0.1 to about 10 mg m^{-3} , a feature it shares with natural cirrus
248 of in-situ origin, as observed by Schumann et al. (2017). Ice crystals within these clouds have
249 formed and enlarged in an ice-cloud environment (Luebke et al., 2016; Krämer et al., 2020). In
250 contrast to contrail cirrus and in situ-origin cirrus, cirrus clouds initiating from liquid often yield a
251 higher IWC since their ice crystals originally form as liquid drops (Krämer et al., 2016, 2020) in a
252 warmer atmosphere with an ambient temperature exceeding 235 K (-38°C), particles undergo
253 freezing as they are lifted into the cirrus temperature region of the atmosphere.

254 Chauvigné et al. (2018) applied a method based on principal component analysis to differentiate
255 between particles in contrail cirrus at various stages and those observed in natural cirrus during
256 the CONCERT 2008 campaign (Voigt et al., 2010). The success of the campaign stemmed from
257 the fact that contrails sampled during the CONCERT initiative were relatively young and exhibited
258 greater distinctiveness compared to natural cirrus formations. Despite this success, the
259 comprehensive acquisition of all necessary optical and microphysical parameters proved
260 challenging during single aircraft campaigns, limiting the widespread application of this method.
261 The CONCERT dataset is relatively small, encompassing approximately 4.0 hours of sampling
262 time in total (Kübbeler et al., 2011). A commonly held assumption regarding the formation and
263 evolution conditions of contrail cirrus is that it tends to persist particularly in ice-supersaturated
264 regions (ISSRs) (Kärcher, 2018).

265 The collective presence of commercial, military, and other aircraft contributes to a global increase
266 in cloudiness, primarily facilitated by the formation of persistent contrails when the surrounding
267 atmosphere reaches supersaturation. Contrail cirrus exhibits both cooling and warming effects,
268 with the nighttime impact being predominantly warming. Previous assessments of aviation's
269 influence on climate (IPCC, 1999; Lee et al., 2009; Brasseur et al., 2016) were limited by the
270 challenge of accurately quantifying the role of cloudiness arising from aging and spreading
271 contrails (Minnis et al., 2013). The formation of a persistent contrail necessitates ice-
272 supersaturated conditions along the aircraft's flight path. The life cycles of contrail cirrus are
273 contingent upon the temporal and spatial scales of ice-supersaturated regions, which exhibit high
274 variability in the troposphere and tropopause region (e.g., Lamquin et al., 2012; Irvine et al., 2013;
275 Bier et al., 2017). Estimating the impact of contrail cirrus on upper tropospheric cloudiness
276 requires the simulation of complex microphysical processes, contrail spreading, overlap with
277 natural clouds, radiative transfer, and interaction with background cloudiness (Burkhardt et al.,
278 2010).

279 Petzold et al. (2020) conducted a study investigating the frequency distribution of ice-
280 supersaturated regions (ISSRs) through regular in-situ observations made by passenger aircraft
281 across northern mid-latitude areas. Their research underscores the seasonal and geographical
282 variability of ISSRs, indicating a higher likelihood of occurrence during winter and in specific
283 geographic regions. This variability underscores the significance of considering the spatial and
284 temporal distributions of ISSRs when assessing the potential for contrail formation.

285 Reutter et al. (2020) delved into the characteristics of ice-supersaturated regions using a
286 combination of in-situ water vapor measurements obtained from the IAGOS research program and

287 data from ERA-Interim reanalysis. Their findings showcase the potential for validating reanalysis
288 data with high-resolution aircraft observations. This validation process is critical for enhancing the
289 accuracy of global models utilized in evaluating contrail formation and their subsequent climatic
290 impacts.

291 The ERF of contrail cirrus was estimated for 2011 (relative to an atmosphere without contrails) as
292 50 mWm^{-2} by Boucher et al. (2013), with uncertainty ranging from 20-150 mWm^{-2} . Lee et al.
293 (2021) presented a new estimate derived from the outcomes of global climate models
294 implementing process-based contrail cirrus parameterizations. Recent analyses by Lee et al. (2021)
295 of the current aviation fleet emissions evaluate the ERF through 2018 as 57 mWm^{-2} , with an
296 uncertainty range of 17-98 mWm^{-2} . Given the limited availability of independent estimates,
297 assessing uncertainty becomes crucial. This necessitates analyzing the sensitivities of relevant
298 processes and incorporating the uncertainties associated with the underlying parameters and fields.

299 Contrails form in the early exhaust plumes of airplanes during flight (Kärcher et al., 2015; aufm
300 Kampe, 1943; Weickmann, 1945; Schumann and Wendling, 1990; Schumann, 1996). This
301 happens when supercooled water droplets freeze into ice particles. At cruising altitudes, the
302 atmospheric relative humidity (RH) is usually too low to sustain liquid water droplets but can
303 support ice-phase particles (Gettelman et al., 2006; Lamquin et al., 2012). Consequently, freezing
304 must occur soon after droplet formation within the moist exhaust plume to create persistent
305 contrails. Appleman (1953) identified a key requirement for contrail formation, suggesting that
306 many aerosol particles in the plume serve as centers for water condensation, known as the "water-
307 saturation constraint." Another essential factor is the visibility constraint, which requires at least
308 10^4 cm^{-3} within a plume age of 0.3 seconds for small-scale research aircraft (Appleman, 1953;
309 Kärcher et al., 1996). These are the main constraints for contrail formation.

310 **2.2 Transition of contrails into contrail cirrus and contrail-cirrus-soot interaction**

311 Contrail cirrus consists of elongated contrails trailing high-altitude aircraft and thin cirrus patches
312 formed by the dispersion of persistent contrails. The morphology of contrails evolves based on
313 factors such as humidity, shear, stratification, waves, turbulence, and radiative heating. Contrails,
314 individually and collectively, interact with other cirrus formations, giving rise to what is termed
315 "contrail cirrus" (Schumann and Wendling, 1990). The total extinction is less pronounced when
316 contrails overlap due to humidity competition. Consequently, the climate impact does not always
317 exhibit a linear correlation with air traffic density (Unterstrasser and Sölch, 2012; Bickel et al.,
318 2020). The transformation of a single contrail into a contrail cirrus is observable during aircraft
319 spiral flights, as depicted in Figure 4 (Haywood et al., 2009). "Contrail outbreaks" describe
320 scenarios where numerous aged and young contrails coexist, often spanning expansive areas within
321 the same airspace (Duda et al., 2001).

322 Soot emissions, composed of black carbon particles from aviation, have the potential to alter cirrus
323 properties independently of contrail processing, leading to the formation of "soot cirrus" (Lee et
324 al., 2010). Climate impact assessments of aviation-induced soot cirrus remain inconclusive due to
325 uncertainties in soot abundance and their ice-nucleating properties (Gettelman and Chen, 2013;
326 Zhou and Penner, 2014; Righi et al., 2021). Increased concentrations of small-sized cirrus particles
327 resembling aviation soot emissions have been detected in cirrus regions with dense air traffic
328 (Kristensson et al. 2000). It remains uncertain whether the soot enters the ice during the initial
329 nucleation process or at a later stage through scavenging. The exact mechanism of soot

330 incorporation into cirrus ice remains unclear. Uncertainties persist regarding whether the soot
331 enters the ice during the initial nucleation process or at a later stage through scavenging.

332 A recent study by Testa et al. (2024) examines the processing of aviation soot within contrails and
333 offered further insights into the potential influence of soot on ice nucleation. They specifically
334 investigate the ice nucleation ability of contrail-processed soot particles at cirrus temperatures and
335 found that these particles were generally poor ice nucleating agents. This suggests that soot cirrus
336 formed from processed aviation soot may have a weaker influence on cirrus cloud formation than
337 previously thought.

338 Dischl et al. (2024) demonstrate a significant reduction in non-volatile particle emissions from
339 aircraft engines using sustainable aviation fuel (SAF) compared to traditional jet fuel. This finding
340 indirectly supports the notion that some soot particles might remain dry throughout contrail
341 formation or that some ice particles might sublimate, as these processes could be influenced by
342 particle properties.

343 The sublimation of cirrus particles containing soot and sulfate may lead to the formation of soot
344 aggregates that can potentially act as efficient ice nuclei. A cirrus pattern observed near Munich,
345 Germany, on November 3, 2012, displayed characteristics suggesting an association with aged
346 soot plumes. The cirrus observed between 9.1 and 9.5 km in height, 8-10 km wide, and 35-50 km
347 long, exhibited a distinctive pattern resembling parallel line clouds. Back trajectories indicated that
348 soot was emitted upstream approximately 12 hours before the event by aircraft. The air ascended,
349 forming a cirrus about 4 hours before the event, lasting for about 1-2 hours before subsiding or
350 sublimating. Analyses propose that this could be cirrus formed on preactivated aircraft soot, but
351 certainty is limited, and it cannot be ruled out that the same pattern might have formed without air
352 traffic. (Schumann and Heymsfield, 2017).

353

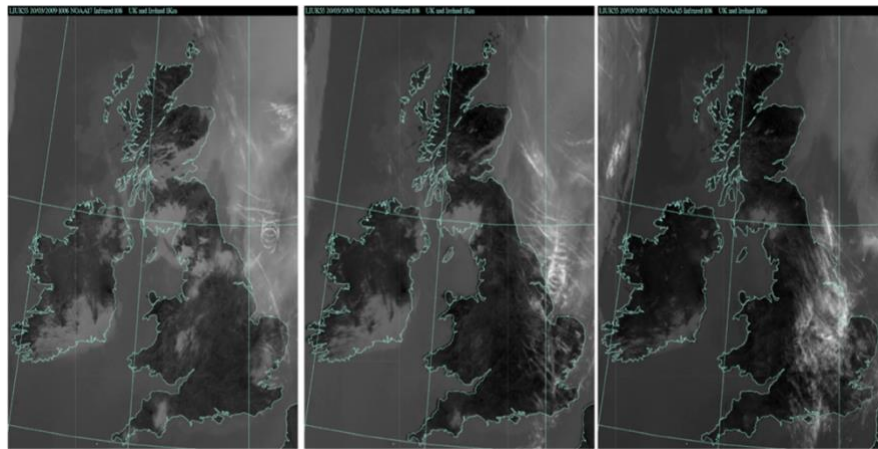


Figure 4. Evolution of contrail cirrus over 1, 3, and 6.5 hours. Contrail cirrus is identified by bright white areas with low infrared (10.8 mm) brightness temperature. The satellite scenes are from NOAA AVHRR for 3 UTC times: (left) 1006 (age after emission = 1 hour), (middle) at 1202 (elapsed time: 3 hours), and (on the right) 1526 (elapsed time: 6.5 hours). Adapted with permission from Haywood et al. (2009).

354

355 A comprehensive understanding of the interplay between contrails, cirrus clouds, and aircraft
356 emissions is essential for accurate assessments of their combined effect on Earth's climate. Recent
357 investigations have illuminated this complex relationship, providing valuable scientific insights.
358 Notably, Urbanek et al. (2018) documented ice clouds exhibiting atypical characteristics over
359 Europe, suggesting potential deviations from standard ice crystal behavior. Additionally, these
360 clouds displayed lower ice supersaturation, hinting at a possible modification in the usual ice
361 formation processes (Urbanek et al., 2018). Intriguingly, the spatial distribution of these cloud
362 formations appeared to correlate with regions experiencing high air traffic. While a definitive
363 causal link between these observations and contrail cirrus formation remains elusive, they do
364 suggest a potential indirect influence stemming from aircraft emissions (Urbanek et al., 2018).

365 In contrast, Kärcher and colleagues (2021) examine the impact of soot particles emitted by aircraft.
366 Kärcher et al. (2021) use modeling to study how these soot particles influence the birth of new
367 cirrus clouds. they found that only a tiny fraction of the soot particles played a role in cloud ice
368 formation via the freezing of liquid aerosol droplets. Consequently, cirrus clouds affected by soot
369 displayed negligible deviations in overall cloud ice content and optical depth compared to their
370 naturally formed counterparts (Kärcher et al., 2021). These findings question the accuracy of
371 current climate models, suggesting they might be overestimating the global radiative impact of
372 interactions between aircraft soot and expansive cirrus clouds.

373 In a related study, Wolf et al. (2023) delve into the radiative effect (RE) of cirrus clouds, shedding
374 light on the pivotal role played by ice crystal properties. Their investigations unveiled that ice
375 crystal size and concentration are the linchpins dictating the overall RE of cirrus clouds.
376 Intriguingly, smaller ice crystals, often associated with contrails, wield a dual-edged radiative
377 effect, inducing both cooling and warming influences. This intricate interplay generally tips the
378 scale towards an overall warming effect exerted by cirrus clouds (Wolf et al., 2023).

379 Beyond the realm of ice crystal properties, Wolf et al. (2023) underscores the importance of other
380 variables. Surface albedo emerges as a contributing factor, with cirrus clouds potentially inducing
381 cooling effects over highly reflective surfaces, like ice, while warming effects over less reflective
382 ones. Additionally, the presence of underlying liquid water clouds and the solar zenith angle also
383 influence the radiative effect. Though their focus primarily centered on plane-parallel clouds, Wolf
384 et al. (2023) acknowledge the potential significance of three-dimensional scattering effects,
385 particularly under high sun angles.

386 **2.3 Evolution of contrails and stages of aviation-induced cloud evolution**

387 The review by Paoli and Shariff (2016) examined the primary physical processes and simulation
388 efforts involved in four distinct phases of contrail evolution. These phases are commonly
389 categorized as the jet, vortex, vortex dissipation, and diffusion phases. Contrail evolution is
390 conveniently divided into these four regimes for clarity (Gerz et al., 1998) (see Fig.5).

391 In the initial seconds after emission (the jet regime), the vortex sheet shed by the wings rolls up
392 into a pair of counter-rotating vortices known as the primary wake. Simultaneously, newly formed
393 ice crystals in the engine exhaust become entrapped around the cores of these vortices. Following
394 this, in the minutes that follow (the vortex regime), the vortices descend into the atmosphere due
395 to their mutually induced downward velocity.

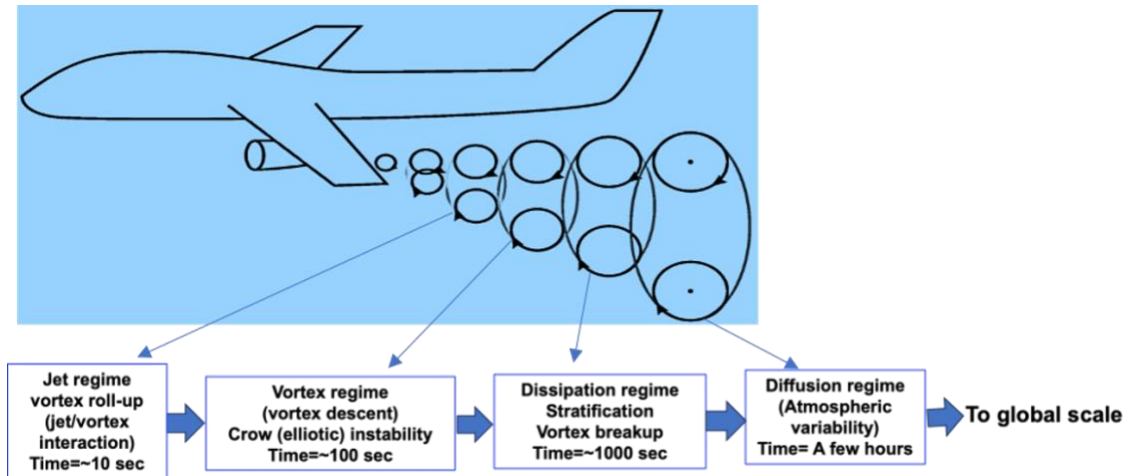


Figure 5. Schematic classification of aircraft wakes evolution into four regimes. Adapted from Paoli and Shariff (2016).

396 The descent of vortices effects in a contrast in density between the air contained within the vortices
 397 (within an oval-shaped region) and the ambient air. This process leads to the generation of vortices
 398 with opposite signs (in a stable stratified atmosphere) along the oval boundary. The vorticity shed
 399 in the upward direction gives birth to a "secondary wake." Within this secondary wake, a portion
 400 of the exhaust gases and ice particles becomes incorporated. Within the regime of vortex
 401 dissipation, the primary vortex pair and secondary vorticity disintegrate and disperse, releasing
 402 both exhaust and ice crystals that eventually endure sublimation. Ice crystals released in the
 403 secondary wake can endure for a longer duration due to the lower temperature. In the fourth
 404 regime, known as the diffusion regime, the horizontal and vertical spreading of the contrail is
 405 influenced by atmospheric turbulence, particle sedimentation, radiative processes, and wind shear
 406 until complete mixing takes place, typically within a few hours.

407 Figure 6 illustrates the processes that influence the various stages of contrail formation. Exhaust
 408 plumes, generated by burning fuel-air mixtures at high temperatures and pressure within turbofan
 409 jet engines, contain both gaseous and particulate matter. In the freely expanding and cooling
 410 plumes (jet regime), particle types include emitted soot particles and aqueous aerosol particles
 411 formed within the exhaust, along with entrained ambient aerosol particles. In scenarios where
 412 turbulent mixing occurs, leading to cooling and generating plume supersaturation over liquid
 413 water, a significant number of plume particles transform water droplets (depicted as gray circles
 414 in Fig. 6).

415 Water droplets rapidly freeze and increase in size by absorbing water vapor from their
 416 surroundings, eventually leading to the formation of a visible contrail. This occurs when the
 417 ambient temperature drops below the formation threshold. In exhaust rich in soot, most droplets
 418 contain soot inclusions. While droxtals, frozen water droplets with faceted surfaces, and hexagonal
 419 prisms and columns likely emerging from them may offer a realistic depiction of small ice crystals
 420 in fresh contrails, there is currently no direct observational evidence for their specific shapes.

421 Plumes from multiple aircraft engines combine with the two wingtip vortices, creating an
 422 inhomogeneous wake. The subsequent evolution of ice crystals is contingent upon fluid-dynamical
 423 processes, particularly in the vortex regime. The downward movement of the vortex pair warms

424 the surrounding air, resulting in the sublimation of ice crystals in the lower portion of the wake. A
 425 small fraction of contrail is amplified by the detrainment of air from the lower wake. Ice crystals
 426 present in the upper wake continue to grow by the uptake of entrained ice-supersaturated ambient
 427 water vapor. A few minutes past emission, the organized flow pattern collapses and mixes with
 428 ambient air (dissipation regime). Table 1 summarizes quantitative comparisons of contrail
 429 characteristics across different stages of evolution, including measurement techniques and
 430 modeling considerations.
 431

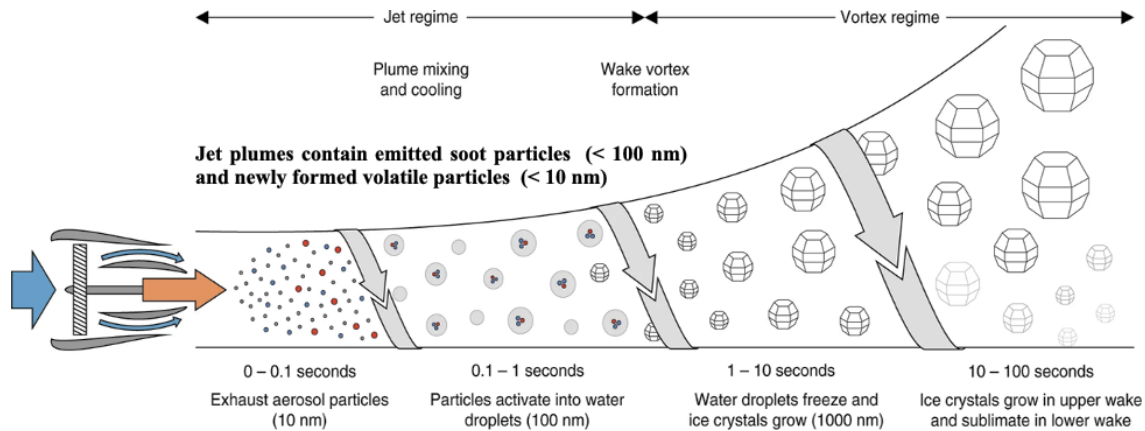


Figure 6. Processes influencing the contrail formation stage. Figure adopted with permission from Kärcher (2018). (Licensed under CC BY 4.0)

432 2.4 Contrail coverage

433 The radiative forcing (RF) for contrails, as determined by Lee et al. (2010), is defined by the
 434 product of contrail coverage and optical depth. For a single contrail segment, this product equates
 435 to total extinction. However, defining contrail coverage presents challenges for several reasons.
 436 Assessing contrail coverage separately from optical depth introduces difficulties. The
 437 identification of young contrails versus other cirrus clouds often relies on their distinctive line
 438 shape. Yet, using geometric characteristics for contrail coverage classification introduces
 439 uncertainty, particularly when contrails undergo deformation or shape changes (Mannstein et al.,
 440 1999). Only a small fraction of all linear contrails is detectable from satellites (Kärcher et al., 2009;
 441 Mannstein et al., 2010; Minnis et al., 2013).

442 Earlier studies examined global contrail coverage using regional satellite observations, estimating
 443 potential contrail coverage based on specific temperature and humidity data and traffic density
 444 (Sausen et al., 1998). The integration of observations to achieve hemispheric coverage has only
 445 recently become available (Duda et al., 2013). The coverage by contrail cirrus may be significantly
 446 higher than determined by line-shaped contrails, and uncertainty factors around an order of 10
 447 have been reported (Burkhardt and Kärcher, 2011). However, this ratio is highly uncertain due to
 448 detection issues. Burkhardt and Kärcher (2011) conducted a quantification of contrail cirrus using
 449 the ECHAM contrail cirrus global climate model (CCmod), which incorporates a subgrid-scale
 450 cloud class representing young contrails. This model captures the life cycle of artificial clouds and
 451 simulates their global coverage, along with the changes in natural cloudiness they induce. Their

452 calculations revealed contrail cirrus coverage to be approximately 0.23%. Similar results were
 453 obtained from recent attempts to quantify contrail cirrus using MODIS data, accounting for more
 454 diffuse contrail contributions (Minnis et al., 2013).

455 **Table 1.** Estimated changes in contrail properties during different stages with measurement
 456 techniques and modeling consideration.

457 (The presented values for different stages of contrail properties and measurement techniques/modeling considerations
 458 are not based on specific references but represent a general understanding from (Schumann et al.,1998; Schumann,
 459 2005; Schumann et al. 2013; Paoli and Shariff, 2016; Schumann et al. 2017; Heymsfield et al., 2017; Bräuer et al.,
 460 2021a, Bräuer et al., 2021b; Schumann et al., 2021; Li et al., 2023; Wang et al., 2023; Geraedts et al., 2024)

461
 462

Stage	Ice Crystal Size (μm)	Number Density (cm^{-3})	Extinction Coefficient (km^{-1})	Width (m)	Length (km)	Optical Depth
Jet	1-10	10^2 - 10^4	10^{-2} - 10^{-1}	10 - 20	10 - 100	0.01 - 0.1
Vortex	10 - 30	10 - 10^2	10^{-3} - 10^{-2}	10^2 - 10^3	1 - 10	0.001 - 0.01
Dissipation	30-100	1 - 10	10^{-4} - 10^{-3}	10^3 - 10^4	0.1 - 1	0.0001 - 0.001
Diffusion	1000-3000	0.1 - 1	10^{-5} - 10^{-4}	10^4 - 10^5	1 - 10	0.00001 - 0.0001
Stage	Measurement Techniques		Modeling Considerations			
Jet	Lidar, satellite imagery		Microphysics, Ice Nucleation rates			
Vortex	Lidar, In-situ probes		Turbulence, Wind shear effects			
Dissipation	Lidar, Ground-based observations		Sedimentation, evaporation rates			
Diffusion	Lidar, satellite imagery		Radiative transfer, ice crystal habit			

463

464 Observations during the COVID-19 pandemic lockdowns provide valuable insights into the
 465 relationship between air traffic and contrail coverage. Dauda et al. (2023) documented a significant
 466 decrease in contrail coverage (up to 41%) over the conterminous United States during the
 467 lockdown period compared to pre-pandemic levels. This decrease highlights the direct impact of
 468 air traffic on contrail formation and underscores the potential for mitigating climate impact through
 469 air traffic management strategies. However, the study also emphasizes the importance of
 470 considering environmental factors alongside air traffic when assessing contrail coverage. While
 471 the reduction in air traffic was the primary driver of the observed decrease in contrail formation,
 472 changes in atmospheric conditions at cruise altitudes likely played a secondary, but significant,
 473 role.

474 In a modeling study, Huszar et al. (2013) adjusted the concentration of a tracer for contrails by
 475 multiplying it with a specific factor and then adding it to the large-scale cloud ice mixing ratio.
 476 They fine-tuned this factor through annual simulations spanning 2005 to achieve an appropriate
 477 global value of the top-of-the-atmosphere radiative forcing attributable to contrails and contrail-
 478 induced cirrus for that year, aiming for a target value of 31 mWm^{-2} as reported by Burkhardt and
 479 Kärcher (2011). The distribution of this forcing aligns with Burkhardt and Kärcher (2011) findings,
 480 showing peak values exceeding 300 mWm^{-2} over central Europe and the eastern U.S., with
 481 significant parts of Europe and the U.S. experiencing a contrail-induced cirrus radiative forcing
 482 above 100 mWm^{-2} . However, their estimates for eastern Asia surpass those of Burkhardt and
 483 Kärcher (2011), with maximum values exceeding 300 mWm^{-2} , while ranging between 100 and
 484 300 mWm^{-2} elsewhere. They suggested these differences could be attributed to how contrail cirrus
 485 is handled (a simpler parameterization in this study versus the more complex contrail-cirrus

486 module used by Burkhardt and Kärcher), variations in simulated thermodynamic conditions over
487 East Asia, and differences in emission inventories.

488 Schumann (2012) developed the Contrail Cirrus Prediction (CoCiP) tool based on a Lagrangian
489 approach. In this model, global contrail coverage is computed by combining the optical depth (τ)
490 contributions from individual contrails and ambient cirrus, counting fractions of areas where
491 contrails cause the optical depth of the total cirrus to surpass a specific threshold (Schumann 2012).

492 Contrails not only augment cloud coverage but also thicken existing cirrus, consequently
493 influencing coverage (Minnis et al., 2013; Schumann and Graf, 2013). This thickening occurs by
494 generating more ice particles with smaller effective radii at constant ice water content (Kristensson
495 et al., 2000). While it is acknowledged that contrails consume humidity and may reduce natural
496 cirrus (Burkhardt and Kärcher, 2011; Unterstrasser and Görsch, 2014; Schumann et al., 2015;
497 Bickel et al., 2020), the prevailing evidence suggests that the thickening effect caused by numerous
498 additional small ice crystals tends to dominate.

499 **2.5 Contrail ice crystal nucleation**

500 Kärcher and Yu (2009) systematically investigated the relationship between nucleated contrail ice
501 crystal numbers and soot particle emissions. In exhaust rich in soot, there is a nearly proportional
502 increase in both ice crystal and soot particle numbers. Close to the contrail threshold, the formation
503 of ice crystals is limited as the low plume supersaturation hinders the activation of water on soot
504 particles, resulting in only a few ice crystals forming. Under conditions rich in soot, the quantity
505 of ice crystals reduces by about one hundred times compared to soot-poor conditions, reaching
506 constant low levels regulated by the number of particles present in the contrail environment. In
507 soot-poor exhaust at low ambient temperatures, there is an increase in ice crystal numbers due to
508 the activation of water and subsequent freezing of abundant aqueous plume particles. Figure 7
509 illustrates the ice crystal number emission index (per kilogram of fuel burnt) in the jet regime,
510 correlating with the number emission index of emitted soot particles as simulated by a parcel model
511 (Kärcher and Yu, 2009). Two sets of results are presented, one for an ambient temperature (T)
512 close to a contrail formation threshold temperature, $\Theta \approx 225$ K (-48°C), commonly encountered in
513 extratropical cruise conditions, and another for a lower temperature of $\Theta -12$ K ≈ 213 K (-60°C).
514 At intermediate ambient temperatures, nucleated ice crystal numbers increase due to enhanced
515 water activation of either soot or ultrafine aqueous plume particles.

516 The hatched area in Figure 7 represents the approximate range of current in-flight soot emission
517 indices. In exhaust rich in soot, the number of soot particles capable of water activation and
518 freezing increases with decreasing ambient temperature. This, in turn, raises plume cooling rates
519 and levels of plume supersaturation over liquid water. It's important to note that the primary driver
520 of the increased cooling and supersaturation is the decreasing ambient temperature, with soot
521 particles acting as additional ice nuclei under these cooler conditions. As the ambient temperature
522 (T) approaches the contrail formation threshold (Θ) in soot-poor exhaust, ambient aerosol particles
523 mixed into exhaust plumes become the sole source of contrail ice crystals. This is because fewer
524 plume particles can be activated due to declining plume supersaturation. The number
525 concentrations of ambient particles in contrails are significantly lower than current levels of soot
526 emissions.

527 The plume cooling rate plays a crucial role in determining the timing of water activation of
528 entrained ambient particles and, consequently, the number of ice crystals derived from them
529 (Kärcher 2015). In soot-poor exhaust, a substantial number of ultrafine aqueous plume particles

530 are formed in the fresh exhaust, especially if the fuel contains condensable vapors besides water
531 vapor. These small particles are anticipated to contribute significantly to ice crystal formation at
532 low ambient temperatures well below average values at cruise levels ($T \approx 218$ K in the extratropic
533 and $T \approx 228$ K in the tropics). If the formation of ultrafine particles cannot be mitigated, ice crystal
534 numbers are expected to be lowest in an intermediate range of soot emissions, specifically between
535 10^{13} and 10^{14} (kg-fuel)⁻¹.

536 Ice crystal number (Ni), which quantifies the concentration of ice crystals in the surrounding
537 atmosphere, plays a significant role in contrail properties (Kärcher, 2015). Studies have shown that
538 Ni can influence factors such as contrail persistence, spreading, and optical characteristics (e.g.,
539 Lewellen, 2014). A higher Ni value typically indicates a greater concentration of ice particles
540 within the contrail, which can affect its behavior in several ways.

541 The signs of variation in the number of ice crystals refer to the alteration in the ice particle
542 concentration within a contrail, such as increased ice particle concentration in the contrail, greater
543 persistence, and spreading of the contrail. Increased optical effects, such as increased brightness
544 and reflectivity. The decreased ice crystal particle concentration in the contrail leads to reduced
545 persistence and spreading of the contrail, and weaker optical effects. These variations in Ni may
546 occur due to several factors, comprising changes in atmospheric conditions, aircraft engine
547 emissions, and the presence of ice nuclei or other particles that impact ice particle formation.

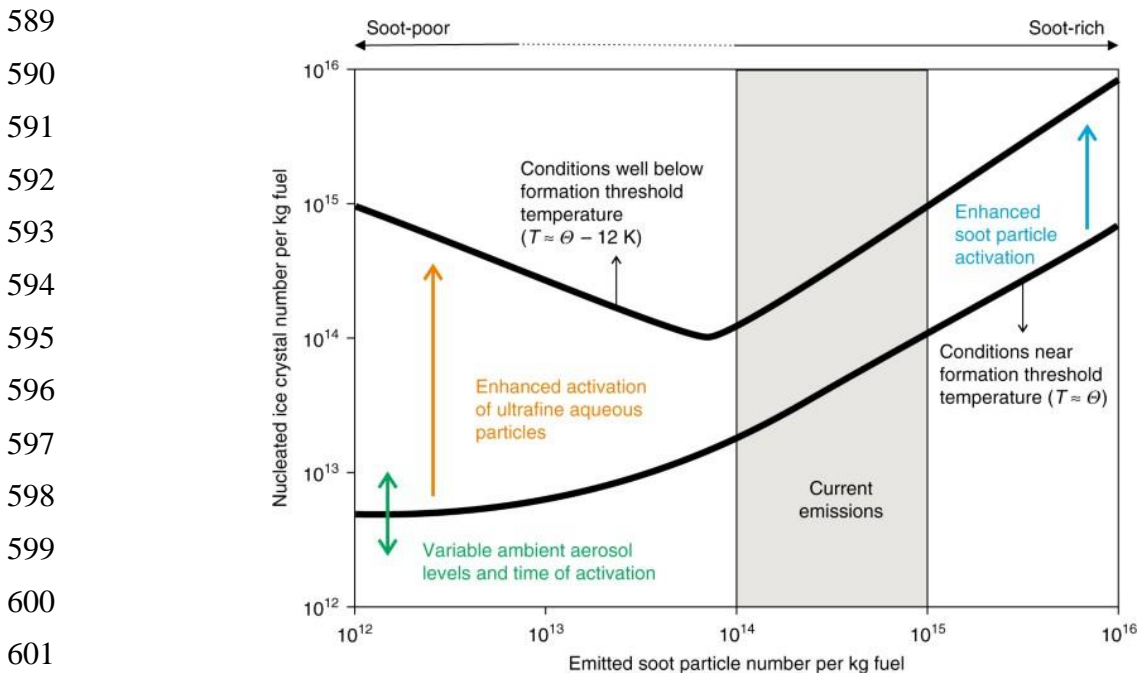
548 Lewellen (2014) elucidates the pivotal role of initial ice crystal concentration (Ni) in contrail
549 dynamics through extensive simulations and the proposition of a simplified model. Their
550 simulations elucidate a discernible correlation between elevated Ni values and several significant
551 effects on contrails. First, contrails characterized by higher Ni values demonstrate prolonged
552 lifetimes, persisting for considerably extended durations, with simulations even indicating
553 lifetimes surpassing 40 hours (Lewellen, 2014). This protracted residence within the atmosphere
554 translates to amplified influence on radiative forcing, as contrails with higher Ni values possess
555 increased temporal opportunities for interaction with incident solar radiation. Second, heightened
556 ice particle concentration within the contrail leads to augmented contrail spreading. As Ni
557 escalates, interactions with atmospheric conditions become more conspicuous, potentially
558 precipitating the formation of contrail cirrus, a prevalent cirrus cloud type intimately associated
559 with contrail genesis (Lewellen, 2014). Finally, higher Ni values correlate with intensified optical
560 effects. A greater abundance of ice crystals within the contrail facilitates more efficient scattering
561 of incident sunlight, engendering brighter and more reflective contrails that perturb the radiative
562 equilibrium in the atmosphere (Lewellen, 2014).

563 Lewellen (2014) delineates a valuable framework for understanding the influence of Ni on contrail
564 significance through their simplified model: $S_{\Sigma} = \alpha N \times D$, where S_{Σ} represents the lifetime-
565 integrated ice crystal surface area, a metric for contrail impact, N is the total crystal number per
566 length of flight path (i.e., ice crystal concentration), and D represents the number-averaged fall
567 distance of ice crystals before sublimation. The coefficient 'α' is approximately constant in the
568 regime of interest. This equation underscores the critical role of Ni (N) in determining the overall
569 radiative forcing exerted by contrails. A higher Ni value translates to a larger S_{Σ} , indicating a more
570 significant impact on the atmosphere due to increased light scattering and longer contrail
571 persistence.

572 **2.6 Stages of aviation-induced cloud evolution and spreading stage**

573 The microphysical and optical characteristics of ice crystals within contrails undergo alterations
 574 as they disperse or transform into contrail cirrus, contingent upon the prevailing meteorological
 575 conditions and microphysical processes (Fig. 8). Over time, persistent contrails undertake a
 576 transformation from their initial linear form to become contrail cirrus. In regions of heavy air
 577 traffic, these contrail cirrus formations overlap and merge, giving rise to extended layers of ice
 578 clouds characterized by alterations in shape, depth, and longevity. These patterns differ from
 579 natural cirrus clouds in terms of microphysical, and optical, additionally, geometric properties also
 580 play a role. The ice-supersaturated layers that sustain these properties exhibit variations in both
 581 vertical structure and horizontal extent, impacting the exchange of water molecules between vapor
 582 and ice phases within them. Collectively, these factors contribute to the radiative forcing (RF)
 583 potential of aviation-induced cirrus (AIC). Figure 8 illustrates the augmentation in cloud coverage
 584 area attributed to the vertical shear of horizontal wind components.

585 The turbulent mixing or entrainment processes result in a gradual reduction (dilution) of ice crystal
 586 concentrations over time. The sizes of ice crystals grow through the absorption (deposition) of
 587 water vapor from layers that are supersaturated with ice. Continuous deposition growth causes
 588 deviations in the shapes (habits) of ice crystals from their initial isometric forms.



602 **Figure 7.** Nucleation of ice crystals in jet aircraft exhaust plumes. Figure adapted with permission
 603 from Kärcher (2018). (Licensed under CC BY 4.0)

604 The shapes and sizes of ice crystals in cirrus clouds significantly impact their growth rates, fall
 605 speeds, and optical properties. Larger ice crystals (>30 micrometers) tend to settle due to gravity
 606 with fall speeds exceeding 100 meters per hour and are more likely to sublimate in warmer or drier
 607 environments. Smaller ice crystals remain suspended around the flight levels due to their negligible
 608 fall speeds, provided that some degree of supersaturation can be maintained, which depends on the
 609 prevailing meteorological conditions.

610 The efficiency of sedimentation, the process by which ice crystals fall from clouds, is influenced
 611 by the depositional growth rate, which in turn is affected by ice supersaturation, the rate of air

612 cooling, and the characteristics of the ice crystals themselves, including their size, shape, and
613 number concentration. Sedimentation increases the vertical extent of cirrus clouds, enhancing their
614 spreading rate and coverage under sheared flow conditions.

615 The settling of ice crystals, known as sedimentation, is a critical factor in determining the lifespan
616 of contrails. As the contrail ages, larger ice particles, due to their increased mass, fall out of the
617 plume more rapidly. This phenomenon can be explained by the concept of terminal velocity
618 (Spichtinger and Gierens, 2009). Researchers have explored methods to calculate this velocity,
619 considering the distribution of ice crystal sizes within the plume (Spichtinger and Gierens, 2009).
620 This approach provides a more comprehensive understanding of the sedimentation process.

621 The size of an individual ice crystal directly influences its falling speed. Larger crystals, typically
622 associated with persistent contrails, descend from the plume quicker than their smaller counterparts
623 found in ephemeral contrails. This sedimentation process significantly impacts the vertical
624 distribution of ice crystals within the contrail and affects its overall persistence. Ice crystals lofted
625 higher, potentially due to weaker updrafts, may experience slower sedimentation and persist for
626 longer durations, especially in colder atmospheric regions.

627

628 **2.7 Lessons learned from observations of contrails and their properties**

629 Contrails, as well as cirrus clouds, are frequently observed in air that lacks saturation (Kübbeler et
630 al., 2011; Krämer et al., 2009). The prevailing explanation suggests that these clouds consist of
631 large ice particles formed under supersaturated conditions, which then descend to lower and drier
632 levels, undergoing slow sublimation. Notably, instances of contrails and contrail cirrus have been
633 documented in ice-sub-saturated air across various scenarios, extending beyond dedicated contrail
634 research flights (Schumann et al., 2017; Voigt et al., 2011; Kübbeler et al., 2011; Gayet et al.,
635 2012; Chauvigné et al., 2018). Such observations have been derived not only from contrail-specific
636 research endeavors but also from In-service Aircraft for a Global Observing System (IAGOS)
637 commercial aircraft data collected in the North Atlantic region (Petzold et al., 2017).

638 Apart from a high number of small contrail ice particles, large particles (ice particle diameter
639 greater than 100 μm) were also detected but at relatively low concentrations (Voigt et al., 2010).
640 Such large ice crystals were also observed in contrail cirrus during the ML-CIRRUS (Midlatitude
641 Cirrus experiment) campaign (Voigt et al., 2017). However, attention to contrail cirrus in ice-sub-
642 saturated environments and the role that large ice particles play in contrail cirrus was raised by
643 Kübbeler et al. (2011) and Schumann (2012).

644
645
646
647
648
649
650
651
652
653
654
655
656
657
658
659
660
661
662
663
664
665
666
667
668
669
670
671
672
673
674
675
676
677
678
679
680
681
682
683

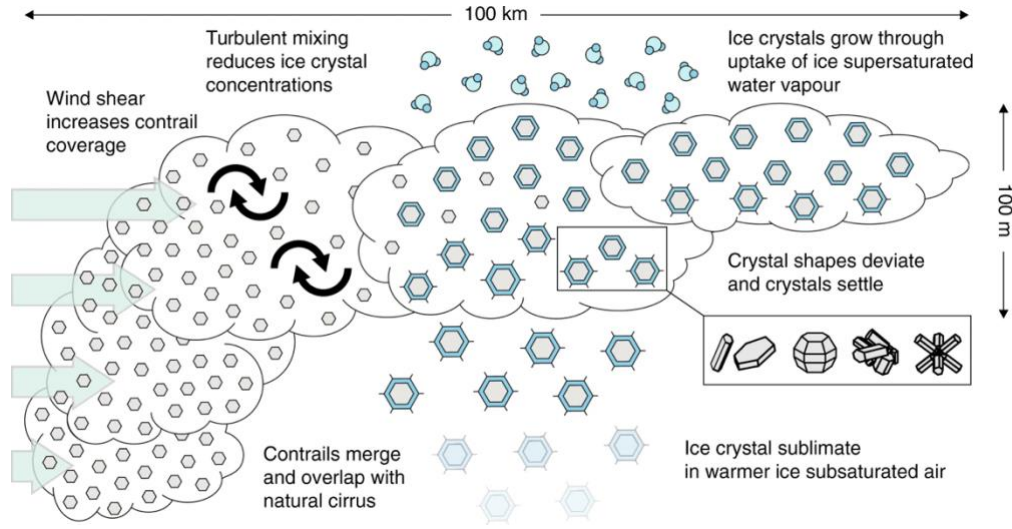


Figure 8. Influential factors in aircraft-induced cloud formation. Figure adopted with permission from Kärcher (2018). (Licensed under CC BY 4.0)

Kübbeler et al. (2011) suggested that the subsaturation observed in contrail cirrus during the CONCERT campaign is caused by the sublimation of large ice particles that may have fallen from higher altitudes after forming under ice supersaturated regions (ISSRs). However, due to the limited contrail cirrus data available, it is difficult to confirm whether contrail cirrus commonly occurs in ice-subsaturated environments.

Li et al. (2023) explored an extended dataset derived from 14.7 hours of cirrus cloud sampling conducted at a frequency of 1 Hz, with a maximum speed of approximately 290 m s^{-1} , obtained during the ML-CIRRUS 2014 campaign. Utilizing readily available parameters that characterize cirrus microphysical properties—including ice number concentration, ice crystal sizes, and ice water content (IWC)—they employed a more straightforward statistical method to distinguish aviation-induced cirrus from natural cirrus, in contrast to the approach adopted by Chauvigné et al. (2018). It consists of the SAC, covering the most common aircraft cruising altitude range, and a recently developed algorithm for detecting aircraft exhaust plumes to identify matured contrail cirrus (>0.5 h lifetime; Voigt et al., 2017; Schumann et al., 2017), and natural cirrus. Contrail cirrus showed sharp differences from natural cirrus during the stages of formation and in the corresponding microphysical properties and occurrence conditions.

Mahnke et al. (2024) investigated the impact of aviation-induced aerosols on cirrus clouds and climate, which remains uncertain. Understanding these properties is vital for assessing aviation's climate effects. From July 2018 to March 2020, the IAGOS-CARIBIC Flying Laboratory identified over 1100 aircraft plume encounters. Findings showed consistent aerosol properties across various altitudes (upper troposphere, tropopause region, and lowermost stratosphere). The exhaust aerosols were primarily externally mixed, even after 1 to 3 hours, with no increase in larger particles (diameter $>250 \text{ nm}$) inside the plumes. The particle number emission indices (EIs) from aged plumes matched engine certification values, indicating that aviation aerosols maintain their emission state during plume expansion and that global models use accurate EI values.

684 **Observational Constraints**

685 While there is growing evidence regarding contrail observations in ice-subsaturated
686 environments, it is imperative to acknowledge the inherent limitations associated with measuring
687 contrail properties. These limitations stem from various factors, including:

688 *Spatial and temporal resolution of instrumentation:* The comprehensive depiction of contrail
689 phenomena may be impeded by the restricted range or sampling frequency of instruments
690 employed for in-situ or remote sensing observations. For instance, satellite-based observations
691 might fail to capture minute-scale contrail features, while in-situ measurements conducted via
692 research aircraft may not fully encompass the spatial extent of a contrail layer.

693 *Discriminating contrails from natural cirrus formations:* The differentiation between contrails
694 and natural cirrus clouds, particularly in ice-subsaturated conditions, presents a significant
695 challenge and often necessitates sophisticated analytical techniques. Both varieties of ice clouds
696 can exhibit comparable characteristics concerning size and ice crystal properties, rendering the
697 definitive identification of their origin based on limited observations a challenging endeavor.

698 *Restricted data availability:* Observational datasets, particularly those focusing on fully
699 developed contrail cirrus, may be scarce. This scarcity impedes the ability to draw definitive
700 conclusions regarding the prevalence of contrails in sub-saturated environments and their
701 enduring influence on the climate system.

702

703 **3 Modeling of Contrails and their Impacts**

704 Understanding the multifaceted impacts of contrails necessitates employing models at various
705 scales. Local-scale process and fluid-dynamic models offer valuable insights into how plume
706 turbulence and wake dynamics influence the nucleation and properties of contrail ice crystals.
707 These simulations can then be validated against in-situ aircraft measurements of nucleated ice
708 crystal concentrations and sublimation losses (Kärcher, 2018). For broader-scale analysis, cloud-
709 resolving and regional models are utilized. These models incorporate meteorological boundary
710 conditions and leverage optical parameterizations to capture the shortwave radiative response of
711 micron-sized ice crystals. By co-locating these simulations with data from aircraft and satellite
712 observations, scientists can gain a more comprehensive understanding of the radiative forcing (RF)
713 exerted by contrail cirrus and its potential influence on pre-existing cirrus clouds (Kärcher, 2018).

714 The limitations of current instrumentation in measuring the microphysical and optical properties
715 of contrail cirrus elevate the importance of models (Table 2) for estimating their RF. To provide
716 robust predictions of climate change driven by aircraft emissions, models simulating ice nucleation
717 and sublimation must effectively translate the current understanding of contrail formation and
718 evolution processes into frameworks that lack the spatial or temporal resolution to explicitly
719 capture the formation stage. This objective can be achieved by synergistically integrating findings
720 from observations with local-scale, process-oriented models.

721 **3.1 Modeling of individual contrails**

722 Individual contrails have been studied by various authors through approaches ranging from
723 simplified parameterizations to more complex numerical models. Parameterization approaches
724 normally depend on simplified assumptions to estimate contrail properties based on simplified
725 atmospheric and emission conditions. On the contrary, more sophisticated numerical models, such
726 as the Contrail Cirrus Prediction model (CoCiP), utilize detailed representations of atmospheric
727 processes, ice particle growth, and radiative transfer to simulate the formation and evolution of
728 contrails.

729 **Table 2.** Modeling the complexities of aircraft-induced cloud radiative effects (Adapted from
 730 Kärcher 2018).

Model scale	Spatial resolution		Contrail stages	Major challenges	Approach/solution
	Horizontal	Vertical			
Local	<10 m	<10 m	Formation stage	Ice crystal number and size distribution	Turbulence microphysics coupling
Regional	<1000 m	<100 m	Spreading stage	Radiative flux changes and interaction with natural clouds	Contrail to contrail cirrus transition
Global	<1000km	<1km	Full life cycle	Ice crystal formation and ice supersaturation	Parameterization and high resolution

Improvements in a hierarchy of local- to global-scale models to be realized in conjunction with observations providing data for cloud and radiation parameterization development and overall model validation.

731 **3.1.1 Contrail Cirrus Prediction Tool (CoCiP) for individual contrails**

732 Schumann et al. (2017) compiled a dataset of contrail properties from various sources, including
 733 previous publications, additional information gathered from experimenters, reanalysis of existing
 734 data, and comparisons with the CoCiP database. The dataset expands upon the work of Schumann
 735 and Heymsfield (2017) by incorporating data from the ML-CIRRUS campaign (Voigt et al., 2016).
 736 The data includes both in-situ measurements of contrails, such as ice particle size spectra obtained
 737 using optical particle spectrometers (Baumgardner et al., 2011; Wendisch and Brenguier, 2013),
 738 and remote sensing data from ground-based and airborne lidar, spectroradiometers, satellites,
 739 cameras, and visual observations. Remote sensing data provides information on contrail properties
 740 such as width and optical depth (Spinhirne et al., 1998; Duda et al., 2004).

741 **3.1.2 MIT Aircraft Plume Chemistry, Emissions, and Microphysics Model (APCEMM)**

742 APCEMM is applied to assess the impact of non-linear plume chemistry and to deliver an initial
 743 estimate of the effects of contrails on atmospheric chemistry. Accurately determining the intricate
 744 relationship between contrail microphysics and chemistry often necessitates the use of costly large
 745 eddy simulations (LESs). APCEMM, through simplified assumptions about plume dynamics,
 746 strives to close the disparity between Gaussian plume models and LESs, as outlined by Fritz et al.
 747 (2020). APCEMM simulates the growth and chemical progression of an individual aircraft plume.
 748 It computes chemical concentrations and aerosol characteristics for a two-dimensional cross-
 749 section of the plume, angled perpendicular to the flight path. Dynamics, chemistry, and
 750 microphysics are explicitly modeled within the plume, using two different approaches depending
 751 on the age of the plume.

752
 753 **3.1.3 NASA’s global model for evaluation of individual linear contrails**

754 The NASA Ames Research Center developed a computationally efficient aircraft contrail model
 755 designed to simulate aircraft-induced contrail formation. This model relies on the Appleman
 756 criterion and operates under static atmospheric conditions (Sridhar et al., 2010; Neil et al., 2010).
 757 Subsequently, researchers from NASA Ames extended this model to simulate the dynamic
 758 transport of contrails by incorporating a Lagrangian dispersion model and a cloud microphysics
 759 model (Li et al., 2013). The computational methods employed are grounded in well-established

760 approaches utilized in other aircraft contrail models (Pruppacher and Klett, 2000; Schumann et al.,
761 1995).

762 In comparison with models from Stanford (Naiman et al., 2009; Naiman et al., 2011; Jacobsen et
763 al., 2011) and DLR (Burkhardt and Kärcher, 2009; Burkhardt and Kärcher, 2011; Bier and
764 Burkhardt, 2022), this dynamic contrail model diverges primarily in two aspects: (1) It excludes
765 the initial contrail ice particles down-wash process caused by airplane wake vortex turbulence.
766 This process, typically lasting less than a minute, is crucial in determining contrail ice nucleation,
767 initial contrail ice particle sizes, and displacements through a complex fluid dynamic process
768 dependent on atmospheric, aircraft, and fuel parameters. In this model, the average initial ice
769 particle size is predefined, and the initial contrail location is set based on the cell where contrail
770 formation conditions are met. (2) The results from this model do not yet include additional
771 radiative forcing caused by aircraft contrails. The researchers are in the process of adding a contrail
772 radiative forcing module capable of computing the total aircraft contrail radiative forcing using
773 inputs from the model, such as ice particle size and linear contrail cloud cover area.

774 **3.1.4 DLR's ICON-LEM regional model**

775 Verma and Burkhardt (2022) developed and implemented a model for contrail formation into the
776 ICON-LEM (ICOsahedral Non-hydrostatic Large-Eddy Model; Zängl et al., 2014; Dipankar et al.,
777 2015). This model includes parameterizations for ice nucleation in the jet phase and ice crystal
778 loss during the contrail's vortex phase. It facilitates the investigation of modifications to cirrus
779 clouds resulting from contrail formation. ICON is the new German Numerical Weather
780 Prediction/Climate Model co-developed by DWD and MPI. It solves a set of equations on an
781 unstructured triangular grid based on successive refinement of a spherical icosahedron (Zängl et
782 al., 2014).

783 The model asserts high horizontal resolution coupled with a vertical resolution of approximately
784 150 m in the upper troposphere, enabling the resolution of pertinent cloud processes. Within
785 ICON-LEM, a contrail scheme has been developed and implemented, incorporating the
786 parameterization of contrail ice nucleation as proposed by Kärcher et al. (2015) and accounting
787 for the survival of ice crystals within the vortex phase. (Unterstrasser, 2016), to study changes in
788 cloud variables due to contrail formation within cirrus. Contrail formation, dependent on
789 atmospheric as well as aircraft and fuel parameters, is calculated, and contrail ice nucleation and
790 ice crystal loss in the contrail's vortex phase are estimated.

791 **3.1.5 Large-eddy simulations covering the entire life cycle, from initiation to termination**

792 Lewellen et al. (2014) outlined the utilization of large-eddy simulations with size-resolved
793 microphysics to model persistent aircraft contrails and the resulting contrail-induced cirrus clouds.
794 These simulations aim to depict the dynamic evolution of contrails, spanning from a few wing
795 spans behind the aircraft to their dissipation over an extended period. The emphasis of the study
796 lies in the modeling approach, discussing the development of schemes for efficient numerical
797 computation. The authors introduced dynamic local ice binning and updating, along with coupled
798 radiation, to accurately capture microphysical processes and radiative properties within individual
799 columns. The paper also addresses the challenge of maintaining realistic ambient turbulence over
800 extended simulation times, proposing a "quasi 3D" approach as a computationally feasible
801 approximation of the full dynamics, allowing for exploration across a broader parameter space.

802

803 Lewellen (2014) provides an extensive analysis encompassing over 200 instances of long-lived
804 contrails, spanning from their formation at several seconds old to their termination. The study
805 investigated the complete lifespan of long-lived contrails originating from a single aircraft. Various
806 factors were explored, including the effective ice crystal number emission index, temperature,
807 relative humidity concerning ice, stratification, shear, supersaturated-layer depth,
808 uplift/subsidence, and coupled radiation. The analysis delved into the scaling behaviors of contrail
809 lifetime, width, ice mass, and surface area. The simulations unveiled contrail lifetimes exceeding
810 40 hours, widths surpassing 100 kilometers, and ice masses exceeding 50 kg per meter of the flight
811 path. The paper identified distinct behavioral regimes influenced by radiative forcing and proposed
812 a simplified model to predict these regimes.

813 Key insights from the simulations highlight the notable impact of ice crystal number loss resulting
814 from competition among different crystal sizes, influencing both young contrails and aging contrail
815 cirrus. The sensitivity of contrail properties to the initial number of ice crystals decreases over
816 time, highlighting the importance of uncertainties in ice crystal deposition coefficients and the
817 Kelvin effect. The influence of atmospheric turbulence on contrail properties and lifetime is also
818 emphasized. Additionally, the paper discusses the effects of ice crystal shape, coupled radiation,
819 precipitation dynamics, and the role of water from fuel consumption in reducing ice crystal loss in
820 colder contrails.

821 Lewellen's simulations provide valuable insights into contrail behavior, shedding light on the
822 significance of crystal number loss mechanisms, the interaction between shear and ice
823 sedimentation, the depth of the supersaturated layer, and the potential impact of "cold" subvisible
824 contrails. The findings from these simulations contribute to estimating the effects of intricate
825 contrail scenarios, formulating mitigation strategies, and enhancing our comprehension of the
826 dynamics of natural cirrus clouds.

827 **3.2 Treatment of contrails in global models**

828 The consideration of contrail cirrus in global climate models has greatly improved in recent years.
829 Despite these advancements, notable uncertainties persist, particularly in the depiction of contrail
830 microphysics and the interaction between contrail-cirrus and cirrus-radiation. As mentioned
831 earlier, the characteristics of young contrail cirrus diverge from those of natural cirrus primarily
832 due to the elevated ice crystal number concentration typical in contrails. Consequently,
833 microphysical process rates in contrail cirrus, influencing its lifespan, can exhibit significant
834 deviations from those observed in natural cirrus. In this section, we examine the treatments of
835 contrail and contrail cirrus in global models. Very few models account for contrails, so our focus
836 is on those models that have been published extensively on contrail impacts, including modeling
837 studies done by the Institute for Atmospheric Physics (DLR), the National Center for Atmospheric
838 Research (NCAR), and Stanford University. The focus is on their modeling approaches and
839 findings. We start with a description of the approach used to treat contrails in these models.

840 **3.2.1 DLR Contrail Cirrus Prediction Model (CoCiP)**

841 CoCiP can be implemented within a GCM and used to study the global distributions of contrails
842 and contrail cirrus (Schumann et al., 2015). The model is specifically crafted for the estimation of
843 contrail cirrus coverage and the analysis of contrail climate impact, particularly in the context of
844 aviation system optimization processes. It is engineered to simulate the entire life cycle of
845 contrails. Contrail segments arise between waypoints along individual aircraft tracks in air masses
846 that are cold and humid enough. The initial characteristics of contrails are contingent upon the

847 specific aircraft involved. The advection and progression of contrails adhere to a Lagrangian
848 Gaussian plume model. This model treats the contrail life cycle using bulk contrail ice physics,
849 incorporating several simplifying assumptions. Notably, the model demonstrates efficiency in
850 handling mixing and cloud processes in a quasi-analytical manner (Schumann, 2012). Contrails
851 become extinct when the bulk ice content endures sublimation or precipitation.

852 The model takes into consideration the impact of both aircraft properties and ambient
853 meteorological conditions. This encompasses established contrail formation thresholds, the effects
854 of advection, turbulent mixing, and the formation of ice mass from both emitted and ambient
855 humidity. The number of ice crystals is contingent upon the quantity of soot particles emitted. The
856 model incorporates simplified approximations for the survival of ice particles in adiabatically
857 sinking wake vortices and the loss of particles in aged contrails (Schumann, 2012).

858 CoCiP (Contrail Cirrus Prediction) depicted in Figure 9 simulates the formation of contrails under
859 specific meteorological conditions, either regionally or globally. Numerical weather prediction
860 data are utilized to determine ambient meteorological conditions through linear interpolation at
861 given positions and times. The model has been effectively employed to simulate contrails in both
862 global and specific cases, and its results have been compared with outcomes from other models
863 and in-situ measurements (Schumann, 2012).

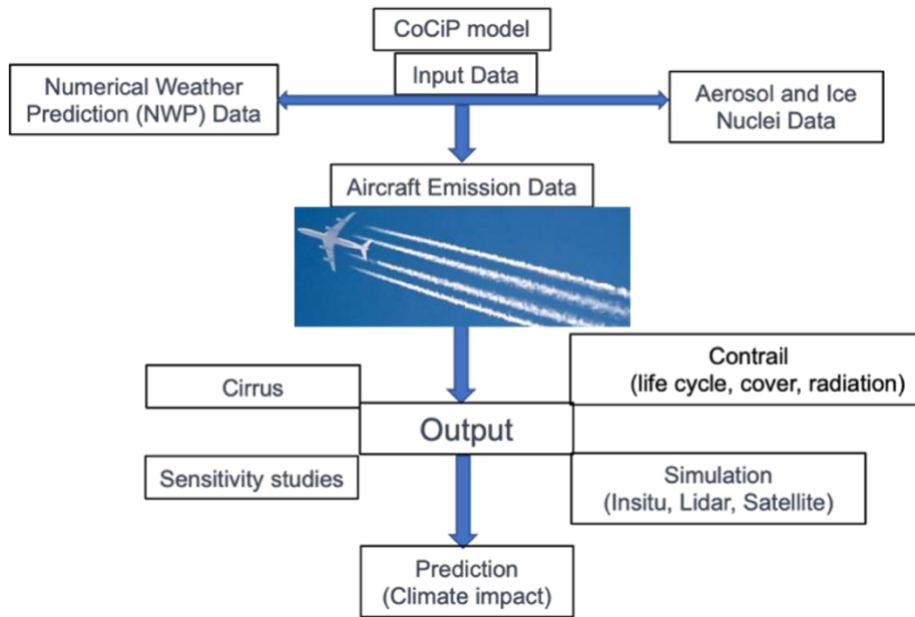
864 **3.2.2 DLR version of the ECHAM5-HAM model**

865 The global climate model ECHAM5-HAM (European Center for Medium-Range Weather
866 Forecasts (ECMWF) and Hamburg) was developed at the Max Planck Institute (MPI) for
867 Meteorology in Hamburg, Germany (Roeckner et al., 2003, 2006; Stier et al., 2005), and adapted
868 to study of aviation effects on climate, including the modeling of the effects from contrails. The
869 aerosol-climate modeling system ECHAM5-HAM is based on a flexible microphysical approach,
870 and it predicts the evolution of an ensemble of microphysically interacting internally and externally
871 mixed aerosol populations as well as their size distribution and composition. Bier and Burkhardt
872 (2022) applied the ECHAM5-HAM model, incorporating a two-moment microphysical scheme
873 that was expanded to introduce a novel cloud category-contrail cirrus. The contrail cirrus scheme
874 encompasses a parameterization addressing contrail ice nucleation, the loss of ice crystals during
875 the vortex phase, plume dilution, the spreading of contrails influenced by vertical wind shear, and
876 inclusive microphysical and macrophysical processes aligned with the natural cloud scheme.

877 The contrail cirrus parameterization implemented in ECHAM5-HAM follows the framework
878 established by Burkhardt and Kärcher (2009), who introduced contrail cirrus as a distinct cloud
879 class alongside natural cirrus clouds within the model's natural cloud scheme. The water and heat
880 budgets are balanced, with natural cirrus and contrails competing for available water vapor.
881 Prognostic variables, including ice water content, contrail coverage, and the length of contrail
882 cirrus, are computed based on factors such as persistence, advection, spreading, and
883 deposition/sublimation.

884

885
886
887
888
889
890
891
892
893
894
895
896
897
898
899



900 **Figure 9.** Schematic of the CoCiP model. Adapted from Schumann (2012). Contrail Image
901 (Credit: Adrian Pingstone (public domain))

902 Bock and Burkhardt (2016) extended this parameterization (CCMod) by incorporating a
903 microphysical two-moment scheme (Lohmann et al., 2008). This enhancement significantly
904 improved the representation of microphysical processes by introducing contrail cirrus ice crystal
905 number concentration and volume as additional prognostic variables. This advancement is crucial
906 for studies investigating the impact of aircraft particle number emissions on contrail cirrus
907 properties and their overall climate influence.

908 Bier and Burkhardt (2022) describe the initialization of contrails within the model. However, the
909 chosen initialization time of 450 seconds (7.5 minutes) warrants further discussion. This value
910 represents half of a model time step, potentially suggesting computational efficiency as a factor in
911 its selection. Nevertheless, a 450-second delay in contrail formation might be too long for accurate
912 simulations, especially for studies focusing on the early stages of contrail evolution. Future
913 investigations need to explore the sensitivity of model results to this initialization time and
914 potentially refine it for a more realistic representation of contrail formation processes.

915 In instances of contrail cirrus volumes exhibiting very low ice crystal number concentrations, as
916 observed in aged contrails associated with heightened ice crystal sedimentation, the deposition of
917 ice water is constrained, aligning with the depositional growth of ice crystals (Bock and Burkhardt,
918 2016). In more recent iterations of the model, specifically, ECHAM5-CCMod, Bier and Burkhardt
919 (2019) incorporated the contrail ice nucleation parameterization proposed by Kärcher et al. (2015).
920 In their model approach, they suggest that the plume cools over time due to continuous mixing of
921 the exhaust with ambient air, eventually becoming water-supersaturated when the SAC criterion
922 is met. The number of activated aerosol particles, stemming from soot and ambient particles, is
923 computed based on ambient conditions, fuel/engine characteristics, and exhaust particle properties.
924 Additionally, Bier and Burkhardt (2022) introduced a parameterization for ice crystal loss during
925 the vortex phase and conducted a thorough evaluation of their model.

926
927
928
929
930
931
932
933
934
935
936
937
938
939
940
941
942
943
944
945
946
947
948
949
950
951
952
953
954
955
956
957
958
959
960
961
962
963
964

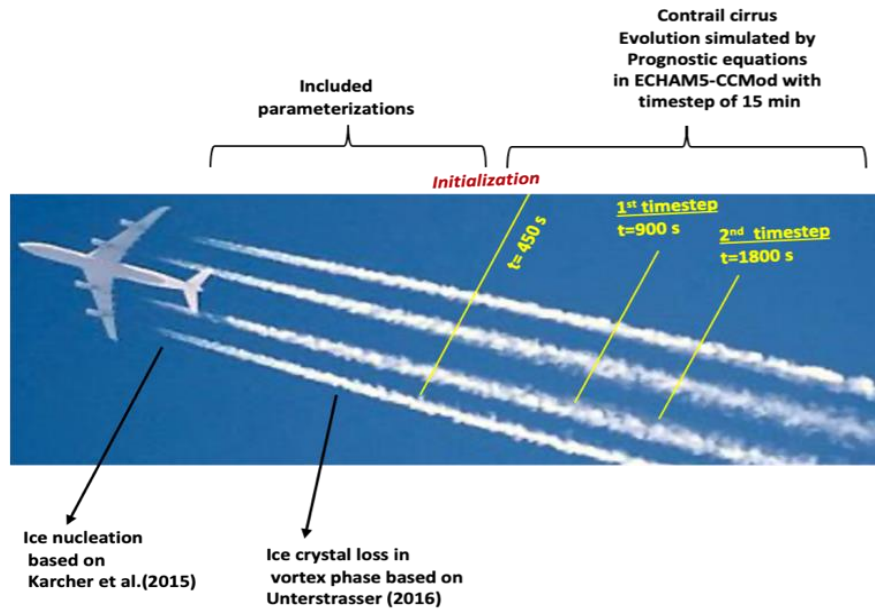


Figure 10. Stages of contrails and their corresponding treatment into the global climate model ECHAM5-CCMod. [Adapted from Bier and Burkhardt (2022). Contrail Image (Credit: Adrian Pingstone (public domain)

3.2.3 NCAR CAM6 model with Contrails

In the first NCAR study of the radiative forcing of linear contrails and contrail cirrus, Chen and Gettelman (2013) used the Community Atmosphere Model version 5 (CAM5), the atmospheric component of the National Center for Atmospheric Research (NCAR) Community Earth System Model (CESM). More recently, they have used the updated atmospheric component from the new version of CESM2 (Danabasoglu et al., 2020). The current atmospheric model implemented in CESM2 is CAM, version 6.2 (CAM6; Gettelman et al., 2020). CAM6 incorporates a detailed two-moment cloud microphysics scheme (Gettelman and Morrison, 2015) coupled with an aerosol microphysics and chemistry model (Liu et al., 2016; Gettelman et al., 2019). The latest version of the contrail parameterization (Chen et al., 2012) was utilized with CAM6 (Gettelman et al., 2021). While the ice cloud microphysics and aerosols exhibit minimal differences between CAM5 and CAM6, the aerosol activation in CAM6 significantly differs, impacting natural cirrus clouds but not contrails. The assumed emission ice particle diameter was adjusted from the original parameterization (10 μm) to 7.5 μm to better align with observations (e.g., Lee et al., 2021).

For contrail studies at NCAR, the standard version of CESM with 32 levels (to 3 hPa) vertical and $\sim 1^\circ$ horizontal resolution was employed. Winds and optional temperatures were relaxed to NASA's data assimilation analyses, specifically the Modern-Era Retrospective analysis for Research and Applications, version 2 (MERRA2; et al., 2015), with wind nudging (Gettelman et al., 2020, 2021). CESM2 features a fully interactive land surface model (the Community Land Model, version 5; et al., 2020). Sea surface temperatures (SSTs) are fixed to MERRA2 SST, and there is no interactive ocean.

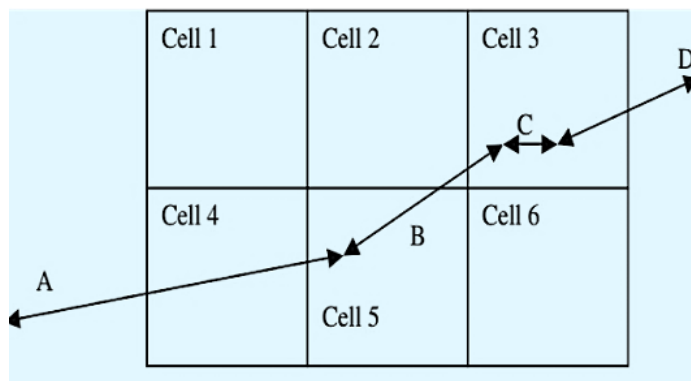
These simulations allow for adjustments in atmospheric and surface temperatures, resulting in radiative flux perturbations representing an Effective Radiative Forcing (ERF). Sensitivity tests were conducted, with temperatures nudged to MERRA2. The results were compared with previous

965 contrail simulations using this model and others, as well as observational data. The pattern of
 966 contrail-induced changes to cloud fraction closely resembled the previous model documented in
 967 CAM5 (Chen and Gettelman 2013), with peak effects observed in the Northern Hemisphere at
 968 mid-latitudes. The radiative forcing in the CAM6 simulations exceeded that of the earlier Chen
 969 and Gettelman (2013) study due to a smaller initial contrail area (100 vs. 300 m) and smaller initial
 970 ice crystal sizes (7.5 vs. 10 μm diameter). The radiative forcing pattern and magnitude were
 971 qualitatively and quantitatively consistent with the analysis conducted by Lee et al. (2021),
 972 aligning with the intercomparison between contrail simulation models.

973 3.2.4 Stanford global model for contrail evaluation

974 Although it is no longer actively utilized in aviation studies, Stanford University developed a low-
 975 order contrail model and a Large Eddy Simulation (LES) model (Naiman et al., 2009; Naiman et
 976 al., 2011; Jacobsen et al., 2011). In their work, Jacobsen et al. (2011) assessed mass-conservative,
 977 positive-definite, unconditionally stable, and non-iterative numerical techniques for simulating the
 978 evolution of discrete, size, and composition-resolved aerosol and contrail particles within
 979 individual aircraft exhaust plumes. This simulation was conducted in a global or regional 3-D
 980 atmospheric model, incorporating the coupling of subgrid exhaust plume information to the grid
 981 scale (see Fig. 11). This approach represents a distinct method for simulating the impacts of aircraft
 982 on climate, contrails, and atmospheric composition.

983 The microphysical processes addressed within each plume include size-resolved coagulation
 984 among and between aerosol and contrail particles, aerosol-to-hydrometeor particle ice and liquid
 985 nucleation, deposition/sublimation, and condensation/evaporation. Each plume is characterized by
 986 its own emission and supersaturation, and the spreading and shearing of each plume’s cross-section
 987 are calculated over time. Aerosol and contrail-particle core compositions are tracked for each size
 988 and affect optical properties within each plume. When linear contrails sublimate or evaporate, their
 989 size and composition-resolved aerosol cores and water vapor are introduced to the grid scale,
 990 where they influence large-scale clouds. The model’s algorithmic properties were analyzed, and
 991 the final model was evaluated against in situ and satellite data. Table 3 summarizes the cross-
 992 model intercomparison of contrail simulation models covered in this study.



993
 994
 995
 996
 997
 998
 999
 1000
 1001 **Figure 11.** Example of how flight segments cross grid cell boundaries in the Jacobsen et al., model.
 1002 Segments A, B, C, and D are original segments. These are partitioned or aggregated into individual
 1003 model grid cells 2, 3, 4, and 5 to form “new” segments. Adapted with permission from Jacobson
 1004 et al. (2011).

1005 **4 Radiative Forcing for Contrail Cirrus in Global Models**

1006 **4.1 Contrail radiative forcing and efficacy**

1007 Contrails during the day can warm or cool depending on optical depth, zenith angle, and ice crystal
1008 shape (Meerkötter et al., 1999; Stuber et al., 2006; Newinger and Burkhardt, 2012). Stuber et al.
1009 (2006) suggested that moving all air traffic to the day decreases RF. Newinger and Burkhardt
1010 (2012) stated that we need to consider the lifetime of the contrails since daytime air traffic can
1011 cause a large contrail coverage at night. After all, it is the long-lived contrail cirrus outbreaks that
1012 are responsible for a large part of the climate impact (Burkhardt et al., 2018). As illustrated in Fig.
1013 1, the overall effect reveals a positive net radiative forcing (RF), signifying a warming impact. The
1014 examination of this phenomenon is undertaken here in contrast to the comprehensive RF, the local
1015 RF (RF') can be defined as the instantaneous change in net incoming radiation for 100% contrail
1016 coverage in a specific location.

1017 Contrail RF comprises both a long-wave (LW) and a short-wave (SW) component, with each
1018 influenced by flight characteristics and the time of day. Unlike the systematic dependency on
1019 optical depth (τ), the relationship between RF and ice water path (IWP) is less consistent (De Leon
1020 et al., 2012; Schumann et al., 2012). The LW RF is positive both day and night, with the largest
1021 impact observed for a cold contrail (located near the tropopause) over a warm, cloud-free Earth
1022 surface. The shortwave radiative forcing (RF) is predominantly negative, with the greatest impact
1023 observed for contrails over darker surfaces, such as cloud-free oceans (Meerkötter et al., 1999).
1024 Studies conducted by Schumann et al. (2012), utilizing both their model and observational
1025 evaluations, suggest the existence of substantial regional RF' values. The calculation of contrail
1026 RF within a global model is contingent on factors such as the representation of contrails, the
1027 atmospheric conditions, and the radiation transfer model employed (Myhre et al., 2009).

1028 While radiative forcing (RF) provides a valuable measure of the impact of contrails on the radiative
1029 balance, it doesn't fully account for the efficacy of different forcing agents in driving surface
1030 temperature changes. Recent studies by Bickel et al. (2020) and Ponater et al. (2021) highlight the
1031 importance of effective radiative forcing (ERF) as a superior metric. ERF considers feedback
1032 mechanisms that can influence the ultimate climate impact of a forcing agent.

1033 In instances of contrail cirrus volumes exhibiting very low ice crystal number concentrations, as
1034 observed in aged contrails associated with heightened ice crystal sedimentation, the deposition of
1035 ice water is constrained, aligning with the depositional growth of ice crystals (Bock and Burkhardt,
1036 2016). In more recent iterations of the model, specifically, ECHAM5-CCMod, Bier and Burkhardt
1037 (2019) incorporated the contrail ice nucleation parameterization proposed by Kärcher et al. (2015).
1038 In their model approach, they suggest that the plume cools over time due to continuous mixing of
1039 the exhaust with ambient air, eventually becoming water-supersaturated when the SAC criterion
1040 is met. The number of activated aerosol particles, stemming from soot and ambient particles, is
1041 computed based on ambient conditions, fuel/engine characteristics, and exhaust particle properties.
1042 Additionally, Bier and Burkhardt (2022) introduced a parameterization for ice crystal loss during
1043 the vortex phase and conducted a thorough evaluation of their model.

1044 Bickel et al. (2020) analyzed the feedback processes and quantified the effective radiative forcing
1045 (ERF) of contrail cirrus, which refers to the cloud formations produced by aircraft engine exhaust.
1046 They highlighted that feedback analysis is a valuable tool for understanding climate sensitivity and
1047 the differences in efficacies between various climate-forcing agents. Previous climate model
1048 simulations have suggested a relatively low efficacy of contrails in forcing global mean surface

1049 temperature changes. They employed a climate model that incorporates a state-of-the-art
 1050 representation of contrail cirrus and conducted the simulations with fixed sea surface temperatures
 1051 to determine the ERF resulting from contrail cirrus.

1052
 1053
 1054

Table 3 Cross-model intercomparison of contrail simulation models

Model Name	Developer	Simulations	Strengths	Weaknesses	Evaluation
CoCiP	DLR	Full life cycle	Efficient computation, considers aircraft/fuel	Simplified mixing, neglects radiation	In-situ measurements, remote sensing data
APCEMM	MIT	Individual microphysics/chemistry	Detailed microphysics	High computational cost, limited global use	Primarily theoretical, limited observations
NASA Global Contrail Model	NASA Ames	Individual formation/transport	Computationally efficient	Neglects downwash, excludes radiative forcing	Reanalysis data
ICON-LEM (Contrail Scheme)	DLR	Contrail formation (regional model)	Considers ice nucleation/survival	Relies on parameterizations, limited microphysics	Satellite data
LES Model	Stanford University	Full life cycle (individual & cirrus)	High-resolution microphysics	Computationally expensive, limited scalability	In-situ measurements
Model Name	Validation Method		Model Uncertainties		
CoCiP	In-situ measurements, remote sensing data		<i>In-situ measurements:</i> May not fully capture contrail variability; calibration and processing uncertainties affect accuracy. <i>Satellite retrievals:</i> Uncertainties in thin contrails; cloud backgrounds can misidentify or underestimate contrails. <i>Data Coverage:</i> CoCiP dataset may not cover all contrail properties, limiting model generalizability.		
APCEMM	Primarily theoretical, limited observations		<i>Validation data:</i> Simplified plume dynamics may not accurately reflect real-world contrail behavior due to limited validation. <i>Parameterization:</i> Uncertainties in microphysical process parameterizations can affect model accuracy.		
NASA Global Contrail Model	Reanalysis data		<i>Reanalysis biases:</i> Temperature and humidity biases in reanalysis data affect contrail formation accuracy. <i>Static atmosphere:</i> Model ignores wind shear and dynamic factors in contrail evolution. <i>Downwash exclusion:</i> Omits ice particle downwash from wake turbulence, impacting contrail properties.		
ICON-LEM (Contrail Scheme)	Satellite data		<i>Satellite retrievals:</i> Cloud backgrounds cause uncertainties in satellite detection and contrail property estimation. <i>Parameterization:</i> Uncertainties in ice nucleation and crystal survival parameterizations affect contrail persistence accuracy.		
LES Model	In-situ measurements		<i>Spatial and temporal coverage:</i> In-situ measurements may miss full variability of contrail properties in large-scale simulations. <i>Computational limits:</i> LES models are expensive, limiting simulation scope and number of contrails, affecting behavior capture. <i>Microphysics schemes:</i> Uncertainties in ice binning and microphysical processes impact contrail microphysics accuracy.		

1055

1056

1057 Bickel et al. (2020) noticed that significant scaling up of aviation density is necessary to obtain
1058 statistically significant results from the simulations. Their study found that the ERF of contrail
1059 cirrus is less than 50% of the respective instantaneous or stratosphere-adjusted radiative forcings.
1060 The best estimate of contrail cirrus ERF is approximately 35%. In comparison, the reduction of
1061 ERF is more substantial for contrail cirrus than for a similar magnitude increase in CO₂
1062 concentrations. They identified the main factor contributing to the reduction in contrail cirrus ERF
1063 as a compensating effect of natural clouds that provide negative feedback. Additionally, they
1064 observed that the combined water vapor and lapse rate adjustment, which affects the distribution
1065 of water vapor in the atmosphere and the lapse rate (temperature decrease with altitude), has a less
1066 positive impact on contrail cirrus ERF compared to the reference case of CO₂ forcing.
1067 Nevertheless, the negative feedback provided by natural clouds has a more pronounced effect in
1068 reducing contrail cirrus ERF compared to these adjustments.

1069 Overall, Bickel et al. (2020) suggested that contrail cirrus has a lower climate impact than initially
1070 thought, with the reduction in ERF attributed to the compensating effect of natural clouds.
1071 Understanding the specific feedback processes and quantifying the ERF of different climate
1072 forcing agents, such as contrail cirrus, is crucial for accurately assessing their contributions to
1073 surface temperature changes and overall climate dynamics.

1074 While radiative forcing (RF) provides a measure of contrail impact on radiative balance, it doesn't
1075 fully account for the efficacy of different forcing agents in driving surface temperature changes.
1076 Recent studies by Ponater et al. (2021) emphasize the importance of effective radiative forcing
1077 (ERF) as a superior metric. ERF considers feedback mechanisms that influence a forcing agent's
1078 ultimate climate impact. Their findings suggest a potentially lower climate impact from contrail
1079 cirrus than previously assumed based on ERF calculations. However, as acknowledged by Ponater
1080 et al. (2021), further research is needed to confirm the efficacy of ERF in assessing the complete
1081 surface temperature response to contrail cirrus. Direct simulations of this response would be
1082 crucial for validating ERF as a reliable metric for contrail cirrus impact.

1083 Similar to findings by Bickel (2023), this study highlights the potential limitations of using RF
1084 alone to estimate contrail cirrus impact. Here, climate model simulations revealed a significant
1085 reduction in the effective radiative forcing (ERF) of contrail cirrus compared to its conventional
1086 RF. This suggests a potentially lower climate impact from contrail cirrus than previously assumed
1087 based solely on RF calculations. The primary contributor to this reduced ERF is likely a negative
1088 cloud adjustment, where contrail cirrus formation leads to a decrease in natural cirrus cover.
1089 Further research is needed to confirm these findings across different climate models and refine our
1090 understanding of contrail cirrus efficacy in driving surface temperature changes.

1091 Long-lasting contrails contribute to global climate change. These contrails can form cirrus clouds,
1092 which are a type of high-altitude cloud that can trap heat in the atmosphere. This trapping of heat
1093 is known as radiative forcing. While the exact contrail contribution to radiative forcing remains
1094 uncertain, it is thought to be a significant factor in climate change (Brasseur et al., 2016). The RF
1095 metric is a backward-looking measure of the effect of emissions on the radiative flux balance and
1096 is commonly used to compare changes in climate forcings (Wuebbles et al., 2010). The RF linked
1097 to non-CO₂ aviation emissions arises from processes occurring over different time scales. Contrails
1098 generally exist for a few hours after an aircraft emissions occur, but other emissions can last much
1099 longer. Effects on the distribution of aerosols and on ozone produced from NO_x emissions can

1100 remain for a few days to months, while changes in CH₄ can be affected for longer than a decade.
1101 The limitations of using RF as a comprehensive metric for global non-CO₂ aviation climate
1102 impacts are well-recognized due to such associated spatiotemporal variations (Wuebbles et al.,
1103 2007). The nonlinear interactions involved make it imprecise to represent the sum of RF for various
1104 non-CO₂ components as a single value. Similarly, distinct climate responses are observed for
1105 different forcing mechanisms.

1106 In 2016, Brasseur et al. investigated the radiative forcing (RF) through analyses involving seven
1107 global models (CAM4, CAM5, IGSM, GISS-E2, GEOSCCM, GATOR-GCMOM, and GEOS-
1108 CHEM) as part of the Federal Aviation Administration's (FAA) Aviation Climate Change
1109 Research Initiative (ACCRI) program. The assessment covered climate impacts for 2006, and the
1110 initial five models projected impacts for 2050 scenarios, specifically focusing on selected aircraft
1111 emission components. In a separate study, Chen and Gettelman (2016) used the CAM5 model to
1112 estimate RF for contrails and contrail cirrus in the 2050 future scenario, employing the 2006 AEDT
1113 dataset. Notably, the research highlighted the tendency to overestimate global linear contrail (LC)
1114 net RF when using the natural ice cloud optical property parameterization as a stand-in for contrail
1115 counterparts in modeling studies. Furthermore, the distribution of regional RF indicated that in
1116 densely trafficked airspaces, such as the United States, RF could be up to ten times higher than the
1117 global average (Brasseur et al., 2016).

1118 Schumann and Graf (2013) determined a more significant AIC impact by using both observational
1119 data and the contrail cirrus prediction model (CoCiP; Schumann, 2012). They found an "aviation
1120 fingerprint" ascribed to a daily air traffic cycle within the diurnal cycle of cirrus properties in the
1121 North Atlantic region (NAR), associating with the annual mean diurnal patterns of cirrus cover
1122 and outgoing longwave radiation (OLR) derived from Meteosat data (Graf et al., 2012).

1123 Figure 12 shows the global average annual radiative forcing (RF) values and uncertainty ranges
1124 for persistent contrails alone and together with contrail cirrus. The values are compiled from
1125 selected studies and assessments published since 1999 and include a recent development by
1126 Kärcher (2018). Over time, early assessments of contrail RF have been confirmed and the range
1127 of uncertainty has been narrowed down considerably.

1128 The figure shows that the RF due to persistent contrails alone is -0.01 W/m² (with an uncertainty
1129 range of 0.005-0.03 W/m²), and the RF due to persistent contrails together with contrail cirrus is
1130 ~0.05 W/m² (with an uncertainty range of 0.02-0.15 W/m²). (Kärcher, 2018). Figure. 12 shows
1131 that analyses accounting only for linear contrails underestimate the total RF for contrails. More
1132 recent analyses tend to show an overall warming of around ~45mWm⁻² (Bier and Burkhardt, 2022).

1133 The models applied by DLR and NCAR's groups are summarized in Table 4 (updated from. Bock
1134 and Burkhardt, 2016). Bock and Burkhardt (2016) evaluated the year 2002 using the AERO2k
1135 inventory and for year 2006 using the AEDT 2006 slant distance inventory. The corrected NCAR
1136 analyses and their more recent results are consistent with those from the DLR modeling studies
1137 (Lee et al., 2021). These findings further amplify the conclusions from Fig. 12.

1138

1139
 1140
 1141
 1142
 1143
 1144
 1145
 1146
 1147
 1148
 1149
 1150
 1151
 1152
 1153
 1154
 1155
 1156
 1157
 1158
 1159
 1160
 1161
 1162
 1163
 1164
 1165
 1166
 1167
 1168
 1169
 1170
 1171
 1172
 1173
 1174
 1175

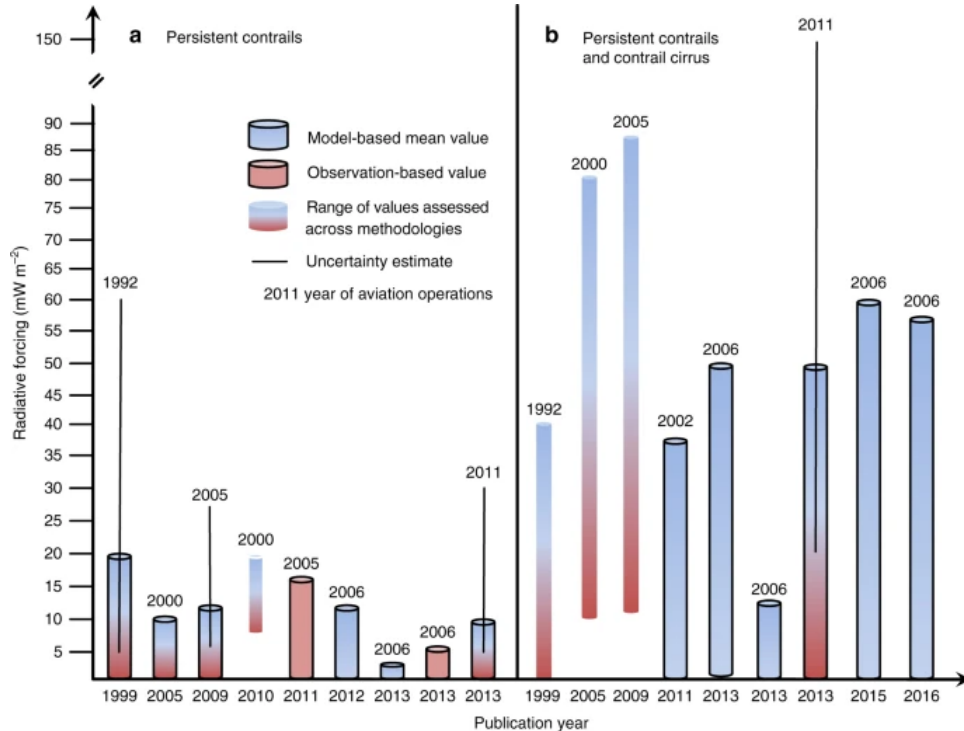


Figure 12. Global annual average amount of radiative forcing caused by aircraft-induced clouds
 Figure adapted with permission from Kärcher (2018). (Licensed under CC BY 4.0)

4.2 Future RF projections

4.2.1 DLR’s study for future RF projections

Bock and Burkhardt (2019) investigated how changes in air traffic between 2006 and 2050, including both volume increase and upward shift in flight altitudes (0.3-1.5 km), would impact contrail cirrus properties and radiative forcing. Table 5 shows their simulations considering this combined scenario. It projects a fourfold increase in air traffic and a maximum flight density at a lower altitude (200 hPa in 2050 compared to 240 hPa in 2006), which has climate implications.

In Table 5, the air traffic distance is specified as the ground-projected track distance. The coverage is sketched out for all contrail cirrus, and the visibility of contrail cirrus (visible optical depth > 0.05) is indicated in brackets (Bock and Burkhardt, 2016). Radiative forcing estimates exist for both track distance and slant distance within brackets (Table 5). Remarkably, Bock and Burkhardt (2019) determined that the projected future increase in air traffic, coupled with a minor shift to higher altitudes, outcomes in a substantial rise in contrail cirrus coverage, optical depth, and radiative forcing. Particularly, air traffic contrail cirrus radiative forcing is estimated to increase threefold, from 49 to 159 mW m⁻² (Fig. 13). The findings are a result of a future air traffic inventory, where the measurement of air traffic is signified in terms of track distance (ground projected) rather than slant distance (3-D). Declining the initial contrail ice particle number by 50% results in a substantial drop in the climate impact of contrail cirrus, leading to a global decline in radiative forcing for the year 2050. The reduction is significant, amounting to a 14% reduction from 160 to 137 mWm⁻² (Fig. 13).

1176 **Table 4.** Summary of existing contrail cirrus simulations and RF from the DLR and NCAR
 1177 models. Adapted from of Bock and Burkhardt (2016).
 1178

Model	Inventory	Flight distance	RF (mW/m ²)	References
ECHAM5-CCMod	AERO2k 2002	track	35	<i>Burkhardt and Kärcher (2011)</i>
ECHAM5-CCMod	AEDT 2006	track	49	
ECHAM5-CCMod	AEDT 2006	slant	56	
ECHAM4-CCMod	AERO2k 2002	track	38	
ECHAM4-CCMod	REACT4C 2006	track	45	<i>Schumann et al. (2015)</i>
COClP	AEDT 2006	flight vectors	63	<i>Schumann et al. (2015)</i>
CAM5	AEDT 2006	slant	13 (57)*	<i>Chen and Gettelman (2013)</i>
CAM6	AEDT 2006	slant	62 (ERF)**	<i>Gettelman et al. (2021)</i>

* The approximation of Chen and Gettelman (2013) was revised.

**ERF (the scaling technique was derived from Lee et al.2021 for 2006 to 2018 and then 9% per year scaled (2018 to 2019) by Gettelman et al. (2021)

AERO2k – Global aircraft emissions data project for climate impacts evaluation

AEDT- Aviation Environmental Design Tool

REACT4C- Reducing Emissions from Aviation by Changing Trajectories for the benefit of Climate

1179

1180 4.2.2 RF projections from the NCAR model

1181 The study conducted by Chen and Gettelman (2016) investigated the radiative forcing curbing
 1182 from aviation-induced cloudiness, using the Community Atmosphere Model Version 5 (CAM5)
 1183 for both present (2006) and future (up to 2050) scenarios. The researchers found a projected four-
 1184 fold increase in global flight distance from 2006 to 2050. Despite this, the simulated radiative
 1185 forcing from contrail cirrus in 2050 is predicted to reach 87 mWm⁻², representing a seven-fold rise
 1186 compared to 2006. This underlines a non-linear correlation between radiative forcing and fuel
 1187 emission mass, accredited to non-uniform regional escalations in air traffic and changes in contrail
 1188 radiative forcing sensitivity through different regions.

1189 The CAM5 simulations also indicate that the negative radiative forcing resulting from the indirect
 1190 effect of aviation sulfate aerosols on liquid clouds in 2050 could be as large as -160 mWm⁻², a
 1191 four-fold increase from 2006. Consequently, when considering both aviation aerosols and contrail
 1192 cirrus, the total radiative forcing in 2050 could possibly employ a cooling impact on the planet.
 1193 Aerosols, particularly aviation sulfate aerosols distributed at cruise altitudes, may be transferred
 1194 to the lower troposphere. This procedure raises aerosol concentrations and consequently enhances
 1195 the cloud drop number concentration and persistence of low-level clouds. On the other hand, the
 1196 study suggests that aviation black carbon aerosols have an insignificant net forcing affect globally,
 1197 both in 2006 and 2050.

1198 The researchers focus on specific regions, for instance, Central Europe, eastern North America,
 1199 and East Asia, and recommend quantitative evaluations of the forcing in each region for several
 1200 scenarios. For example, in Central Europe, the predicted contrail cirrus radiative forcing in 2050
 1201 is anticipated to locally peak at 2 Wm⁻², marking a 2 to 3-fold increase compared to 2006. In the
 1202 eastern United States, the contrail cirrus radiative forcing could reach 800 mWm⁻² in 2050,
 1203 revealing a higher percentage increase compared to 2006. The most prominent rise in contrail

1204 cirrus radiative forcing is estimated in East Asia, where a 6-fold increase is projected for 2050,
 1205 associated with the region's anticipated significant rise in consumption of aviation fuel.

1206 **Table 5.** Overview of the model simulations: Air traffic distance exists as ground-projected track
 1207 distance. Coverage is furnished for all contrail cirrus, with coverage for visible contrail cirrus
 1208 (visible optical depth > 0.05) shown in brackets (Bock and Burkhardt, 2016). The radiative
 1209 forcing is represented for both track distance and slant distance, with values enclosed in brackets.
 1210 (Adapted from Bock and Burkhardt (2019))

Background	Inventory	Air traffic volume (km yr ⁻¹)	Propulsion efficiency	Initial ice number concentration (cm ⁻³)	Coverage (%)	RF (mW m ⁻²)
2006	2006	3.7 × 10 ¹⁰	0.3	150	1.1 (0.7)	49 (56)
2006	2050 Baseline	15.4 × 10 ¹⁰	0.3	150	2.9 (2.0)	159 (182*)
2050 (RCP6)	2050 Baseline	15.4 × 10 ¹⁰	0.3	150	2.8 (2.0)	160 (183*)
2050 (RCP6)	2050 Scenario1	15.4 × 10 ¹⁰	0.42	75	2.98(1.7)	137 (157*)

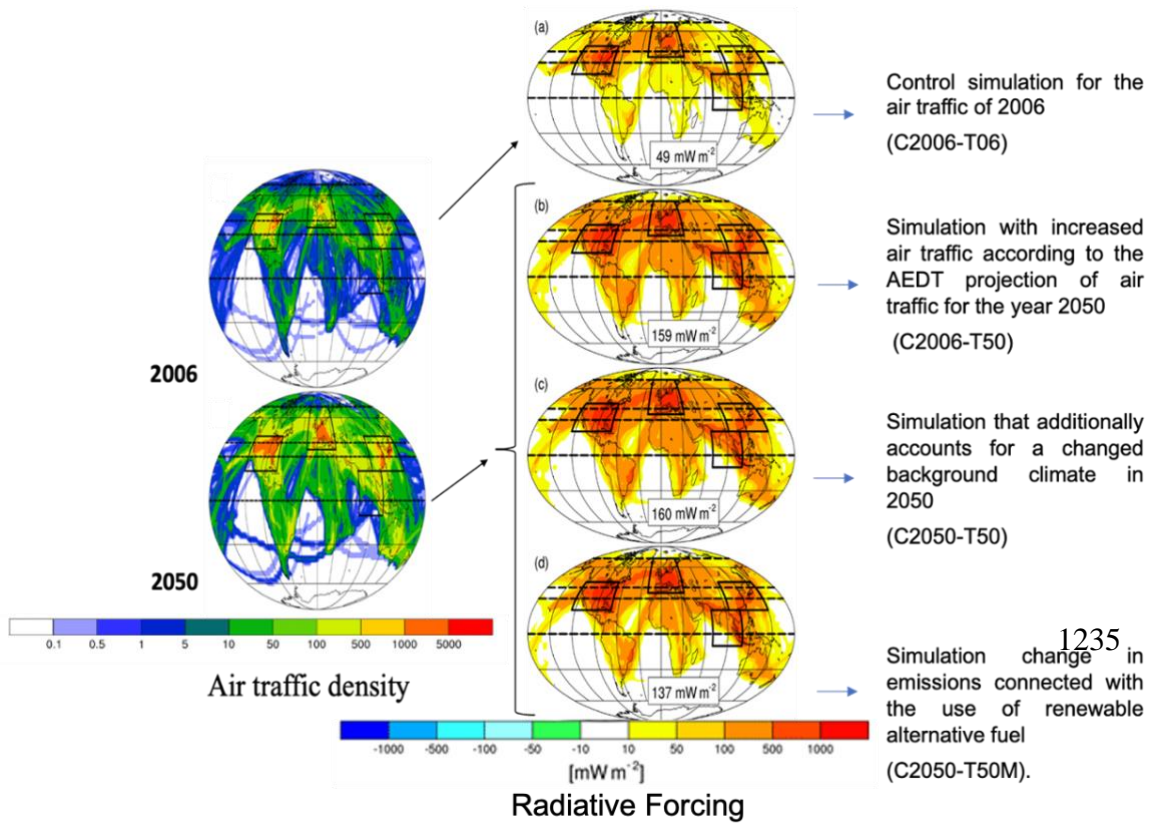
RCP6-Representative Concentration Pathway 6.0

*Asterisks denote extrapolated values resultant from the factor resolute by the radiative forcing in 2006, which is connected to air traffic volume and computed using slant distance and track distance (Bock and Burkhardt, 2016).

1211 The inclusion of aviation aerosols in the simulations suggests a slight reduction in positive forcing
 1212 over land, as compared to the forcing solely caused by contrail cirrus. On the other hand, over the
 1213 ocean, a negative forcing rising from aviation emissions is measured. This can be accredited to the
 1214 lower surface albedo and cleaner environment (fewer aerosols) in comparison to land areas. In the
 1215 three regions with the highest projected air traffic in 2050 (eastern United States, Central Europe,
 1216 and East Asia), aviation aerosols reduce the regionally averaged positive radiative forcing induced
 1217 by contrail cirrus by approximately 50%, as indicated by the blue boxes in Fig. 14. The peak
 1218 positive forcing within each of these regions is also reduced by 50% due to aviation aerosols. The
 1219 study provides detailed regional estimates of these effects (Table 6).

1220 The negative radiative forcing result from aviation aerosols, as detected in this study, supports the
 1221 inferences represented by Righi et al. (2013). The extent of the cooling effect is estimated to be
 1222 affected by the background cloud drop number concentration.

1223
 1224
 1225
 1226
 1227
 1228
 1229
 1230
 1231
 1232
 1233
 1234
 1236
 1237
 1238
 1239

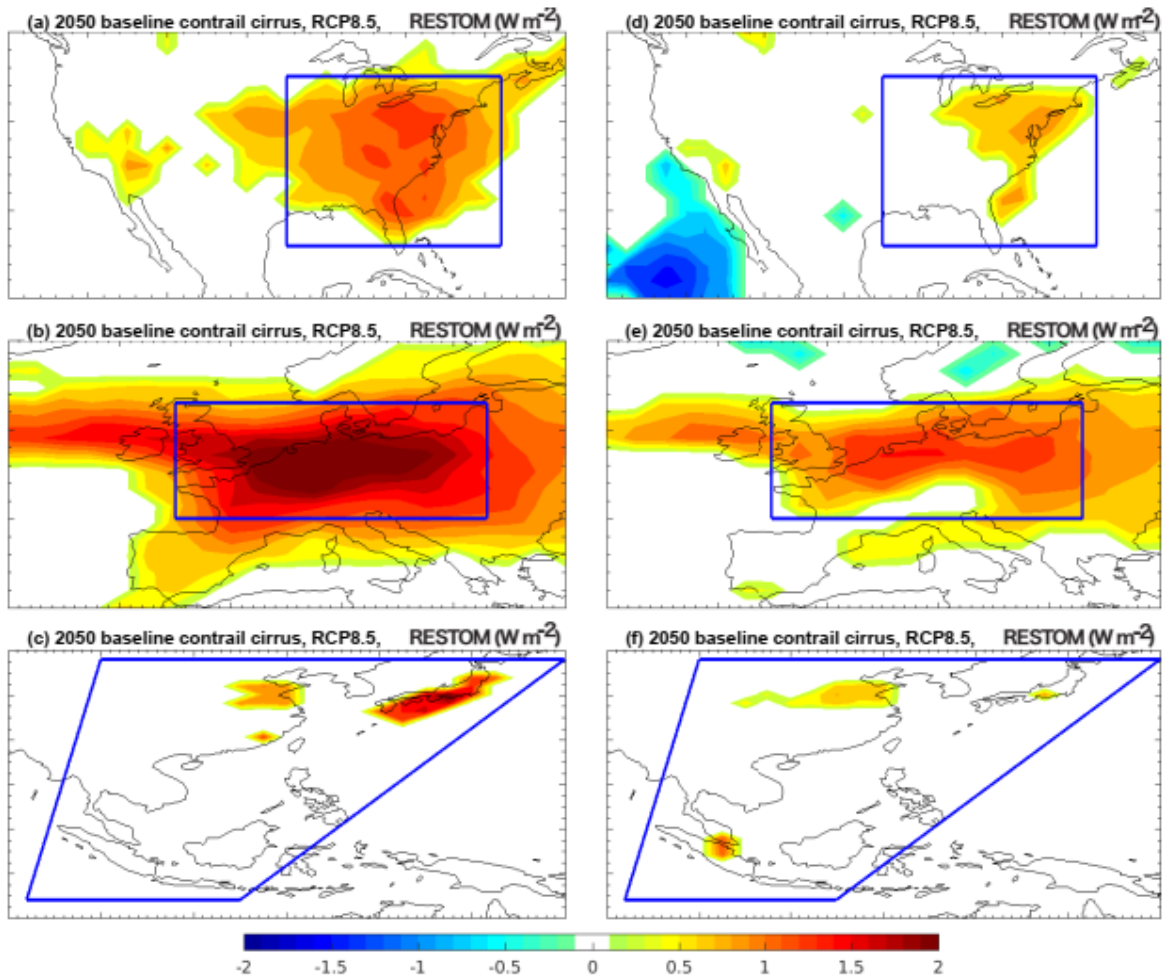


1240 **Figure 13.** The horizontal distribution depicts the vertically incorporated air traffic density ($\text{km m}^{-2}\text{s}^{-1}$) for the years 2006 and 2050, along with the radiative forcing in scenarios C2006-T06 (a),
 1241 C2006-T50 (b), C2050-T50 (c), and C2050-T50M (d) Figure adapted with permission from Bock
 1242 and Burkhardt (2019). (Licensed under CC BY 4.0).
 1243

1244 **Table 6.** Radiative forcing (mWm^{-2}) attributed to aviation H_2O emissions, with uncertainties
 1245 derived from 2 standard deviations of the four-member ensemble. (Adapted from Chen and
 1246 Gettelman, 2016)

Meteorology	Scenario	Global	North America	Central Europe	East Asia
Present	2006 AIR	12 ± 4	195 ± 30	483 ± 69	41 ± 8
2050 RCP4.5	2050 BL	87 ± 6	798 ± 152	1682 ± 535	272 ± 39
2050 RCP4.5	2050 SC1	76 ± 7	724 ± 136	1568 ± 489	231 ± 36
2050 RCP4.5	2050 SC2	76 ± 7	724 ± 136	1568 ± 489	231 ± 36
2050 RCP4.5	2050 SC3	80	681	1952	213
2050 RCP8.5	2050 BL	83 ± 3	852 ± 92	1558 ± 226	248 ± 25
2050 RCP8.5	2050 SC1	73 ± 4	777 ± 96	1442 ± 235	211 ± 24
2050 RCP8.5	2050 SC2	73 ± 4	777 ± 96	1442 ± 235	211 ± 24
2050 RCP8.5	2050 SC3	75	865	1597	221

1247 RCP4.5-Representative Concentration Pathway 4.5
 1248 RCP8.5 -Representative Concentration Pathway 8.5. BL-Base line
 1249 SC1, SC2, and SC3- Scenarios 1, 2 and 3



1250

1251 **Figure 14.** Ensemble of the average regional radiative forcing in Wm⁻², utilizing the baseline
 1252 emission scenario for the year 2050 with RCP8.5 meteorology, focusing on contrail cirrus alone
 1253 (a–c) and contrail cirrus combined with aviation aerosols (d–f). The term "RESTOM" represents
 1254 the alteration in the net residual radiative flux at the top of the model. The plot includes only
 1255 ensemble-mean perturbations that surpass 2 standard deviations of the averaged control
 1256 simulations. (Figure adopted with permission from Chen and Gettelman, 2016) (Licensed under
 1257 CC BY 4.0)

1258 4.3 Issues representing cloud-contrail and contrail-contrail overlaps in modeling studies

1259 A thorough examination of past methodologies for modeling cloud layer overlaps and several
 1260 modeling studies recommends that overlapping with other cloud layers is prone to reduce both the
 1261 shortwave (cooling) and longwave (warming) radiative forcing linked to contrails (Sanz-Morère
 1262 et al., 2021). However, there is inadequate agreement on how the overlap between clouds and
 1263 contrails might modify the net radiative forcing due to uncertainties regarding whether it would
 1264 more strongly mitigate the shortwave or longwave components. Particularly, the precise impact of
 1265 contrail-contrail overlap on global contrail radiative forcing has yet to be measured. In this section,
 1266 we review previous literature referring to the treatment of multiple-layer overlap in the context of
 1267 contrail radiative forcing calculations.

1268 Schumann et al. (2012) determined that the net radiative forcing may augment if contrails overlap
 1269 with low-level clouds but could go through significant variations when passing under natural cirrus
 1270 clouds. This underscores the significance of precisely modeling natural clouds in contrail
 1271 simulations. Nevertheless, when utilizing this method to simulate single contrails, accounting for
 1272 the radiative interactions among multiple contrails turns into a challenging task. In prior examples
 1273 of modeling contrail-contrail overlap, when simulating contrails in global climate models, various
 1274 treatments have been utilized, as outlined in. Contrail parametrizations have been formulated for
 1275 ECHAM4 (Ponater et al., 2002; Burkhardt and Kärcher, 2009), where maximum-random overlap
 1276 is presumed between contrail and cloud layers, as well as among different contrails (Burkhardt and
 1277 Kärcher, 2011; Marquart et al., 2003; Bock and Burkhardt, 2016; Frömming et al., 2011). Rädels
 1278 and Shine (2008) and Rap et al. (2010) also use this parameterization, calibrating the outcomes by
 1279 using satellite observations. Table 7 summarizes the existing methods for modeling contrail-
 1280 contrail overlaps.

1281
 1282 **Table 7.** Existing methods for modeling contrail-contrail overlap when estimating global contrail
 1283 RF. MRO: maximum-random overlap, defined by Geleyn and Hollingsworth (1978) as assuming
 1284 that clouds in adjacent layers maximally overlap, while clouds separated by one or more clear
 1285 layers randomly overlap (Adapted from Sanz-Morère et al. 2021).

Source	Model used to represent contrail-contrail overlap
Minnis et al. (1999)	No overlap considered (fractional coverage from observations)
Marquart et al. (2003)	MRO in the vertical for each column
Rädels and Shine (2008)	Random overlap
Rap et al. (2010)	Random overlap
Frömming et al. (2011)	MRO in the vertical for each column
Burkhardt and Kärcher (2011)	MRO in the vertical for each column
Chen and Gettelman (2013)	Zero contrail-contrail overlap in grid box
Schumann and Graf. (2013)	Linear RF addition
Bock and Burkhardt (2016)	MRO in the vertical for each column

1286
 1287 Chen and Gettelman (2013) included contrails in the CAM5 model by portraying them as an
 1288 increase in the 3-D cloud fraction, where the model presumes maximum-random overlap.
 1289 Nevertheless, in their method, they considered zero overlaps between newly formed contrails when
 1290 placed at the same vertical level (approximately 1 km). Finally, the CoCiP Lagrangian contrail
 1291 model (Schumann, 2012) reports contrail-contrail overlaps indirectly by linearly summing the
 1292 radiative forcing of all contrails, taking into consideration any observed cirrus present above the
 1293 simulated contrail. Nonetheless, this method does not clearly consider the overlap between
 1294 simulated contrails. Inconsistencies rise in how contrail-contrail overlaps are modeled across
 1295 various studies. The most efficient approach remains uncertain, and as of now, no analysis has
 1296 measured the impact of contrail-contrail overlaps on global contrail RF. Since further expansion
 1297 of the aviation sector is expected, it is anticipated that an increased number of instances of contrail
 1298 overlap will occur. Hence, a more inclusive understanding of the degree and dynamics of contrail-
 1299 contrail overlap is a necessity. Table 8 summarizes the agreement and disagreement between
 1300 climate models on contrail cirrus radiative forcing.

1301 **5 Observation Datasets for Contrail Studies**

1302 The vast majority of observations, comprised of airborne, satellite, and ground-based approaches,
1303 encompass jet aircraft exhaust contrails from 1972 onward. Nevertheless, it is remarkable that
1304 records of contrail observations date back to as early as 1915, as published by Ettenreich in 1919.

1305 Early measurements performed behind a propeller-driven aircraft offered data supporting the
1306 concept that contrail ice formation requires liquid saturation to originate, associating with the
1307 Schmidt-Appleman criterion that is now well-established (Schmidt, 1941, Appleman, 1953 and
1308 Schumann, 1996.). These remarks, which encompassed the collection of ice particles on impactors
1309 and halo observations, also furnished initial insights into the size and shape of both contrail and
1310 cirrus ice particles (Weickmann, 1945).

1311 The precise testing of models necessitates reliable quantitative data, covering not only information
1312 on contrail and plume properties but also on contrail age, the generating aircraft, atmospheric
1313 conditions during contrail formation, and the observational methods employed (Schumann et al.,
1314 2017). Mean properties of individual contrails are characterized for a wide range of jet aircraft as
1315 a function of age during their life cycle from seconds to 11.5 h (7.4-18.7 km altitude, -88 to -31°C
1316 ambient temperature), based on a compilation of about 230 in-situ and remote sensing
1317 measurements (Schumann et al., 2017). Contrails from individual aircraft can remain visible for
1318 extended periods, as reported in analyses by Minnis et al. 1998, 2013) and Vázquez-Navarro et al.
1319 (2015). Schumann et al. (2017) furnished a brief description of individual datasets, integrating new
1320 analyses for their study, and combined them to create a "contrail library" (COLI). This dataset was
1321 then compared with the outcomes of the Contrail Cirrus Prediction (CoCiP) model. The
1322 observations corroborate that the quantity of ice particles in contrails is controlled by both the
1323 engine exhaust and the formation process in the jet phase. Some particle losses ensue in the wake
1324 vortex phase, with succeeding gradually diminishes over time.

1325 Publicly available air traffic data are usually limited, but certain projects have gathered flight data
1326 from sources such as air traffic control or ground-based observations (Schumann et al., 2013;
1327 Schumann et al., 2017). Distinguishable projects with air traffic subsets since 2005 are accredited.
1328 Garber et al. (2005) compiled traffic data for the United States and southern Canada for the years
1329 2000-2005. In Germany, the Deutsche Flugsicherung (DFS) has been gathering and filing away
1330 traffic data from 2006 onwards for more new projects. The Aviation and Climate Change Research
1331 Initiative (ACCRI; Basseur et al., 2016) furnished a global waypoint dataset for the year 2006 to
1332 researchers included in the ACCRI project.

1333 The existing observation datasets on contrail properties and formation conditions are constantly
1334 expanding with the inclusion of innovative resources. The recently developed Global Aviation
1335 Emissions Inventory based on ADS-B (GAIA) (Teoh et al., 2024). leverages historical flight paths
1336 derived from Automatic Dependent Surveillance-Broadcast (ADS-B) technology, coupled with
1337 reanalyzed weather data from 2019 to 2021. GAIA paints a detailed picture of global aviation
1338 activity, encompassing the spatial and temporal variations in flight patterns, fuel consumption, and
1339 emissions of key pollutants like CO₂, NO_x, and particulate matter. This information proves
1340 particularly valuable for contrail research by offering insights into the connections between aircraft
1341 types, flight routes, and the potential for contrail formation in diverse regions. For example, by
1342 analyzing short-haul versus long-haul flight emissions within GAIA, researchers can glean insights
1343 into the contribution of various aircraft categories to contrail formation patterns across different
1344 geographical areas.

1345
1346
1347
1348

Table 8 . Agreement and disagreement between climate models on contrail cirrus radiative forcing. (The models discussed include CoCiP, ECHAM5-HAM, CAM6, and the Stanford Global Model. Detailed descriptions of these models can be found in Sections 3.2.1 through 3.2.4).

Aspect	Agreement	Disagreement	Potential Causes	Recommendations for Future Research
Net Radiative Forcing (RF)	Likely positive net RF, signifying warming			
Longwave vs. Shortwave RF		Models show some variation in the relative contribution of longwave (warming) and shortwave (cooling) components to the net RF depending on factors like ice crystal shape and optical depth.	Complexity of ice crystal parameterizations Treatment of solar radiation transfer	Improve ice crystal parameterizations in models to better capture the variation in radiative properties. Conduct studies to refine the treatment of solar radiation transfer in contrail simulations.
Regional Variations	Models concur on significant regional variations in RF			
High-traffic vs. Low-traffic areas		Models show discrepancies in the magnitude of the regional variations.	Input data on air traffic patterns	Improve the quality and resolution of air traffic data used in climate models.
Future RF Projections	Models predict a significant increase in contrail cirrus RF by 2050 due to rising air traffic and flight altitude			
Impact of aviation aerosols		Models show variations in the projected net effect (warming vs. cooling) due to the counteracting impact of aviation aerosols on low-level clouds.	Uncertainties in how models represent aviation aerosol properties and their interactions with clouds.	Conduct dedicated studies to improve the representation of aviation aerosols and their interactions with clouds in climate models.
Cloud Overlap	Overlap with other clouds (natural cirrus, low-level clouds) can affect RF, but the extent of impact (shortwave vs. longwave dominance) is uncertain.	Contrail-contrail overlap is not well understood and might be more frequent in the future.	Need for a better understanding of cloud-contrail and contrail-contrail overlap and their impact on global RF.	Develop improved methods for simulating cloud-contrail and contrail-contrail overlap in climate models. Conduct observational studies to quantify the frequency and radiative effects of contrail overlap.

- *CoCiP*: Agreements on overall contrail effects, but some discrepancies in initial ice crystal formation.
- *ECHAM5-HAM*: Captures basic contrail formation but has different ice crystal properties affecting long-term impacts.
- *CAM6*: Aligns with others in radiative forcing but shows minor differences in contrail-induced cloud changes.
- *Stanford Global Model*: Agrees on initial formation but has contrasting plume mixing and microphysical schemes leading to varied impact predictions.

1349 By seamlessly integrating GAIA with existing observation datasets like COLI (Schumann et al.,
1350 2017), researchers can cultivate a more nuanced understanding of the interplay between aviation
1351 activity, atmospheric conditions, and contrail occurrence. This enhanced knowledge ultimately
1352 empowers the improvement of contrail prediction models and informs strategies to mitigate their
1353 impact on climate.

1354 Particulars about aircraft assets, including size, mass, speed, fuel consumption, and propulsion
1355 efficiency, were tracked from various references, including the BADA (EUROCONTROL, 2009).
1356 Added engine properties, such as fuel consumption and emissions at surface pressure, can be
1357 attained from the ICAO Aircraft Engine Emissions Databank (EASA, 2023) and the 2006 AEDT
1358 emissions inventory (Barrett, 2010; Wilkerson, 2010).

1359 Poll (2018) devised a straightforward model to estimate fuel burn for commercial aircraft, offering
1360 a transparent, publicly accessible option apart from the BADA and PIANO codes (Piano-X,
1361 software, Lissys Ltd., 2008)). Utilizing this method necessitates understanding the Mach number
1362 and flight level where an aircraft, under specific conditions, achieves its absolute minimum fuel
1363 burn rate. Yet, acquiring this data proves challenging, although an initial effort is outlined in Poll
1364 and Schumann (Poll, 2018), where input files are supplied for 53 aircraft types.

1365 Two sets of observational-based capabilities exist that can provide the coverage needed to help
1366 evaluate the global modeling analyses for treating the effects of contrails, the Contrail Library
1367 (COLI) and the satellite-based record. The Contrail Library results are useful for evaluating limited
1368 areas of contrails but not for global analyses.

1369 **5.1 Contrail Library (COLI)**

1370 The COLI database includes 236 entries describing properties of contrails with known ages,
1371 including mean data for one hundred cases of in-situ measurements, more than 70 cases from
1372 ground-based and airborne lidar observations, 50 cases from satellites, and a few camera
1373 observations. The data come from 33 observation projects during the last 45 years. The comparison
1374 of the data from various measurements shows notable differences among the various instruments
1375 utilized across the dataset. Nevertheless, a notable accord endures among each approach, as well
1376 as uniformity between in-situ and remote sensing results, along with agreement with Schumann et
1377 al (2017) model outcomes. Moreover, in-situ data resultant from contrail measurements, the
1378 investigation integrates remote sensing data found from ground-based or airborne lidar and
1379 spectroradiometer, satellites, cameras, and visual interpretations. Table 9 summarizes some of the
1380 projects that contributed to the COLI database, including the aircraft used and the primary location,
1381 the mode of reference, and the primary reference of the study.

1382 Accurate forecasting of contrail occurrence and persistence holds significant importance in
1383 addressing their potential climate impact. For this purpose, research conducted by Gierens et al.
1384 (2020) underscores the limitations of reanalysis data, primarily due to their coarse vertical
1385 resolution. This study shows the necessity for high-resolution observational data, especially
1386 concerning temperature and relative humidity in the upper troposphere and tropopause region, to
1387 understand contrail formation and behavior better. Initiatives such as the In-service Aircraft for a
1388 Global Observing System (IAGOS) (Gierens et al., 2020) are pivotal in providing such data by
1389 utilizing advanced instruments installed on passenger aircraft. The assessment of contrail
1390 formation models demands dependable data encompassing both contrail characteristics and
1391 atmospheric conditions during their formation. While the study by (Gierens et al., 2020) evaluates
1392 the predictability of contrails using the Schmidt-Appleman criterion based on reanalysis data, it

1393 underscores the critical role of high-resolution data in assessing more advanced contrail prediction
1394 models. The availability of observational datasets containing parameters such as temperature,
1395 relative humidity, and air traffic data, as discussed in this section, is indispensable for such model
1396 assessments.
1397

1398 **5.2 Satellite-based datasets**

1399 Over the past two decades, the detection of contrail in satellite imagery has primarily depended on
1400 the algorithm developed by Mannstein et al. (2003) (e.g., Palikonda et al., 2005; Vazquez-Navarro
1401 et al., 2010). This algorithm contains a series of convolution and thresholding operations related
1402 to brightness temperature images and, subsequently the detection of linear associated components
1403 of fitting size. While the algorithm has been fine-tuned to attain either high precision or high
1404 remembrance in contrail detections, no single model has simultaneously surpassed in both aspects.
1405 Subsequently, empirical observations of contrail coverage often need broad lower-bound/upper-
1406 bound approaches (Duda et al., 2013). Minnis et al. (2013) reported the properties of contrail cirrus
1407 clouds formed during 11 different contrail outbreaks, in the context of objectively determined
1408 linear contrails and their properties. It was observed that the ratio of contrail cirrus to linear
1409 contrails is substantially affected by the satellite analysis algorithm utilized to allocate linear
1410 contrails. Furthermore, this ratio seems to be affected by the presence of overlapping contrails,
1411 which can obscure individual contrails.

1412 The contrail cirrus optical depths were found to be 2-3 times greater than their linear contrail
1413 counterparts and the associated ice crystal particle diameters were 20% greater than the contrail
1414 particle sizes. The analyses of such satellite datasets are likely to be useful for evaluating global
1415 models of contrail radiative effects.

1416 An exception to the application of the Mannstein et al. (2013) algorithm is prominent in Kulik
1417 (2019) and Meijer et al. (2021). These analyses employed a deep learning model for pixel-level
1418 contrail detection using GOES-16 satellite imagery. Upon detecting a contrail, these studies
1419 facilitate the assessment of its lifetime impact and the ascription of potentially relevant flights
1420 (Vazquez-Navarro et al., 2010; Vazquez-Navarro et al., 2013; Vazquez-Navarro et al., 2015.
1421 Mutually, these practices furnish a means to evaluate the efficacy of flight diversions in avoiding
1422 contrail formations. McCloskey et al. (2021) officially released the first large dataset of pixel-level
1423 contrail locations in Landsat-8 satellite imagery labeled by humans. Labelers should be able to
1424 accurately differentiate contrails from naturally occurring cirrus due to Landsat-8's high spatial
1425 resolution and the advected flight history information provided. This dataset will be useful in
1426 benchmarking contrail detection models and validating contrail research in collocated
1427 geostationary satellite imagery.

1428 Satellite-based datasets offer valuable insights into global contrail occurrence and variability,
1429 although challenges arise when estimating contrail radiative forcing. Retrieving contrail optical
1430 thickness, a crucial parameter for such calculations, from current satellite observations, is
1431 particularly difficult. Moreover, distinguishing contrails from overlapping features and natural
1432 cirrus clouds remains challenging, especially with limited spatial resolution. Addressing these
1433 challenges is essential for enhancing the contribution of satellite observations to contrail radiative
1434 forcing estimations. Advancements in retrieval algorithms for contrail optical thickness and
1435 methods to differentiate contrails from overlapping features are necessary for more accurate
1436 assessments.

1437

1438 Despite these challenges, satellite-based contrail datasets have significant potential for monitoring
 1439 contrail occurrence and coverage over time. This information is valuable for evaluating the
 1440 effectiveness of flight diversion strategies aimed at minimizing contrail formation. Furthermore,
 1441 the emergence of human-labeled contrail datasets like McCloskey et al. (2021) provides a valuable
 1442 resource for training and validating future advancements in contrail detection using deep learning
 1443 and machine learning algorithms. Continuous collaboration among satellite data providers,
 1444 atmospheric scientists, and AI researchers is vital for realizing the full potential of satellite-based
 1445 contrail datasets for contrail mitigation and climate impact assessments.

1446

1447 Ng et al. (2023) presented a human-labeled dataset named open contrails to train and evaluate
 1448 contrail detection models based on GOES-16 Advanced Baseline Imager (ABI) data. Ng et al.
 1449 (2023) proposed and evaluated a contrail detection model that incorporates temporal context for
 1450 improved detection accuracy. The human-labeled dataset and the contrail detection outputs are
 1451 publicly available on Google Cloud Storage at gs://goes_contrails_dataset.

1452 Persuading policymakers and airlines about the climate benefits of flight diversions becomes more
 1453 reasonable with the availability of satellite corroboration capabilities. Geostationary satellites like
 1454 GOES-16 and low-earth orbit satellites such as Landsat-8 present both complementary strengths
 1455 and weaknesses when employed for the task of contrail detection (i.e., coverage versus persistence
 1456 of the observations). An automated contrail detection system is essential for developing and
 1457 evaluating contrail avoidance systems. Deep neural networks can be employed as an automated
 1458 contrail detection system, a form of artificial intelligence (AI) and machine learning (ML), that
 1459 has been advanced to connect and categorize contrails in satellite imagery or other relevant data
 1460 sources. This system can effectively analyze complex patterns and features associated with
 1461 contrails, by leveraging the competencies of deep neural networks. By utilizing deep neural
 1462 networks and machine learning techniques, the automated contrail detection system offers an
 1463 efficient and reliable solution for detecting and monitoring contrails, facilitating further research
 1464 and analysis of their impact on climate and aviation.

1465 **Table 9.** Observations from the year 2000 to 2014 were incorporated into the COLI for the study
 1466 of contrail (Adapted from Schumann et al. 2016).

Year	Project name	Source aircraft	Carrier/location	Measurement	Reference
2000	Cluster	airliners	Great Lakes	satellite	Duda et al.,(2004)
2001	Shutdown	B747+C fighters	Northwestern USA	satellites	Minnis et al.,(2002)
2002	CRYSTAL-FACE	WB-57	NASA WB-57	in situ	Gao et al.,(2006)
2003	Fallstreaks 2003	airliners	Goddard	lidar	Atlas and Wang (2010)
2005	PAZI-2	airliners	DLR Falcon	in situ	Febvre et al.,(2009)
2006	CR-AVE	WB-57	NASA WB-57	in situ	Flores et al.,(2006)
2008	CONCERT	airliners	DLR Falcon	in situ	Voigt et al.,(2010)
2008	ACTA	airliners	Europe andNorth Atlantic	satellite	Vázquez-Navarro et al.,(2015)
2011	CONCERT2011	airliners	DLR Falcon	in situ	Kaufmann et al.,(2014)
2011	COSIC	Bae 146	FAAM Bae-146	in situ	Jones et al.,(2012)
2012	Cameras	airliners	Munich	cameras	Schumann et al.,(2013)
2014	ML-CIRRUS	B772 or F900	HALO	in situ	Voigt et al.,(2016)

1467

1468 Siddiqui (2020) conducted a study where a neural network was used to distinguish contrail cirrus
1469 clouds from regular cirrus clouds on TSI images. The study found that the neural network
1470 triumphed with a high accuracy of 98.5% on the validation set, implying that the model was able
1471 to learn significant visual features of contrails that differentiate them from regular cirrus clouds.
1472 The success of this model opens various practical applications for studying contrails. For instance,
1473 the model can be used to analyze images from different months of data, agreeing for researchers
1474 to investigate the frequencies of contrail occurrences. This can impart valuable insights into air
1475 traffic trends, as well as how physical conditions like temperature and humidity vary seasonally
1476 and their potential impact on contrail formation. Researchers can better understand contrail
1477 behavior and their relationship with various environmental factors by leveraging the neural
1478 network's ability to detect and classify contrails accurately. This knowledge can be used to refine
1479 models and predictions related to contrail formation and persistence and contribute to a more
1480 comprehensive understanding of aviation's impact on the atmosphere.

1481 **6 Supersonic contrails**

1482 Contrail studies have primarily focused on subsonic aviation due to the predominance of subsonic
1483 air traffic since the retirement of the Concorde in 2003. Contrail formation and persistence for
1484 supersonic commercial aircraft pose challenges -- persistent contrails are unlikely to form in the
1485 stratosphere when these aircraft are flying at supersonic speeds but societal requirements for flying
1486 at subsonic speeds over land to avoid noise issues would still potentially produce persistent
1487 contrails. The importance of understanding the global climate effect of contrails linked to
1488 supersonic aviation is well-established (Stenke et al., 2008). Matthes et al. (2022) recently
1489 published a comprehensive review on the climate effects of supersonic aviation, encompassing
1490 non-CO2 effects like contrail formation. Their work highlights the need for a thorough
1491 understanding of existing research in this area and uncertainties persist regarding parameters
1492 controlling contrail ice crystal distribution evolution for these aircraft. Consequently, the presence
1493 or absence of contrails becomes a discernible marker of the aircraft's speed regime. Additionally,
1494 limited research, such as observations by Schumann et al. (2017) suggested the possibility of
1495 contrail formation even at high altitudes (18.7 km) under specific atmospheric conditions. These
1496 factors highlight the need for a comprehensive understanding of contrail formation and persistence
1497 for future supersonic aircraft.

1498 **7 Uncertainties and Research Gaps**

1499 **7.1 Uncertainties**

1500 There are several crucial areas of uncertainty and research gaps that require focused investigation
1501 to achieve a more comprehensive understanding of contrail formation, evolution, and their effects:

- 1502 • *Humidity Observations and Predictions:* An important uncertainty lies in the accuracy and
1503 reliability of humidity observations and predictions at different altitudes. Improved
1504 measurements and modeling of humidity are critical for assessing the conditions conducive to
1505 persistent contrail formation and their subsequent behavior. Addressing this uncertainty will
1506 lead to more precise insights into contrail persistence and its associated radiative impacts.
- 1507 • *Interaction with Natural Cirrus Clouds:* The interplay between natural cirrus clouds and
1508 contrails initiates an additional level of uncertainty, fostering obscuring the understanding of
1509 their individual and mutual effects on radiative forcing (RF).
- 1510 • *Regional Variations in Atmospheric Conditions:* The sensitivity of contrail radiative impacts
1511 to regional variations in atmospheric conditions is not well understood and remains uncertain.

- 1512 • *Uncertainties and Soot Particles*: The role of soot particles in contrail formation remains
 1513 subject to uncertainties, particularly regarding their ability to nucleate ice. Despite the presence
 1514 of numerous ice particles in fresh contrails, ongoing debates, as highlighted in recent studies
 1515 such as Righi et al. (2021), question whether soot particles directly facilitate ice nucleation.
 1516 Clarifying this relationship is essential for comprehending the impact of soot emissions on
 1517 contrail formation and subsequent evolution. To address this knowledge gap, further research
 1518 efforts are imperative to explore the influence of soot particles on ice nucleation processes
 1519 within contrails.
- 1520 • *Radiative Transfer Scheme*: Quantifying the radiative forcing exerted by contrails on Earth's
 1521 climate remains an intricate task. Studies by Schumann and Graf (2013) identified a distinct
 1522 signature, an "aviation fingerprint," in cirrus cloud cover and outgoing longwave radiation
 1523 (OLR) that mirrored air traffic patterns. This observation suggests a robust correlation between
 1524 aviation activity and cirrus cloud formation. Their analysis even estimated a regional increase
 1525 in heat-trapping (longwave radiative forcing) of 600-900 mWm⁻², highlighting the potential
 1526 influence of aviation on these high-altitude ice clouds. However, a crucial challenge lies in
 1527 accurately modeling the net impact on Earth's energy balance. This difficulty stems from the
 1528 fact that different climate models employ various approaches to simulate radiative transfer
 1529 processes, which govern the movement of heat through the atmosphere. These variations in
 1530 how models handle these radiative processes can significantly influence the estimated impact
 1531 of contrails on our planet's energy equilibrium.

1532 Significant uncertainties persist regarding the radiative forcing caused by aircraft contrails. These
 1533 uncertainties arise from numerous factors, starting with uncertainties in the background
 1534 meteorology and specific aircraft emissions. When assessing the climate impact of contrail cirrus,
 1535 the primary uncertainties lie in (1) determining upper tropospheric water vapor concentrations and
 1536 regions of supersaturation; (2) adequately representing contrail cirrus processes in global models;
 1537 and (3) understanding the radiative response resulting from the contrail cirrus presence, typically,
 1538 only approximate assessments of uncertainties associated with these processes are furnished.

1539 Assessing the radiative response of contrail cirrus involves handling several crucial uncertainties,
 1540 including:

1541 *Uncertainties in Contrail Cirrus Radiative Forcing*: Estimating the radiative forcing (RF) of
 1542 contrail cirrus clouds is inherently uncertain. Lee et al. (2021) categorizes these uncertainties into
 1543 two main areas: (A) uncertainties related to the radiative response of contrail cirrus and (B)
 1544 uncertainties associated with the upper-tropospheric water budget and the contrail cirrus scheme
 1545 within climate models.

1546 (A) *Uncertainties in Radiative Response*

1547 Radiative Transfer Scheme (A1): Myhre et al. (2009) estimated an uncertainty of approximately
 1548 35% arising from the radiative transfer scheme employed in climate models. This scheme
 1549 simulates how different wavelengths of radiation interact with various atmospheric components,
 1550 including contrail cirrus.

1551 *Cloud Heterogeneity (A2)*: The inhomogeneity of ice crystals within a model grid box, vertical
 1552 cloud overlap, and limitations of plane-parallel geometry contribute an estimated uncertainty of
 1553 35% (Carlin et al., 2002; Pomroy and Illingworth, 2000; Gounou and Hogan, 2007).

1554 *Ice Crystal Habit (A4)*: Variations in the shape and form (habit) of ice crystals within contrail
1555 cirrus can significantly impact how they interact with radiation. Markowicz and Witek (2011)
1556 suggest an uncertainty of 20% due to this factor.

1557 *Soot Core Impact (A5)*: The radiative transfer uncertainty associated with soot cores embedded
1558 within contrail cirrus ice crystals is significant, particularly for shortwave albedo (reflectivity), but
1559 remains unquantified (Liou et al., 2013). Soot cores can absorb radiation, potentially leading to a
1560 warming effect that is not currently accounted for in models.

1561 (B) Uncertainties in Water Budget and Contrail Cirrus Scheme

1562 *Ice Supersaturation (B1)*: Uncertainties in the representation of upper-tropospheric ice
1563 supersaturation (Lamquin et al., 2012) contribute an estimated 20% uncertainty.

1564 *Ice Crystal Number Density (B2)*: and Radiative Transfer for Young Contrails (A3): Uncertainties
1565 in ice crystal number densities (Karcher et al., 2015, 2018) are linked to factors like water vapor
1566 saturation and soot emissions. Lee et al. (2021) recognized the dependence between A3 (radiative
1567 transfer for young contrails) and B2 (ice crystal number density). Consequently, they included the
1568 uncertainty from A3 within their overall category B uncertainty estimate.

1569 *Contrail Cirrus Lifetime (B3)*: The effect of contrail cirrus lifetime on estimated RF is relatively
1570 small, with an associated uncertainty estimated at 5-10% (Chen and Gettelman, 2013; Newinger
1571 and Burkhardt, 2012). While Lewellen (2014) highlights the potential importance of lifetime
1572 through large-eddy simulations demonstrating contrail cirrus lifetimes exceeding 40 hours and
1573 widths exceeding 100 km, several factors contribute to the seemingly counterintuitive finding in
1574 this context of estimated RF. Lewellen's (2014) simulations highlight the potential significance
1575 of contrail cirrus with extended lifetimes, particularly for their ice crystal surface area and overall
1576 radiative impact. However, the study focuses on the integrated effect over the entire lifetime,
1577 whereas the uncertainty estimate (5-10%) pertains to the impact of variations in lifetime on the
1578 average RF. Further research is needed to better understand the complex interplay between contrail
1579 cirrus lifetime, ice crystal growth processes, atmospheric conditions, and their combined effect on
1580 radiative forcing.

1581 *Air Traffic Data Resolution (B4)*: Sensitivity studies suggest an uncertainty of about 10% arising
1582 from the temporal resolution of air traffic data used in climate models (Lee et al., 2021).

1583 *Natural Cloud Feedback (B5)*: The feedback mechanism by which contrail cirrus alters the upper
1584 tropospheric water budget, affecting natural clouds, introduces a significant uncertainty that
1585 remains unquantified (Burkhardt and Karcher, 2011; Schumann et al., 2015). Lee et al. (2021)
1586 assumed an uncertainty of 15% for this factor.

1587 *Initial Ice Crystal Assumptions (B6)*: The estimation of RF by Chen and Gettelman (2013) is
1588 subject to uncertainties associated with assumptions about initial ice crystal radii and contrail
1589 cross-sectional areas, leading to an estimated uncertainty of 33%.

1590 Overall Uncertainty

1591 Following Lee et al. (2021), the uncertainty in the radiative response to contrail cirrus (excluding
1592 soot cores) is estimated to be around 55%, assuming independence of different uncertainties. This
1593 aligns with their findings and highlights the dominance of radiative response uncertainties
1594 (category A) in the overall uncertainty budget. Category B uncertainties (water budget and contrail

1595 cirrus scheme) remain significant and require further investigation, particularly the combined
1596 effect of ice crystal number density and radiative transfer for young contrails.

1597 The Uncertainty Tightrope

1598 While scientists continue to refine their understanding of how contrails form and influence our
1599 climate, the ever-present threat of climate change demands that we don't wait for complete
1600 certainty before taking action. The evidence of our warming planet is undeniable, and aviation's
1601 contribution to this issue necessitates exploring all possible solutions, even in the face of some
1602 lingering unknowns.

1603 Fortunately, research like that conducted by Frias et al. (2024) offers a glimmer of hope. Their
1604 study suggests that practical strategies to avoid contrail formation can be implemented with
1605 minimal disruption to flight operations, while significantly reducing the overall climate impact of
1606 these contrails. This finding underscores the potential for immediate action alongside ongoing
1607 scientific inquiry. By embracing a two-pronged approach that combines continued research with
1608 real-world mitigation efforts, we can work towards minimizing aviation's environmental footprint.

1609

1610 **7.2 Research needs and gaps**

1611 In the pursuit of a comprehensive understanding of contrail impacts on climate, there is a critical
1612 need to establish clear research needs and requirements.

1613 Improving weather models demands better predictions of humidity and clouds with enhanced
1614 resolution in time, space, and altitude. The models must also adapt to evolving weather conditions.
1615 Accurate water vapor data during cruise altitudes is crucial, emphasizing the need for small, cost-
1616 effective humidity sensors. To achieve this, there is a need for the production, testing, and
1617 evaluation of precise sensors. Lidar technology and weather model assessments play a key role in
1618 advancing observational capabilities for more accurate predictions. Enhancing cirrus cloud
1619 forecasts requires a dual focus on data and artificial intelligence. Ensemble simulations are vital
1620 for estimating uncertainties in cirrus cloud predictions. Additionally, there is an urgent need for
1621 more climate and contrail models, ensuring a comprehensive understanding and evaluation of these
1622 complex atmospheric processes.

1623 Gierens et al. (2020) highlighted a significant issue with the ERA-5 reanalysis data, showing that
1624 it underestimates the frequency and degree of ice supersaturation. This underestimation impacts
1625 the reliability of forecasts for contrail persistence and the accuracy of estimates for contrail optical
1626 thickness and instantaneous radiative forcing. Their research, which involved comparing
1627 predictions from weather and climate models with actual atmospheric data from the
1628 IAGOS/MOZAIC project and the EMAC model, revealed that while temperature predictions are
1629 generally accurate, relative humidity predictions are often significantly off. This discrepancy
1630 undermines the effectiveness of using reanalysis data to predict real-world contrail formation along
1631 aircraft trajectories. The study underscores the necessity of improving ice supersaturation
1632 predictions to enhance the reliability of contrail avoidance strategies and ensure they can be
1633 operationally viable (Gierens et al.,2020).

1634 Research by Ovarlez et al. (2000) highlights discrepancies between measured water vapor content
1635 and data from weather forecasts. Their findings emphasize the importance of accurate humidity
1636 measurements, particularly for studies on contrail formation and persistence. Weather forecasts
1637 might underestimate actual humidity, potentially leading to inaccurate assessments of contrail

1638 behavior. This underlines the need for ongoing research to improve the accuracy of humidity data
1639 in weather models.

1640 Furthermore, high-quality observations, effectively integrated into weather models, are crucial for
1641 setting accurate starting points for forecasts (Bauer et al., 2015). This highlights the need for robust
1642 data collection strategies that combine information from diverse sources. These sources can
1643 include in-situ measurements taken directly within the atmosphere, radar systems that track
1644 precipitation patterns, and satellite sensors that provide a global view. Advanced data assimilation
1645 techniques then play a vital role by merging these observations with model outputs. This combined
1646 approach creates a more precise picture of the initial atmospheric state, ultimately leading to
1647 improved weather forecasts (Bauer et al., 2015).

1648 Sun and Roosenbrand (2023) reported the limitations in traditional computer vision approaches
1649 for contrail detection, particularly in handling the complexity of satellite images under varying
1650 conditions. Earlier machine learning methods relied on simpler convolutional neural network
1651 models, primarily demanding extensive labeled data for contrail presence determination. Notably,
1652 there is a gap in the existing literature, lacking research specifically tailored to machine learning
1653 approaches for contrail detection, setting it apart from other image segmentation or detection tasks.
1654 A significant challenge lies in the absence of adequate loss functions optimized for linear features
1655 like contrails during training, making detection notably difficult at lower resolutions, especially
1656 when multiple contrails are close. Addressing these gaps is crucial for advancing the efficacy of
1657 contrail detection methods (Sun and Roosenbrand, 2023).

1658 While a complete understanding of contrail effects on climate may not be achievable, further
1659 research is crucial to reduce uncertainties and improve our ability to predict and mitigate their
1660 impact. Here are some of the key areas of research gaps that should be explored to address existing
1661 uncertainties:

- 1662 ▪ *Properties of Contrail Particles:* Understanding contrail effects on climate requires
1663 reflection of key factors such as particle size, layer height, cloud overlap, and optical
1664 properties. Larger particles tend to have a different radiative impact than smaller ones. The
1665 altitude of contrail formation impacts their interaction with solar and terrestrial radiation.
1666 Precise climate modeling requires proper accounting for cloud overlap, impacting radiative
1667 calculations. Contrail optical properties, comprising albedo and emissivity, determine their
1668 reflective and trapping abilities for solar and terrestrial radiation. The concentration and
1669 size distribution of contrail particles affect their formation and radiative impact. Accurate
1670 estimation of contrail forcing, important for climate modeling and policy decisions,
1671 depends on understanding particle number, size, and layer height.
- 1672 ▪ *Assessment of Effective Radiative Forcing:* Effective Radiative Forcing (ERF) is a valuable
1673 tool for evaluating the global mean radiative impact of contrail cirrus on climate. However,
1674 it's important to recognize that ERF primarily focuses on this average effect and may not
1675 fully capture regional variations or complex feedback mechanisms associated with contrail
1676 formation and persistence.
- 1677 ▪ *Emissions and Alternative Fuels:* Corroborating a precise connection between soot and
1678 contrail ice crystal numbers is important for understanding the environmental impact of
1679 sustainable aviation fuels, such as biofuels. Biofuels are being studied as a more sustainable
1680 alternative to conventional aviation fuels, and evaluating their impact on contrail formation
1681 is crucial for assessing environmental benefits. Scientific research, notifying regulatory
1682 decisions, relies on the interpretation of the correlation between soot and ice crystal

1683 numbers. This connection is integral for complete visions of the environmental
1684 implications of alternative aviation fuels. Precise data on contrail formation, containing the
1685 impact of biofuels, is crucial for climate models predicting the impact of aviation emissions
1686 on climate. The experimental establishment of the soot-ice crystal connection gives this
1687 understanding.

- 1688 ■ *Properties of Soot Particle*: A study into the bimodal size distributions of soot particles in
1689 aircraft emissions is critical for focusing uncertainties on contrail formation and properties,
1690 with inferences for climate science and aviation practices (Schumann et al., 2002). In-flight
1691 measurements typically show a single peak in the number-size distribution of freshly
1692 emitted soot particles (Schumann et al., 2002). However, some cases reveal a second, larger
1693 particle mode in near-field contrails and dry plumes. The source of this larger mode
1694 remains uncertain, suggesting that the bimodal distribution might be present in unrefined
1695 jet engine emissions rather than being solely caused by contrail processing or coagulation
1696 during plume development (Schumann et al., 2002). Precise data on soot particle
1697 properties, including any potential bimodal size distribution, is essential for climate models
1698 incorporating contrail effects. Resolving the origin of this bimodal distribution is crucial to
1699 improving model representations of contrail properties. Policymakers and regulatory
1700 bodies rely on scientific research for progressing aviation-related environmental policies,
1701 making an understanding of soot particle size distributions significant for up-to-date
1702 decision-making.
- 1703 ■ Examining the microphysical interaction between soot particles and contrail ice crystals
1704 emerges as a critical research priority. Laboratory experiments simulating contrail
1705 formation conditions offer valuable insights into the ice nucleating potential of soot
1706 particles under controlled environments. Moreover, field measurements focusing on the
1707 in-situ characterization of soot particles and ice crystals within nascent contrails provide
1708 indispensable data for validating models. By integrating these methodologies, researchers
1709 can advance their understanding of the role of soot particles in contrail formation and
1710 refine climate models accordingly.
- 1711 ■ *Remote Sensing for Contrail-Cirrus*: Organized regional campaigns are important for
1712 estimating key variables in aging contrail-cirrus and aircraft plumes. This contains in-situ
1713 and remote sensing to portray the growth, decay, and trajectories of contrail ice particles,
1714 delivering essential data for interpretation of transformation and radiative effects.
1715 Estimation of contrail particles, ambient aerosols, and gaseous aerosol precursors notifies
1716 climate modeling and environmental assessments, connecting emissions to contrail
1717 properties. Gathered data validates climate models, enhancing their accuracy and
1718 improving the representation of contrail-cirrus effects. Understanding contrail-cirrus
1719 development supports developing mitigation strategies, informing contrail avoidance, and
1720 reducing aviation's climate impact.

1721 In addition to these research issues, there is a need to bridge the gaps with the assessment of the
1722 above-reported uncertainties and to investigate and improve the understanding of contrail
1723 avoidance and climate tradeoffs. Research should explore how to mitigate the climate impact of
1724 contrails without compromising aviation safety and efficiency.

1725
1726
1727

1728 7.3 Contrail avoidance and climate tradeoffs

1729 While existing studies explore contrail avoidance strategies and their impact on fuel burn and
1730 climate, a comprehensive large-scale evaluation remains elusive. Ideally, such an evaluation would
1731 encompass a significant number of routes, account for weather variations, enable full flight level
1732 optimization, quantify contrail impacts on individual flights, and compare results to a fuel-optimal
1733 baseline to isolate the specific effects of contrail avoidance. This comprehensive approach would
1734 provide a more definitive understanding of the fuel-climate tradeoffs associated with contrail
1735 avoidance strategies.

1736 Recent studies investigating targeted contrail avoidance strategies offer promising results. Teoh et
1737 al. (2020) suggest that focusing on a small percentage of flights with the highest contrail impact
1738 could be an effective approach, minimizing the overall increase in fuel consumption and CO2
1739 emissions. Additionally, advancements in engine design hold promise as a long-term solution for
1740 reducing contrail formation.

1741 Molloy et al. (2022) address a critical step towards implementing effective contrail avoidance
1742 strategies in practice. Their work outlines the practical considerations for conducting large-scale
1743 trials, which are essential for evaluating the feasibility and effectiveness of these strategies in real-
1744 world conditions. The proposed deployable options based on existing air traffic management
1745 processes offer a promising path forward for initiating such trials.

1746 Frias et al. (2024) present a compelling case for the practicality and economic viability of contrail
1747 avoidance. Their findings demonstrate that significant reductions in contrail climate impact can be
1748 achieved with minimal operational burdens. This study provides strong motivation for airlines and
1749 air traffic controllers to embrace contrail avoidance strategies as a means to reduce aviation's
1750 overall climate footprint.

1751 Gierens et al. (2008) proposed several potential ways to mitigate the impact of contrails,
1752 encompassing both technical and operational approaches. Regarding the technical aspect, they
1753 recognized the challenge of completely preventing contrail formation due to its primarily
1754 thermodynamic nature. However, they suggested the exploration of new engine cycles and
1755 technical infrastructures that might help suppress contrails. Additionally, reducing the number of
1756 emitted particles was considered to mitigate contrail formation. While such evaluations would not
1757 eliminate contrails completely, they would produce thinner contrails with rarer but larger crystals.
1758 These heavier ice crystals would incline more rapidly on average, causing shorter contrail
1759 lifetimes. The analysis also investigated operational mitigation options. Striking strict constraints,
1760 such as fixed maximum flight levels, was studied unreasonably due to the significant challenges it
1761 would pose for air traffic controllers and the resulting safety concerns. Their proposed strategies
1762 focused on addressing contrail formation both at the technical level through engine and
1763 infrastructure improvements and at the operational level by implementing flexible measures that
1764 consider real-time weather conditions. These approaches aimed to strike a balance between
1765 contrail reduction and the practical needs of aviation.

1766 In a recent study, Sausen et al. (2023) presented an experiment that aimed to avoid contrail
1767 formation during real-world operations. This experiment took place in the Maastricht Upper Area
1768 Control region, covering parts of Germany, the Benelux countries, and the North Sea, in the year
1769 2021. The researchers highlighted that contrail avoidance could serve as an effective method for
1770 mitigating the climate impact of aviation. To conduct their trial experiment, air traffic was

1771 deliberately diverted every other day by adjusting the flight altitude, either increasing or decreasing
1772 it by up to 2000 ft, whenever potential persistent contrails were predicted. The effectiveness of
1773 these deviations was assessed by analyzing satellite images of high clouds and employing a
1774 contrail detection algorithm that utilized contrail properties. Despite the ongoing challenge of
1775 accurately forecasting persistent contrails, the trial achieved a significant level of success, reaching
1776 97.5%, suggesting that on average, persistent contrails can be avoided during regular flights in the
1777 real world through minor adjustments in the vertical flight path. Contrail avoidance through minor
1778 adjustments in flight paths represents a practical approach to mitigate the formation of persistent
1779 contrails. It demonstrates the feasibility of implementing such measures within air traffic
1780 management to reduce the environmental impact of aviation. The study highlights the potential for
1781 real-world applications of contrail avoidance as a means of addressing the climate effects of
1782 contrails. The findings of this experiment mark an important milestone in implementing
1783 operational measures in air traffic management to decrease the impact of climate from aviation.

1784 The limitations of simply avoiding all contrails become evident when we consider their diverse
1785 climate effects. While some contrails can have a net cooling effect, others contribute to warming.
1786 This distinction necessitates a more nuanced approach to contrail avoidance. We should focus on
1787 mitigating the formation of contrails that contribute to warming, while potentially allowing or even
1788 encouraging the formation of those with a net cooling effect. This distinction requires reliable
1789 methods for differentiating between the two contrail types.

1790 *Future considerations: optimizing contrail avoidance.*

1791 The Sausen et al. (2023) study represents a significant step forward, demonstrating the feasibility
1792 of operational contrail avoidance through minor flight adjustments. To optimize this approach for
1793 maximum climate benefit, future research should focus on three key areas:

1794 *Distinguishing warming from cooling contrails:* Developing robust methods to differentiate
1795 between these contrail types is crucial. Improved weather forecasting models and contrail
1796 prediction algorithms that consider factors like altitude, atmospheric conditions, and cirrus cloud
1797 cover can contribute to this goal.

1798 *Large-scale implementation:* Evaluating the broader applicability of contrail avoidance strategies
1799 necessitates conducting large-scale trials across diverse airspace with varying weather patterns.
1800 This will provide a more comprehensive understanding of the effectiveness and potential trade-
1801 offs associated with contrail avoidance in different operational contexts.

1802 *Integration with air traffic management:* For widespread adoption, efficient protocols for
1803 integrating contrail avoidance measures within existing air traffic management systems are
1804 essential. This may involve developing streamlined decision-making tools and communication
1805 channels for air traffic controllers and pilots.

1806 By addressing these considerations, contrail avoidance can evolve from a general strategy to a
1807 targeted approach that maximizes its potential for mitigating aviation's climate impact. This
1808 approach would focus on reducing the formation of warming contrails while allowing for or even
1809 encouraging the formation of cooling contrails.

1810 In a recent Ph.D. thesis, Elmourad (2023) evaluated the fuel-climate tradeoffs arising from contrail
1811 avoidance strategies applied on a large scale. This study raises several key questions about
1812 contrails avoidance: What fraction of aviation's global total contrail length can be avoided using
1813 vertical re-routing exclusively? What is the fuel penalty of such an avoidance strategy? How does

1814 the fuel penalty or contrail reduction vary between flights or seasons? Can the fuel penalty be
1815 constrained? What effect does that have on the ability to do contrail avoidance? What net climate
1816 benefit can be achieved from contrail avoidance strategies? How does this differ from avoiding all
1817 contrails or only nighttime contrails? What are the relative orders of magnitude between the
1818 climate benefits from contrail avoidance and the climate damages from additional fuel burn? How
1819 does this difference compare with the uncertainties associated with contrail impacts?

1820 As the global volume of air traffic continues to rise, the aviation industry grapples with a
1821 significant challenge in mitigating its environmental impact on climate change. Contrails, which
1822 contribute to global warming by trapping terrestrial radiation, have the potential to counteract the
1823 benefits of reduced emissions resulting from optimized flight paths. In a study by Roosenbrand et
1824 al. (2023), the authors conducted a global assessment of flights that contribute to contrail formation
1825 and assessed the altitude adjustments required to avoid these contrail-prone areas. This analysis
1826 utilized a combination of data from the Integrated Global Radiosonde Archive (IGRA), which
1827 provides measurements from weather balloons with global coverage and high vertical resolution,
1828 and flight data from OpenSky. The study identified Mid-Western Europe, the Eastern United States
1829 of America, and Japan as regions characterized by both high air traffic volumes and a substantial
1830 percentage of flights forming contrails. Importantly, these regions offer opportunities for altitude
1831 adjustments of less than one kilometer to minimize contrail formation. The research also
1832 pinpointed other regions where relatively minor operational interventions could yield significant
1833 climate benefits.

1834 *Fuel-climate tradeoffs*: While there have been numerous studies on operational contrail avoidance,
1835 there are still some research gaps in the field when it comes to understanding the fuel-climate
1836 tradeoffs that would follow a large-scale global application of contrail avoidance strategies.

1837 *Sustainable Aviation Fuel (SAF)*: Much still needs to be understood about what SAF will look like
1838 as it becomes the dominant fuel of the future. The emissions of soot and other particles from SAF
1839 are still not well understood and will have a significant effect on future contrail production and
1840 lifetimes. According to Bräuer et al. (2021b), sustainable aviation fuels have been identified as
1841 capable of reducing both contrail ice numbers and the radiative forcing caused by contrail cirrus.
1842 Their study involved the measurement of apparent ice emission indices across different fuels with
1843 varying aromatic content at altitudes ranging from 9.1 to 9.8 km and 11.4 to 11.6 km. The data
1844 were collected during the ECLIF II/NDMAX flight experiment in January 2018, encompassing a
1845 variety of fuels differing in aromatic quantity and type. A comparison between a sustainable
1846 aviation fuel blend and a reference fuel Jet A-1 revealed a maximum reduction of 40% in apparent
1847 ice emission indices, highlighting the potential impact of sustainable aviation fuels on mitigating
1848 contrail-related environmental effects.

1849 Moore et al. (2017) examined the impact of biofuel blends compared to traditional jet fuel on
1850 aircraft emissions. They found that biofuel blends significantly reduced the quantity and weight of
1851 particles emitted, suggesting biofuels can reduce aviation's environmental impact. Their
1852 measurements showed a notable decrease in total and non-volatile particles with the biofuel blend
1853 and a shift to smaller particle sizes. This is due to a larger reduction in bigger soot particles acting
1854 as condensation nuclei. The drop in soot emissions enhances the formation of new particles.
1855 Mixing petroleum fuels with HEFA bio-jet fuel cut volatile and non-volatile particle emissions by
1856 50%-70% during cruise conditions. However, soot particle emissions remain high, indicating
1857 biofuels help but don't eliminate issues related to contrail formation.

1858 *Alternative aircraft and new fuels:* There is a lot of ongoing discussion about the potential
1859 development of aircraft using hydrogen as fuel. Such an aircraft engine would still emit water
1860 vapor and therefore could produce contrails. However, the major reduction in particulates, e.g., no
1861 soot, could affect the lifetime of the contrail and whether it could result in contrail cirrus. Research
1862 is needed to evaluate the potential for contrail production and resulting lifetimes. Other alternative
1863 fuels would also need to be evaluated.

1864 There is a necessity for government research organizations as well as industry partners to venture
1865 into the investigation and establishment of sensor prototypes. An example is a humidity sensor
1866 prototype with a range of great precision covering 20 parts per million by volume to more than
1867 10,000 ppmv. The purpose is to improve the accuracy of measurements, especially on parameters
1868 like temperature and relative humidity, at altitudes preserved during flight to counteract contrail
1869 mitigation. Additionally, improving measurement at lower altitudes is vital for improving the
1870 precision of weather forecasting. This accumulated data will play a pivotal role in evaluating and
1871 integrating these insights into forecast models, enhancing the robustness of these calculations. An
1872 additional area of focus is the refinement of model calculations on the impact of contrails,
1873 necessitating improved handling of variables such as clouds, aerosols, and specific aircraft
1874 characteristics.

1875 Tackling the pressing challenge of climate change requires the exploration and adoption of
1876 effective contrail mitigation strategies. Recent studies show promise in the utilization of alternative
1877 fuels, particularly sustainable aviation fuels (SAFs), which boast lower soot particle emissions
1878 compared to conventional jet fuel. Initial flight trials have shown a marked decrease in contrail
1879 formation when SAFs are used, potentially attributed to the reduced concentration of ice nucleation
1880 particles in SAF exhaust. Moreover, ongoing research focuses on optimizing flight path planning
1881 and air traffic management (ATM) to minimize contrail formation and persistence. Research
1882 conducted by Sausen et al. (2023) demonstrates the feasibility of contrail avoidance through minor
1883 adjustments in flight paths during real-world operations. Continued progress and application of
1884 these strategies, coupled with advancements in contrail observation technologies such as high-
1885 precision humidity sensors, offer significant potential to mitigate the climate impact of aviation.
1886

1887 **8 Conclusions**

1888 This study reviews the current understanding of the impacts of contrail formation by aircraft on
1889 the Earth's climate system; it provides insights into the current state of contrail research, offering
1890 perspectives on contrail formation, characteristics, life cycle, and potential future impacts. The
1891 study underscores the importance of confronting uncertainties in climate models and emphasizes
1892 the need for further research to enhance our understanding of contrail effects.

1893 Aviation emissions, encompassing both contrail cirrus clouds and carbon dioxide emissions, exert
1894 an important influence on the Earth's climate. Extensive research efforts have significantly
1895 improved our understanding of contrail formation and aging; however, key microphysical
1896 processes remain a subject of ongoing investigation. Our examination of global observational data
1897 and projections highlights the potential for a significant increase in contrail cirrus radiative forcing
1898 by the mid-21st century, driven by factors such as anticipated growth in air traffic, potential
1899 improvements in fuel efficiency, and evolving atmospheric conditions. While uncertainties
1900 regarding the precise magnitude of this increase exist, the potential consequences necessitate
1901 proactive mitigation strategies. Several promising approaches are being explored, including
1902 operational measures to optimize flight paths, the development of new contrail suppression

1903 technologies, and the adoption of sustainable aviation fuels. Implementing a combination of these
1904 strategies, while continuously refining our understanding of contrail effects, is crucial for
1905 minimizing the overall climate impact of aviation.

1906 **Author contributions.** DKS prepared the manuscript with partial support from SS and supervision
1907 from DJW

1908
1909 **Competing interests.** The author declares that they have no competing interests.

1910
1911 **Acknowledgment.**

1912 This work was supported by the National Aeronautics and Space Administration (NASA) under
1913 award number NNA16BD14C for NASA Academic Mission Services (NAMS).

1914 We thank Drs. Andrew Gettelman (Pacific Northwest National Laboratory, PNNL, USA), Ulrike
1915 Burkhardt (German Aerospace Center, DLR, Germany), Bernd Kärcher (DLR), Phillip J Ansell
1916 (University of Illinois at Urbana-Champaign, USA), D.S. Lee (Manchester Metropolitan
1917 University, UK), and Steven L Baughcum (The Boeing Company) for reviewing prior drafts of
1918 this report.

1919 **Financial support.** The authors would like to thank for support from the Universities Space
1920 Research Association (USRA) through project subcontract 08600-031.

1921
1922
1923 **References**

1924
1925 Airbus Global Market Forecast: 2023-2042. Retrieved from <https://www.airbus.com/en/products>
1926 [services/commercial-aircraft/market/global-market-forecast](https://www.airbus.com/en/products/services/commercial-aircraft/market/global-market-forecast)), 2022.

1927 Appleman, H.: The formation of exhaust condensation trails by jet aircraft. *Bull. Amer. Meteor.*
1928 *Soc.*, 34(1), 14-20, <https://doi.org/10.1175/1520-0477-34.1.14>, 1953.

1929 Atlas, D., Wang, Z., and Duda, D. P.: Contrails to cirrus: Morphology, microphysics, and radiative
1930 properties. *J. Appl. Meteor.*, 45, 5–19, <https://doi.org/10.1175/JAM2335.1>, 2006.

1931 Aufm Kampe, H. J.: Die Physik der Auspuffwolken hinter Flugzeugen, *Luftwissen*, 10, 171–173,
1932 1943.

1933 Barrett, S., Prather, M., Penner, J., Selkirk, H., Balasubramanian, S., Doppelheuer, A., Fleming, G.,
1934 Gupta, M., Halthore, R., Hileman, J., Jacobson, M.: Guidance on the use of AEDT gridded
1935 aircraft emissions in atmospheric models. A technical note, Aug 17,
1936 <https://doi.org/10.2172/993261>, 2010.

1937 Bauer, H.S., Schwitalla, T., Wulfmeyer, V., Bakhshaii, A., Ehret, U., Neuper, M. and Caumont,
1938 O.: Quantitative precipitation estimation based on high-resolution numerical weather
1939 prediction and data assimilation with WRF—a performance test. *Tellus A: Dynamic*
1940 *Meteorology and Oceanography*, 67(1), p.25047, <https://doi.org/10.3402/tellusa.v67.25047>,
1941 2015.

1942 Baumgardner, D., Brenguier, J. L., Bucholtz, A., Coe, H., DeMott, P., Garrett, T. J., Gayet, J. F.,
1943 Hermann, M., Heymsfield, A., Korolev, A., Krämer, M.: Airborne instruments to measure
1944 atmospheric aerosol particles, clouds and radiation: A cook's tour of mature and emerging
1945 technology. *Atmos. Res.*, 102(1-2), 10-29. Oct 1,
1946 <https://doi.org/10.1016/j.atmosres.2011.08.010>, 2011.

1947 Bickel, M., Ponater, M., Bock, L., Burkhardt, U. and Reineke, S., Estimating the effective
1948 radiative forcing of contrail cirrus. *Journal of Climate*, 33(5), pp.1991-2005,
1949 <https://doi.org/10.1175/JCLI-D-19-0531.1>, 2020.

1950 Bickel, M.: *Climate Impact of Contrail Cirrus*. Ph.D. Thesis, Ludwig-Maximilians-Universität
1951 München, 133 pp. doi: 10.57676/mzmg-r403., 2023.

1952 Bier, A., and Burkhardt, U.: Variability in contrail ice nucleation and its dependence on soot
1953 number emissions. *J. Geophys. Res. Atmos.*, 124(6), 3384–3400,
1954 <https://doi.org/10.1029/2018JD030132>, 2019.

1955 Bier, A., and Burkhardt, U.: Impact of parametrizing microphysical processes in the jet and vortex
1956 phase on contrail cirrus properties and radiative forcing. *J. Geophys. Res. Atmos.*, 127,
1957 e2022JD036677, <https://doi.org/10.1029/2022JD036677>, 2022.

1958 Bier, A., Burkhardt, U., and Bock, L.: Synoptic control of contrail cirrus life cycles and their
1959 modification due to reduced soot number emissions. *J. Geophys. Res. Atmos.*, 122(21),
1960 11,584–11,603, <https://doi.org/10.1002/2017JD027182>, 2017.

1961 Bock, L., and Burkhardt, U.: Reassessing properties and radiative forcing of contrail cirrus using
1962 a global climate model. *J. Geophys. Res. Atmos.*, 121(16), 9717–9736,
1963 <https://doi.org/10.1002/2015JD024688>, 2016.

1964 Bock, L., and Burkhardt, U.: The temporal evolution of a long-lived contrail cirrus cluster:
1965 Simulations with a global climate model, *J. Geophys. Res. Atmos.*, 121, 3548–3565,
1966 <https://doi.org/10.1002/2015JD024282>, 2016.

1967 Bock, L., and Burkhardt, U.: Contrail cirrus radiative forcing for future air traffic. *Atmos. Chem.*
1968 *Phys.*, 19(12), 8163–8174, <https://doi.org/10.5194/acp-19-8163-2019>, 2019

1969 Boeing: *Commercial Market Outlook 2022–2041*.
1970 <https://www.boeing.com/commercial/market/commercial-market-outlook/index.page>, 2022.

1971 Bräuer, T., Voigt, C., Sauer, D., Kaufmann, S., Hahn, V., Scheibe, M., Schlager, H., Diskin, G. S.,
1972 Nowak, J. B., DiGangi, J. P., Huber, F.: Airborne measurements of contrail ice properties-
1973 Dependence on temperature and humidity, *Geophys. Res. Lett.*, 48(8), e2020GL092166,
1974 <https://doi.org/10.1029/2020GL092166>, 2021a.

1975 Bräuer T, Voigt C, Sauer D, Kaufmann S, Hahn V, Scheibe M, Schlager H, Huber F, Le Clercq P,
1976 Moore RH, Anderson BE. Reduced ice number concentrations in contrails from low-aromatic
1977 biofuel blends. *Atmos. Chem. Phys.*, 21(22), 16817-26., <https://doi.org/10.5194/acp-21-16817-2021>, 2021b.

1979 Burkhardt, U., Kärcher, B., Ponater, M., Gierens, K., and Gettelman, A.: Contrail cirrus supporting
1980 areas in model and observations. *Geophys. Res. Lett.*, 35,
1981 <https://doi.org/10.1029/2008GL034056>, 2008.

1982 Burkhardt, U., and Kärcher, B.: Process-based simulation of contrail cirrus in a global climate
1983 model. *J. Geophys. Res. Atmos.*, 114(D16), D16201, <https://doi.org/10.1029/2008JD011675>,
1984 2009.

1985 Burkhardt, U., Bock, L., and Bier, A.: Mitigating the contrail cirrus climate impact by reducing
1986 aircraft soot number emissions. *npj Clim. Atmos. Sci.*, 1, 37, <https://doi.org/10.1038/s41612-018-0044-x>, 2018.

1987
1988 Burkhardt, U., and Kärcher, B.: Global radiative forcing from contrail cirrus. *Nat. Clim. Change.*,
1989 1, 54–58, <https://doi.org/10.1038/nclimate1068>, 2011.

1990 Burkhardt, U., Kärcher, B., and Schumann, U.: Global modeling of the contrail and contrail cirrus
1991 climate impact. *Bull. Am. Meteorol. Soc.*, 91(4), 479–484,
1992 <https://doi.org/10.1175/2010BAMS2966.1>, 2010.

- 1993 Caiazzo, F., Agarwal, A., Speth, R. L., and Barrett, S. R. H.: Impact of biofuels on contrail
 1994 warming. *Environ. Res. Lett.*, 12, 114013, <https://doi.org/10.1088/1748-9326/aa8c25>, 2017.
- 1995 Carlin, B., Fu, Q., Lohmann, U., Mace, G., Sassen, K., and Comstock, J.: High-cloud horizontal
 1996 inhomogeneity and solar albedo bias. *J. Climate*, 15, 2321–2339, [https://doi.org/10.1175/1520-0442\(2002\)15](https://doi.org/10.1175/1520-0442(2002)15), 2002.
- 1997
 1998 Chauvigné, A., Jourdan, O., Schwarzenboeck, A., Gourbeyre, C., Gayet, J. F., Voigt, C., Schlager,
 1999 H., Kaufmann, S., Borrmann, S., Molleker, S., Minikin, A.: Statistical analysis of contrail to
 2000 cirrus evolution during the Contrail and Cirrus Experiment (CONCERT). *Atmos. Chem. Phys.*,
 2001 18(13), 9803–22, Jul 12, <https://doi.org/10.5194/acp-18-9803-2018>, 2018.
- 2002 Chen, C.-C., Gettelman, A., Craig, C., Minnis, P., and Duda, D.: Global contrail coverage
 2003 simulated by CAM5 with the inventory of 2006 global aircraft emissions. *J. Adv. Model. Earth*
 2004 *Syst.*, 4(4), <https://doi.org/10.1029/2012MS000088>, 2012.
- 2005 Chen, C.-C., and Gettelman, A.: Simulated radiative forcing from contrails and contrail cirrus.
 2006 *Atmos. Chem. Phys. Discuss.*, 13, 10,939–10,959, [https://doi.org/10.5194/acpd-13-10939-](https://doi.org/10.5194/acpd-13-10939-2013)
 2007 2013, 2013.
- 2008 Chen, C.-C., and Gettelman, A.: Simulated 2050 Aviation Radiative Forcing from Contrails and
 2009 Aerosols. *Atmos. Chem. Phys.*, 16 (11), 7317–33, <https://doi.org/10.5194/acp-16-7317-2016>,
 2010 2016.
- 2011 Comstock, J. M., Ackerman, T. P., and Turner, D. D.: Evidence of high ice supersaturation in
 2012 cirrus clouds using ARM Raman lidar measurements. *Geophys. Res. Lett.*, 31, L11106,
 2013 <https://doi.org/10.1029/2004GL019705>, 2004.
- 2014 Danabasoglu, G., Lamarque, J. F., Bacmeister, J., Bailey, D. A., DuVivier, A. K., Edwards, J.,
 2015 Emmons, L. K., Fasullo, J., Garcia, R., Gettelman, A., Hannay, C.: The community earth
 2016 system model version 2 (CESM2). *J. Adv. Model. Earth Syst.*, 12(2), e2019MS001916,
 2017 <https://doi.org/10.1029/2019MS001916>, Feb, 2020.
- 2018 De Leon, R. R., M. Krämer, M., Lee, D. S., and Thelen, J. C.: Sensitivity of radiative properties
 2019 of persistent contrails to the ice water path. *Atmos. Chem. Phys.*, 12, 7893–7901,
 2020 <https://doi.org/10.5194/acp-12-7893-2012>, 2012.
- 2021 Dischl, R. K., Sauer, D., Voigt, C., Harlaß, T., Sakellariou, F., Märkl, R. S., Schumann, U.,
 2022 Scheibe, M., Kaufmann, S., Roiger, A., Dörnbrack, A., Renard, C., Gauthier, M., Swann, P.,
 2023 Madden, P., Luff, D., Johnson, M., Ahrens, D., Sallinen, R., Schripp, T., Eckel, G., Bauder,
 2024 U., and Le Clercq, P.: Measurements of particle emissions of an A350-941 burning 100 %
 2025 sustainable aviation fuels in cruise, EGUsphere [preprint], [https://doi.org/10.5194/egusphere-](https://doi.org/10.5194/egusphere-2024-1224)
 2026 2024-1224, 2024.
- 2027 Dietmüller, S., et al.: A new radiation infrastructure for the Modular Earth Submodel System
 2028 (MESSy, based on version 2.51). *Geosci. Model Dev.*, 9, 2209–2222,
 2029 <https://doi.org/10.5194/gmd-9-2209-2016>, 2016.
- 2030 Dipankar, A., Stevens, B., Heinze, R., Moseley, C., Zängl, G., Giorgetta, M., and Brdar, S.: Large
 2031 eddy simulation using the general circulation model ICON. *J. Adv. Model. Earth Syst.*, 7, 963–
 2032 986, <https://doi.org/10.1002/2015MS000431>, 2015.
- 2033 Duda, D. P., Minnis, P., Nguyen, L., and Palikonda, R.: A case study of the development of contrail
 2034 clusters over the Great Lakes. *J. Atmos. Sci.*, 61, 1132–1146, [https://doi.org/10.1175/1520-0469\(2004\)061<1132:ACOTDO>2.0.CO;2](https://doi.org/10.1175/1520-0469(2004)061<1132:ACOTDO>2.0.CO;2), 2004.
- 2035
 2036 Duda, D. P., Minnis, P., Khlopenkov, K., Chee, T. L., and Boeke, R.: Estimation of 2006 Northern
 2037 Hemisphere contrail coverage using MODIS data. *Geophys. Res. Lett.*, 40, 612–617,
 2038 <https://doi.org/10.1002/grl.50126>, 2013.

2039 Duda, D. P., Smith, W. L., Bedka, S., Spangenberg, D., Chee, T., and Minnis, P.: Impact of
2040 COVID-19-Related Air Traffic Reductions on the Coverage and Radiative Effects of Linear
2041 Microphysical Persistent Contrails Over Conterminous United States and Surrounding Oceanic
2042 Routes, *J. Geophys. Res.-Atmos.*, 128, e2022JD037554,
2043 <https://doi.org/10.1029/2022JD037554>, 2023.

2044 EASA (European Union Aviation Safety Agency) ICAO Aircraft Engine Emissions Databank
2045 2023: <http://www.easa.europa.eu/document-library/icao-aircraft-engine-emissions-databank>.

2046 Ettenreich, R.: Wolkenbildung über einer Feuersbrunst und an Flugzeugabgasen. *Meteorol. Z.*, 36,
2047 355–356, 1919.

2048 Elmourad, J. A.: Evaluating Fuel-Climate Tradeoffs in Contrail Avoidance (Doctoral dissertation,
2049 Massachusetts Institute of Technology), 2023.

2050 EUROCONTROL.: Aircraft Performance Summary Tables for the Base of Aircraft Date (BADA),
2051 3.7, European Organisation for the Safety of Air Navigation, Brétigny-sur-Orge, 103, 2009.

2052 Frias, A.M., Shapiro, M.L., Engberg, Z., Zopp, R., Soler, M. and Stettler, M.E.J.: Feasibility of
2053 contrail avoidance in a commercial flight planning system: an operational analysis.
2054 *Environmental Research: Infrastructure and Sustainability*, 4(1), p.015013, doi 10.1088/2634-
2055 4505/ad310c, 2024.

2056 Fritz, T. M., Eastham, S. D., Speth, R. L., and Barrett, S. R. H.: The role of plume-scale processes
2057 in long-term impacts of aircraft emissions. *Atmos. Chem. Phys.*, 20, 5697–5714,
2058 <https://doi.org/10.5194/acp-20-5697-2020>, 2020.

2059 Frömming, C., Ponater, M., Burkhardt, U., Stenke, A., Pechtl, S., and Sausen, R.: Sensitivity of
2060 contrail coverage and contrail radiative forcing to selected key parameters, *Atmos. Environ.*,
2061 45, 1483–1490, <https://doi.org/10.1016/j.atmosenv.2010.12.039>, 2011.

2062 Fuglestvedt, J. S., and coauthors: Transport impacts on atmosphere and climate: Metrics. *Atmos.*
2063 *Environ*, 44, 4648–4677, <https://doi.org/10.1016/j.atmosenv.2009.04.044>, 2010.

2064 Garber, D. P., Minnis, P., and Costulis, P. K.: A commercial flight track database for upper
2065 tropospheric aircraft emission studies over the USA and southern Canada, *Meteorologische*
2066 *Zeitschrift*, 14, 445–452, <https://doi.org/10.1127/0941-2948/2005/0040>, 2005.

2067 Gayet, J. F., Shcherbakov, V., Voigt, C., Schumann, U., Schäuble, D., Jessberger, P., Petzold, A.,
2068 Minikin, A., Schlager, H., Dubovik, O., Lapyonok, T.: The evolution of microphysical and
2069 optical properties of an A380 contrail in the vortex phase, *Atmos. Chem. Phys.*, 12(14), 6629-
2070 6643, <https://doi.org/10.5194/acp-12-6629-2012>, 2012.

2071 Geleyn, J. F., Hollingsworth, A.: An economical analytical method for the computation of the
2072 interaction between scattering and line absorption of radiation, *Beiträge zur Physik der*
2073 *Atmosphäre*, 52, 1–16, 1978.

2074 Gerz, T., Durbeck, T., Konopka, P.: Transport and effective diffusion of aircraft emissions, *J.*
2075 *Geophys. Res.*, 103, 25905–25914, <https://doi.org/10.1029/98JD01819>, 1998.

2076 Geraedts, S., Brand, E., Dean, T. R., Eastham, S., Elkin, C., Engberg, Z., Hager, U., Langmore, I.,
2077 McCloskey, K., Ng, J. Y. H., and Platt, J. C.: A scalable system to measure contrail formation
2078 on a per-flight basis, *Environ. Res. Commun.*, 6, 015008, 2024.

2079 Gettelman, A., Chen, C. C., Bardeen, C. G.: The climate impact of COVID-19-induced contrail
2080 changes, *Atmos. Chem. Phys.*, 21(12), 9405-9416, <https://doi.org/10.5194/acp-21-9405-2021>,
2081 2021.

2082 Gettelman, A., Chen, C.: The climate impact of aviation aerosols, *Geophys. Res. Lett.*, 40(11),
2083 2785-2789, <https://doi.org/10.1002/grl.50539>, 2013.

2084 Gettelman, A., Morrison, H.: Advanced Two-Moment Bulk Microphysics for Global Models. Part
2085 I: Off-Line Tests and Comparison with Other Schemes, *J. Climate*, 28, 1268–1287,
2086 <https://doi.org/10.1175/JCLI-D-14-00102.1>, 2015.

2087 Gettelman, A., Bardeen, C. G., McCluskey, C. S., Järvinen, E., Stith, J., Bretherton, C.,
2088 McFarquhar, G., Twohy, C., D’Alessandro, J., Wu, W.: Simulating Observations of Southern
2089 Ocean Clouds and Implications for Climate, *J. Geophys. Res.*, 125,
2090 <https://doi.org/10.1029/2019JD031872>, 2020.

2091 Gettelman, A., Gagne, D. J., Chen, C.-C., Christensen, M. W., Lebo, Z. J., Morrison, H., Gantos,
2092 G.: Machine Learning the Warm Rain Process, *J. Adv. Model. Earth Syst.*, 13,
2093 <https://doi.org/10.1029/2020MS002273>, 2021.

2094 Gettelman, A., Hannay, C., Bacmeister, J. T., Neale, R. B., Pendergrass, A. G., Danabasoglu, G.,
2095 Lamarque, J.-F., Fasullo, J. T., Bailey, D. A., Lawrence, D. M., Mills, M. J.: High Climate
2096 Sensitivity in the Community Earth System Model Version 2 (CESM2), *Geophys. Res. Lett.*,
2097 46, <https://doi.org/10.1029/2019GL083978>, 2019.

2098 Gierens, K. M., Lim, L., Eleftheratos, K.: A review of various strategies for contrail avoidance,
2099 *Open Atmos. Sci. J.*, 2, 1-7, <https://doi.org/10.2174/1874282300802010001>, 2008.

2100 Gierens, K., Matthes, S., Rohs, S.: How Well Can Persistent Contrails Be Predicted?, *Aerospace*,
2101 7, 169, <https://doi.org/10.3390/aerospace7110169>, 2020.

2102 Gounou, A., Hogan, R. J.: A sensitivity study of the effect of horizontal photon transport on the
2103 radiative forcing of contrails, *J. Atmos. Sci.*, 64, 1706–1716,
2104 <https://doi.org/10.1175/JAS3943.1>, 2007.

2105 Graf, K., Schumann, U., Mannstein, H., Mayer, B.: Aviation induced diurnal North Atlantic cirrus
2106 cover cycle, *Geophys. Res. Lett.*, 39, <https://doi.org/10.1029/2012GL053403>, 2012.

2107 Grewe, V., Gangoli Rao, A., Grönstedt, T., Xisto, C., Linke, F., Melkert, J., Middel, J., Ohlenforst,
2108 B., Blakey, S., Christie, S., Matthes, S., Dahmann, K.: Evaluating the climate impact of
2109 aviation emission scenarios towards the Paris agreement including COVID-19 effects, *Nat.*
2110 *Commun.*, 12, 3841, <https://doi.org/10.1038/s41467-021-24046-4>, 2021.

2111 Haywood, J. M., Allan, R. P., Bornemann, J., Forster, P. M., Francis, P. N., Milton, S., Rädcl, G.,
2112 Rap, A., Shine, K. P., Thorpe, R.: A case study of the radiative forcing of persistent contrails
2113 evolving into contrail-induced cirrus. *J. Geophys. Res. Atmos.*, 114(D24),
2114 <https://doi.org/10.1029/2009JD012650>, 2009.

2115 Heymsfield, A. J., Krämer, M., Luebke, A., Brown, P., Cziczo, D. J., Franklin, C., Lawson, P.,
2116 Lohmann, U., McFarquhar, G., Ulanowski, Z., and Van Tricht, K.: Cirrus clouds, *Meteorol.*
2117 *Monogr.*, 58, 2.1–2.26, 2017.

2118 Huszar, P., Teyssède, H., Michou, M., Voldoire, A., Olivié, D. J. L., Saint-Martin, D., Cariolle,
2119 D., Senesi, S., Salas Y Melia, D., Alias, A., Karcher, F., Ricaud, P., and Halenka, T.: Modeling
2120 the present and future impact of aviation on climate: an AOGCM approach with online coupled
2121 chemistry, *Atmos. Chem. Phys.*, 13, 10027–10048, [https://doi.org/10.5194/acp-13-10027-](https://doi.org/10.5194/acp-13-10027-2013)
2122 2013, 2013.

2123 ICAO Future Of Aviation 2012, 2012. Retrieved from
2124 <https://www.icao.int/Meetings/FutureOfAviation/Pages/default.aspx>

2125 Immler, F., Treffeisen, R., Engelbart, D., Krüger, K., Schrems, O.: Cirrus contrails, and ice
2126 supersaturated regions in high-pressure systems at northern mid-latitudes, *Atmos. Chem.*
2127 *Phys.*, 8, 1689–1699, <https://doi.org/10.5194/acp-8-1689-2008>, 2008.

2128 IPCC: Climate Change 2021: The Physical Science Basis. Contribution of Working Group I to the
2129 Sixth Assessment Report of the Intergovernmental Panel on Climate Change, 2021.

2130 IPCC: Summary for Policymakers 2018: In V. Masson-Delmotte, P. Zhai, H. O. Pörtner, et al.
2131 (Eds.), *Global warming of 1.5°C. An IPCC Special Report on the Impacts of Global Warming*
2132 *of 1.5°C above Pre-industrial Levels and Related Global Greenhouse Gas Emission Pathways,*
2133 *World Meteorological Organization Technical Document, pp. 32, 2018.*
2134 IPCC: Aviation and the global atmosphere 1999: In: Penner, J.E., Lister, D.H., Griggs, D. J.,
2135 Dokken, D.J., McFarland, M. (Eds.), *Intergovernmental Panel on Climate Change Special*
2136 *Report. Cambridge University Press, Cambridge, UK, 1999.*
2137 Irvine, E. A., Hoskins, B. J., Shine, K. P.: A Lagrangian analysis of ice-supersaturated air over the
2138 North Atlantic, *J. Geophys. Res.: Atmospheres*, 119, 90–100,
2139 <https://doi.org/10.1002/2013JD019843>, 2013.
2140 Iwabuchi, H., Yang, P., Liou, K.N. and Minnis, P.: Physical and optical properties of persistent
2141 contrails: Climatology and interpretation. *J. Geophys. Res: Atmospheres*, 117(D6),
2142 <https://doi.org/10.1029/2011JD017003>, 2012.
2143 Jacobson, M. Z., Wilkerson, J. T., Naiman, A. D., Lele, S. K.: The effects of aircraft on climate
2144 and pollution. Part I: Numerical methods for treating the subgrid evolution of discrete size-and
2145 composition-resolved contrails from all commercial flights worldwide. *J. Comput. Phys.*,
2146 230(12), 5115-32, <https://doi.org/10.1016/j.jcp.2011.03.021>, Jun 1, 2011.
2147 Jacobson, M. Z.: Short-term effects of controlling fossil-fuel soot, biofuel soot and gases, and
2148 methane on climate, Arctic ice, and air pollution health. *J. Geophys. Res.*, 115, D14209,
2149 <https://doi.org/10.1029/2009JD013795>, 2010.
2150 Jensen, E., Ackermann, A.S., Stevens, D.E., Toon, O.B., Minnis, P.: Spreading and growth of
2151 contrails in a sheared environment. *J. Geophys. Res.*, 103, 13557–13567,
2152 <https://doi.org/10.1029/98JD00642>, 1998.
2153 Jensen, E., Toon, O., Vay, S., Ovarlez, J., May, R., Bui, T., Twohy, C., Gandrud, B., Pueschel, R.,
2154 and Schumann, U.: Prevalence of ice-supersaturated regions in the upper troposphere:
2155 Implications for optically thin ice cloud formation, *J. Geophys. Res.*, 106, 17253–17266,
2156 <https://doi.org/10.1029/2000JD900774>, 2001.
2157 Kärcher, B.: Formation and radiative forcing of contrail cirrus. *Nat. Commun.*, 9, 1824,
2158 <https://doi.org/10.1038/s41467-018-04272-2>, 2018.
2159 Kärcher, B., Burkhardt, U., Bier, A., Bock, L., and Ford, I. J.: The microphysical pathway to
2160 contrail formation. *J. Geophys. Res. Atmos.*, 120, 7893–7927,
2161 <https://doi.org/10.1002/2015JD023293>, 2015.
2162 Kärcher, B.: Formation and radiative forcing of contrail cirrus. *Nat. Commun.*, 9(1), 1824,
2163 <https://doi.org/10.1038/s41467-018-04272-2>, 2018.
2164 Kärcher, B., and Yu, F.: Role of aircraft soot emissions in contrail formation. *Geophys. Res. Lett.*,
2165 36(1), L01804, <https://doi.org/10.1029/2008GL036649>, 2009.
2166 Kärcher, B., Burkhardt, U., Bier, A., Bock, L., and Ford, I. J.: The microphysical pathway to
2167 contrail formation. *J. Geophys. Res. Atmos.*, 120(15), 7893–7927,
2168 <https://doi.org/10.1002/2015JD023293>, 2015.
2169 Klöwer, M., Allen, M. R., Lee, D. S., Proud, S. R., Gallagher, L., and Skowron, A.: Quantifying
2170 aviation’s contribution to global warming. *Environ. Res. Lett.*, 16, 104027,
2171 <https://doi.org/10.1088/1748-9326/ac24ff>, 2021.
2172 Krämer, M., Rolf, C., Spelten, N., Afchine, A., Fahey, D., Jensen, E., Khaykin, S., Kuhn, T.,
2173 Lawson, P., Lykov, A., Pan, L. L. (2020 Nov 2). A microphysics guide to cirrus–Part 2:
2174 Climatologies of clouds and humidity from observations. *Atmos. Chem. Phys.*, 20(21), 12569-
2175 608, <https://doi.org/10.5194/acp-20-12569-2020>, 2020.

2176 Krämer, M., Schiller, C., Afchine, A., Bauer, R., Gensch, I., Mangold, A., Schlicht, S., Spelten,
2177 N., Sitnikov, N., Borrmann, S., de Reus, M., and Spichtinger, P.: Ice supersaturations and cirrus
2178 cloud crystal numbers, *Atmos. Chem. Phys.*, 9, 3505–3522, [https://doi.org/10.5194/acp-9-](https://doi.org/10.5194/acp-9-3505-2009)
2179 3505-2009, 2009.

2180 Kristensson, A., Gayet, J.-F., Ström, J., and Auriol, F.: In situ observations of a reduction in
2181 effective crystal diameter in cirrus clouds near flight corridors, *Geophys. Res. Lett.*, 27, 681–
2182 684, <https://doi.org/10.1029/1999GL010858>, 2000.

2183 Kübbeler, M., Hildebrandt, M., Meyer, J., Schiller, C., Hamburger, Th., Jurkat, T., Minikin, A.,
2184 Petzold, A., Rautenhaus, M., Schlager, H., Schumann, U., Voigt, C., Spichtinger, P., Gayet, J.-
2185 F., Goubeyre, C., and Krämer, M.: Thin and subvisible cirrus and contrails in a subsaturated
2186 environment, *Atmos. Chem. Phys.*, 11, 5853–5865, [https://doi.org/10.5194/acp-11-5853-](https://doi.org/10.5194/acp-11-5853-2011)
2187 2011, 2011.

2188 Kulik, L.: Satellite-based detection of contrails using deep learning, Master's thesis, Massachusetts
2189 Institute of Technology, 2019.

2190 Kurz, C.: Entwicklung und Anwendung eines gekoppelten Klima-Chemie-Modellsystems:
2191 Globale Spurengastransporte und chemische Umwandlungsprozesse (Doctoral thesis),
2192 Ludwigs-Maximilians-University Munich, DLR Forschungsbericht, 2007.

2193 Lamquin, N., Stubenrauch, C.J., Gierens, K., Burkhardt, U., and Smit, H.: A global climatology
2194 of upper tropospheric ice supersaturation occurrence inferred from the Atmospheric Infrared
2195 Sounder calibrated by MOZAIC, *Atmos. Chem. Phys.*, 12, 381–405,
2196 <https://doi.org/10.5194/acp-12-381-2012>, 2012.

2197 Lee, D.S., Pitari, G., Grewe, V., Gierens, K., Penner, J.E., Petzold, A., Prather, M.J., Schumann,
2198 U., Bais, A., Bernsten, T. and Iachetti, D.: Transport impacts on atmosphere and climate:
2199 Aviation, *Atmospheric environment*, 44(37), pp.4678-4734,
2200 <https://doi.org/10.1016/j.atmosenv.2010.06.045>, 2010.

2201 Lee, D. S., Fahey, D. W., Forster, P. M., Newton, P. J., Wit, R. C. N., Lim, L. L., Owen, B., and
2202 Sausen, R.: Aviation and global climate change in the 21st century, *Atmos. Environ.*, 43, 3520-
2203 3537, <https://doi.org/10.1016/j.atmosenv.2009.04.024>, 2009.

2204 Lee, D. S., Fahey, D. W., Skowron, A., Allen, M. R., Burkhardt, U., Chen, Q., Doherty, S. J.,
2205 Freeman, S., Forster, P. M., Fuglestedt, J., Gettelman, A., De León, R. R., Lim, L. L., Lund,
2206 M. T., Millar, R. J., Owen, B., Penner, J. E., Pitari, G., Prather, M. J., Sausen, R., and Wilcox,
2207 L. J.: The contribution of global aviation to anthropogenic climate forcing for 2000 to 2018,
2208 *Atmos. Environ.*, 244, 117834, <https://doi.org/10.1016/j.atmosenv.2020.117834>, 2021.

2209 Lewellen, D. C.: Analytic Solutions for Evolving Size Distributions of Spherical Crystals or
2210 Droplets Undergoing Diffusional Growth in Different Regimes, *J. Atmos. Sci.*, 69, 417–434,
2211 <https://doi.org/10.1175/JAS-D-11-0193.1>, 2012.

2212 Lewellen, D. C.: Persistent contrails and contrail cirrus. Part II: Full lifetime behavior, *J. Atmos.*
2213 *Sci.*, 71, 4420–4438, <https://doi.org/10.1175/JAS-D-14-0004.1>, 2014.

2214 Lewellen, D. C., Meza, O., Huebsch, W.: Persistent contrails and contrail cirrus. Part 1: Large-
2215 eddy simulations from inception to demise, *J. Atmos. Sci.*, 71, 4399–4419,
2216 <https://doi.org/10.1175/JAS-D-14-0003.1>, 2014.

2217 Li, J., Caiazzo, F., Chen, N. Y., Sridhar, B., Ng, H., and Barrett, S.: Evaluation of aircraft contrails
2218 using dynamic dispersion model, *AIAA Guidance Navigation, and Control (GNC) Conf.*,
2219 2013–5178 pp., <https://doi.org/10.2514/6.2013-5178>, 2013.

2220 Li, Y., Mahnke, C., Rohs, S., Bundke, U., Spelten, N., Dekoutsidis, G., Groß, S., Voigt, C.,
2221 Schumann, U., Petzold, A., and Krämer, M.: Upper-tropospheric slightly ice-subsaturated

2222 regions: frequency of occurrence and statistical evidence for the appearance of contrail cirrus,
 2223 Atmos. Chem. Phys., 23, 2251–2271, <https://doi.org/10.5194/acp-23-2251-2023>, 2023

2224 Li, J., Kim, J. H., Sridhar, B., and Ng, H. K.: Ames Contrail Simulation Model: Modeling Aviation
 2225 Induced Contrails and the Computation of Contrail Radiative Forcing Using Air Traffic Data,
 2226 NASA Tech. Memo., NASA/TM-20230014633, 2023.

2227 Liou, K.N., Takano, Y., Yue, Q., and Yang, P.: On the radiative forcing of contrail cirrus
 2228 contaminated by black carbon, Geophys. Res. Lett., 40, 778–784,
 2229 <https://doi.org/10.1002/grl.50214>, 2013.

2230 Liu, X., Ma, P.-L., Wang, H., Tilmes, S., Singh, B., Easter, R. C., Ghan, S. J., and Rasch, P. J.:
 2231 Description and evaluation of a new four-mode version of the Modal Aerosol Module (MAM4)
 2232 within version 5.3 of the Community Atmosphere Model, Geosci. Model Dev., 9, 505–522,
 2233 <https://doi.org/10.5194/gmd-9-505-2016>, 2016.

2234 Lohmann, U., Spichtinger, P., Heidt, S., Peter, T., and Smit, H.: Cirrus clouds and ice
 2235 supersaturation regions in a global climate model, Environ. Res. Lett., 3(4), 045022,
 2236 <https://doi.org/10.1088/1748-9326/3/4/045022>, 2008.

2237 Luebke, A. E., Afchine, A., Costa, A., Groß, J.-U., Meyer, J., Rolf, C., Spelten, N., Avallone, L.
 2238 M., Baumgardner, D., and Krämer, M.: The origin of midlatitude ice clouds and the resulting
 2239 influence on their microphysical properties, Atmos. Chem. Phys., 16, 5793–5809,
 2240 <https://doi.org/10.5194/acp-16-5793-2016>, 2016.

2241 Mahnke, C., Gomes, R., Bundke, U., Berg, M., Ziereis, H., Sharma, M., Righi, M., Hendricks, J.,
 2242 Zahn, A., Wahner, A., and Petzold, A.: Properties and Processing of Aviation Exhaust Aerosol
 2243 at Cruise Altitude Observed from the IAGOS-CARIBIC Flying Laboratory, Environ. Sci.
 2244 Technol., 58, 6945–6953, 2024.

2245 Mannstein, H., Brömser, A., and Bugliaro, L.: Ground-based observations for the validation of
 2246 contrails and cirrus detection in satellite imagery, Atmos. Meas. Tech., 3, 655–669,
 2247 <https://doi.org/10.5194/amt-3-655-2010>, 2010.

2248 Mannstein, H., Meyer, R., and Wendling, P.: Operational detection of contrails from NOAA-
 2249 AVHRR data, Int. J. Remote Sens., 20, 1641–1660,
 2250 <https://doi.org/10.1080/014311699212470>, 1999.

2251 Märkl, R. S., Voigt, C., Sauer, D., Dischl, R. K., Kaufmann, S., Harlaß, T., Hahn, V., Roiger, A.,
 2252 Weiß-Rehm, C., Burkhardt, U., Schumann, U., Marsing, A., Scheibe, M., Dörnbrack, A.,
 2253 Renard, C., Gauthier, M., Swann, P., Madden, P., Luff, D., Sallinen, R., Schripp, T., and Le
 2254 Clercq, P.: Powering aircraft with 100 % sustainable aviation fuel reduces ice crystals in
 2255 contrails, Atmos. Chem. Phys., 24, 3813–3837, <https://doi.org/10.5194/acp-24-3813-2024>,
 2256 2024.

2257 Markowicz, K. M., Witek, M. L.: Simulations of contrail optical properties and radiative forcing
 2258 for various crystal shapes, J. Appl. Meteorol. Climatol., 50, 1740–1755,
 2259 <https://doi.org/10.1175/JAMC-D-11-071.1>, 2011.

2260 Marquart, S., Ponater, M., Mager, F., and Sausen, R.: Future Development of Contrail Cover,
 2261 Optical Depth, and Radiative Forcing: Impacts of Increasing Air Traffic and Climate Change,
 2262 J. Climate, 16, 2890–2904, [https://doi.org/10.1175/1520-0442\(2003\)016<2890:FDOCCO>2.0.CO;2](https://doi.org/10.1175/1520-0442(2003)016<2890:FDOCCO>2.0.CO;2),
 2263 2003.

2264 Matthes S, Lee DS, De Leon RR, Lim L, Owen B, Skowron A, Thor RN, Terrenoire E.: The effects
 2265 of supersonic aviation on ozone and climate, Aerospace, 9(1), 41,
 2266 <https://doi.org/10.3390/aerospace9010041>, 2022.

2267 Mayer, B., and Kylling, A.: The libRadtran software package for radiative transfer calculations:
2268 Description and examples of use, *Atmos. Chem. Phys.*, 5, 1855–1877,
2269 <https://doi.org/10.5194/acp-5-1855-2005>, 2005.

2270 McCloskey, K., Geraedts, S., Van Arsdale, C., and Brand, E.: A human-labeled landsat-8 contrails
2271 dataset. In *ICML 2021 Workshop on Tackling Climate Change with Machine Learning*,
2272 <https://www.climatechange.ai/events/iclr2023#about>, 2021.

2273 Meerkötter, R., Schumann, U., Doelling, D. R., Minnis, P., Nakajima, T., and Tsushima, Y.:
2274 Radiative forcing by contrails, *Ann. Geophys.*, 17, 1080–1094,
2275 <https://doi.org/10.1007/s00585-999-1080-0>, 1999.

2276 Meijer, V. R., Kulik, L., Eastham, S. D., Allroggen, F., Speth, R. L., Karaman, S., and Barrett, S.
2277 R.: Contrail coverage over the United States before and during the COVID-19 pandemic,
2278 *Environ. Res. Lett.*, 17, 034039, <https://doi.org/10.1088/1748-9326/ac52f4>, 2021.

2279 Minnis, P.: Contrails. In G. R. North (Ed.), *Encyclopedia of Atmospheric Sciences* (2nd ed., Vol.
2280 2, pp. 121-132). Oxford, UK: Elsevier Ltd., 2015.

2281 Minnis, P., Bedka, S. T., Duda, D. P., Bedka, K. M., Chee, T., Ayers, J. K., Palikonda, R.,
2282 Spangenberg, D. A., Khlopenkov, K. V., and Boeke, R.: Linear contrail and contrail cirrus
2283 properties determined from satellite data, *Geophys. Res. Lett.*, 40, 3220–3226,
2284 <https://doi.org/10.1002/grl.50557>, 2013.

2285 Minnis, P., Schumann, U., Doelling, D. R., Gierens, K. M., and Fahey, D. W.: Global distribution
2286 of contrail radiative forcing, *Geophys. Res. Lett.*, 26, 1853–1856,
2287 <https://doi.org/10.1029/1999GL900391>, 1999.

2288 Molod, A., Takacs, L., Suarez, M., and Bacmeister, J.: Development of the GEOS-5 atmospheric
2289 general circulation model: evolution from MERRA to MERRA2, *Geosci. Model Dev.*, 8,
2290 1339–1356, <https://doi.org/10.5194/gmd-8-1339-2015>, 2015.

2291 Molloy, J., Teoh, R., Harty, S., Koudis, G., Schumann, U., Poll, I. and Stettler, M.E.: Design
2292 principles for a contrail-minimizing trial in the north atlantic, *Aerospace*, 9(7), p.37,
2293 <https://doi.org/10.3390/aerospace9070037>, 2022.

2294 Moore, R.H., Thornhill, K.L., Weinzierl, B., Sauer, D., D’Ascoli, E., Kim, J., Lichtenstern, M.,
2295 Scheibe, M., Beaton, B., Beyersdorf, A.J. and Barrick, J.: Biofuel blending reduces particle
2296 emissions from aircraft engines at cruise conditions, *Nature*, 543(7645), pp.411-415,
2297 <https://doi.org/10.1038/nature21420>, 2017.

2298 Myhre, G., and Stordal, F.: On the tradeoff of the solar and thermal infrared radiative impact of
2299 contrails, *Geophys. Res. Lett.*, 28, 3119–3122, <https://doi.org/10.1029/2001GL013916>, 2001.

2300 Myhre, G., Kvalevåg, M., Rädcl, G., Cook, J., Shine, K. P., Clark, H., Kärcher, F., Markowicz,
2301 K., Kardas, A., Wolkenberg, P., Balkanski, Y., Ponater, M., Forster, P., Rap, A., and De Leon,
2302 R. R.: Intercomparison of radiative forcing calculations of stratospheric water vapour and
2303 contrails, *Meteorol. Z.*, 18, 585–596, <https://doi.org/10.1127/0941-2948/2009/0405>, 2009.

2304 Naiman, A. D., Lele, S. K., Wilkerson, J. T., and Jacobson, M. Z.: Parameterization of subgrid
2305 plume dilution for use in large-scale atmospheric simulations, *Atmos. Chem. Phys.*, 10, 2551–
2306 2560, <https://doi.org/10.5194/acp-10-2551-2010>, 2009.

2307 Naiman, A. D., Lele, S. K., Wilkerson, J. T., and Jacobson, M. Z.: A low order contrail model for
2308 use with global-scale climate models, 47th AIAA Aerospace Science Meeting, Orlando, FL,
2309 2011.

2310 Naiman, A. D., Lele, S. K., and Jacobson, M. Z.: Large Eddy simulations of persistent aircraft
2311 contrails, 49th AIAA Aerospace Science Meeting, Orlando, 2011.

2312 Newinger, C., Burkhardt, U.: Sensitivity of contrail cirrus radiative forcing to air traffic
2313 scheduling, *J. Geophys. Res. Atmos.*, 117, D1020, <https://doi.org/10.1029/2011JD016815>,
2314 2012.

2315 Neil Y. Chen, N., Sridhar, B., and Ng, H. K.: Prediction and use of contrail frequency index for
2316 contrail reduction strategies, *AIAA Guidance, Navigation, and Control Conference*, Toronto,
2317 Canada, 2010.

2318 Ng, J. Y. H., McCloskey, K., Cui, J., Brand, E., Sarna, A., Goyal, N., ... and Geraedts, S.:
2319 OpenContrails: Benchmarking Contrail Detection on GOES-16 ABI, arXiv preprint
2320 arXiv:2304.02122, 2023.

2321 Niklaß, M., Grewe, V., Gollnick, V., and Dahlmann, K.: Concept of climate-charged airspaces: a
2322 potential policy instrument for internalizing aviation's climate impact of non-CO2 effects,
2323 *Climate Policy*, 21, 1066–1085, <https://doi.org/10.1080/14693062.2020.1809243>, 2021.

2324 Ovarlez, J., van Velthoven, P., Sachse, G., Vay, S., Schlager, H., and Ovarlez, H.: Comparison of
2325 water vapor measurements from POLINAT 2 with ECMWF analyses in high-humidity
2326 conditions, *J. Geophys. Res.*, 105, 3737–3744, <https://doi.org/10.1029/1999JD900591>, 2000.

2327 Ovarlez, J., Gayet, J.-F., Gierens, K., Strom, J., Ovarlez, H., Auriol, F., Busen, R., and Schumann,
2328 U.: Water vapour measurements inside cirrus clouds in Northern and Southern hemispheres
2329 during INCA, *Geophys. Res. Lett.*, 29, 1813–1817, <https://doi.org/10.1029/2002GL016301>,
2330 2002.

2331 Palikonda, R., Minnis, P., Duda, D. P., and Mannstein, H.: Contrail coverage derived from 2001
2332 AVHRR data over the continental United States of America and surrounding areas, *Meteorol.*
2333 *Z.*, 14, 525–536, <https://doi.org/10.1127/0941-2948/2005/0055>, 2005.

2334 Paoli, R. and Shariff, K.: Contrail Modeling and Simulation, *Annu. Rev. Fluid Mech.*, 48, 393–
2335 427, <https://doi.org/10.1146/annurev-fluid-010719-060304>, 2016.

2336 Penner, J. E., Lister, D. H., Griggs, D. J., Dokken, D. J., and McFarland, M., Eds.: *Aviation and
2337 the Global Atmosphere*, Cambridge University Press, 373 pp., 1999.

2338 Petters, M. D., and Kreidenweis, S. M.: A single parameter representation of hygroscopic growth
2339 and cloud condensation nucleus activity, *Atmos. Chem. Phys.*, 7(8), 1961–1971,
2340 <https://doi.org/10.5194/acp-7-1961-2007>, 2007.

2341 Petzold, A., Busen, R., Schröder, F. P., Baumann, R., Kuhn, M., Ström, J., Hagen, D. E.,
2342 Whitefield, P. D., Baumgardner, D., Arnold, F., Borrmann, S., and Schumann, U.: Near-field
2343 measurements on contrail properties from fuels with different sulfur content, *J. Geophys. Res.*
2344 *Atmos.*, 102, 29867–29880, <https://doi.org/10.1029/97JD02686>, 1997.

2345 Petzold, A., Krämer, M., Neis, P., Rolf, C., Rohs, S., Berkes, F., Smit, H. G. J., Gallagher, M.,
2346 Beswick, K., Lloyd, G., Baumgardner, D., Spichtinger, P., Nédélec, P., Ebert, V., Buchholz,
2347 B., Riese, M., and Wahner, A.: Upper tropospheric water vapor and its interaction with cirrus
2348 clouds as seen from IAGOS long-term routine in situ observations, *Faraday Discuss*, 200, 229–
2349 249, <https://doi.org/10.1039/C7FD00040A>, 2017.

2350 Petzold, A., Hoor, P., Järvinen, E., Lauer, A., Meyer, J., Neuberger, T., Schiller, C., Veselovskii,
2351 I., and Woiwode, W.: Ice-supersaturated air masses in the northern mid-latitudes from regular
2352 in situ observations by passenger aircraft: vertical distribution, seasonality and tropospheric
2353 fingerprint, *Atmos. Chem. Phys.*, 20, 8157–8179, <https://doi.org/10.5194/acp-20-8157-2020>,
2354 2020.

2355 Poellot, M. R., Arnott, W. P., and Hallett, J.: In situ observations of contrail microphysics and
2356 implications for their radiative impact, *J. Geophys. Res.*, 104, 12 077–12 084,
2357 <https://doi.org/10.1029/1999JD900006>, 1999.

2358 Poll DI. On the relationship between non-optimum operations and fuel requirement for large civil
2359 transport aircraft, with reference to environmental impact and contrail avoidance strategy, *The*
2360 *Aeronautical Journal*, Dec;122(1258):1827-70, 2018.

2361 Pomroy, H.R., and Illingworth, J.A.: Ice cloud inhomogeneity: quantifying bias in emissivity from
2362 radar observations, *Geophys. Res. Lett.*, 27, 2101–2104,
2363 <https://doi.org/10.1029/2000GL011429>, 2000.

2364 Ponater, M., Marquart, S., and Sausen, R.: Contrails in a comprehensive global climate model:
2365 Parameterization and radiative forcing results, *J. Geophys. Res. Atmos.*, 107, ACL 2-1–ACL
2366 2-15, <https://doi.org/10.1029/2001JD001227>, 2002.

2367 Ponater, M., Bickel, M., Bock, L. and Burkhardt, U.: Towards determining the contrail cirrus
2368 efficacy, *Aerospace*, 8(2), p.42, <https://doi.org/10.3390/aerospace8020042>, 2021.

2369 Pruppacher, H. R. and Klett, J. D.: *Microphysics of Clouds and Precipitation*, Atmospheric and
2370 Oceanographic Sciences Library, 2nd Edn., Kluwer Academic Publishers, Dordrecht, the
2371 Netherlands, ISBN 978-0792344094, 1997.

2372 Pruppacher, H. R. and Klett, J. D.: *Microphysics of clouds and precipitation*, Kluwer Academic,
2373 Norwell, Mass., 2000.

2374 Rädcl, G. and Shine, K. P.: Radiative forcing by persistent contrails and its dependence on cruise
2375 altitudes, *J. Geophys. Res. Atmos.*, 113, D07105, <https://doi.org/10.1029/2007JD009401>,
2376 2008.

2377 Rap, A., Forster, P. M., Jones, A., Boucher, O., Haywood, J. M., Bellouin, N., and De Leon, R.
2378 R.: Parameterization of contrails in the UK Met Office Climate Model, *J. Geophys. Res.*, 115,
2379 D10205, <https://doi.org/10.1029/2009JD012152>, 2010.

2380 Reutter, P., Konopka, P., Pappalardo, L., Lembras, A., Müller, R., Euler, F., Baklanov, A., and
2381 Hegerl, G.: Ice supersaturated regions: properties and validation of ERA-Interim reanalysis
2382 with IAGOS in situ water vapor measurements, *Atmos. Chem. Phys.*, 20, 787–804,
2383 <https://doi.org/10.5194/acp-20-787-2020>, 2020.

2384 Righi, M., Hendricks, J., and Sausen, R.: The global impact of the transport sectors on atmospheric
2385 aerosol: simulations for year 2000 emissions, *Atmos. Chem. Phys.*, 13, 9939–9970,
2386 <https://doi.org/10.5194/acp-13-9939-2013>, 2013.

2387 Righi M, Hendricks J, Beer CG. Exploring the uncertainties in the aviation soot–cirrus effect,
2388 *Atmos. Chem. Phys.*, 21(23), pp.17267-17289, <https://doi.org/10.5194/acp-21-17267-2021>,
2389 2021.

2390 Roeckner, E., Baeuml, G., Bonventura, L., Brokopf, R., Esch, M., Giorgetta, M., Hagemann, S.,
2391 Kirchner, I., Kornblueh, L., Manzini, E., Rhodin, A., Schlese, U., Schulzweida, U., and
2392 Tompkins, A.: The atmospheric general circulation model ECHAM5. PART I Model
2393 description, Report 349. Max Planck Institute for Meteorology, Hamburg, Germany.

2394 Roosenbrand, E., Sun, J., & Hoekstra, J.: Optimizing Global Flight Altitudes for Contrail
2395 Reduction. Insights from Open Flight and Weather Balloon Data. In: Fifteenth USA/Europe
2396 Air Traffic Management Research and Development Seminar (ATM2023), 2023.

2397 Sanz-Morère, I., Eastham, S. D., Allroggen, F., Speth, R. L., & Barrett, S. R. H.: Impacts of multi-
2398 layer overlap on contrail radiative forcing. *Atmos. Chem. Phys.*, 21, 1649–1681,
2399 [doi:10.5194/acp-21-1649-2021](https://doi.org/10.5194/acp-21-1649-2021), 2021.

2400 Sausen, R., Gierens, K., Ponater, M., & Schumann, U.: A diagnostic study of the global
2401 distribution of contrails. Part I: Present-day climate. *Theor. Appl. Climatol.*, 61, 127–141,
2402 [doi:10.1007/s007040050076](https://doi.org/10.1007/s007040050076), 1998.

2403 Sausen, R., Hofer, S. M., Gierens, K. M., Bugliaro Goggia, L., Ehrmanntraut, R., Sitova, I., ... &
2404 Miller, N.: Can we successfully avoid persistent contrails by small altitude adjustments of
2405 flights in the real world?. *Meteorol. Z.*, 2023.

2406 Schmidt, E.: Die Entstehung von Eisnebel aus den Auspuffgasen von Flugmotoren. *Schr. Dtsch.*
2407 *Akad. Luftfahrtforsch.*, 44, 1–15, 1941.

2408 Schröder, F., Kärcher, B., Duroure, C., Ström, J., Petzold, A., Gayet, J.-F., ... & Borrmann, S.: On
2409 the Transition of Contrails into Cirrus Clouds. *J. Atmos. Sci.*, 57, 464–480, doi:10.1175/1520-
2410 0469(2000)057<0464:OTTOCI>2.0.CO;2, 2000.

2411 Schumann, U., & Graf, K.: Aviation-induced cirrus and radiation changes at diurnal timescales. *J.*
2412 *Geophys. Res.*, 118, 2404–2421, doi:10.1002/jgrd.50283, 2013.

2413 Schumann, U., & Heymsfield, A.: On the lifecycle of individual contrails and contrail cirrus-Ice
2414 Formation and Evolution in Clouds and Precipitation: Measurement and Modeling Challenges:
2415 Chapter 3, *Meteor. Monogr*, 3.1–3.24, 2017.

2416 Schumann, U., & Wendling, P.: Determination of contrails from satellite data and observational
2417 results. In: *Air Traffic and the Environment-Background, Tendencies and Potential Global*
2418 *Atmospheric Effects*, U. Schumann (Ed.), *Lecture Notes in Engineering*, Springer-Verlag,
2419 138–153, 1990.

2420 Schumann, U., Baumann, R., Baumgardner, D., Bedka, S. T., Duda, D. P., Freudenthaler, V., ... &
2421 Wang, Z.: Properties of individual contrails: a compilation of observations and some
2422 comparisons. *Atmos. Chem. Phys.*, 17, 403–438, doi:10.5194/acp-17-403-2017, 2017.

2423 Schumann, U., Bugliaro, L., Dörnbrack, A., Baumann, R., & Voigt, C.: Aviation Contrail Cirrus
2424 and Radiative Forcing Over Europe During 6 Months of COVID-19. *Geophys. Res. Lett.*, 48,
2425 doi:10.1029/2021GL096230, 2021.

2426 Schumann, U., Penner, J. E., Chen, Y., Zhou, C., & Graf, K.: Dehydration effects from contrails
2427 in a coupled contrail-climate model. *Atmos. Chem. Phys.*, 15, 11179–11199, doi:10.5194/acp-
2428 15-11179-2015, 2015.

2429 Schumann, U., Ström, J., Busen, R., Baumann, R., Gierens, K., Krautstrunk, M., ... & Stiggl, J.: In
2430 situ observations of particles in jet aircraft exhausts and contrails for different sulfur-containing
2431 fuels. *J. Geophys. Res.*, 101, 6853–6870, doi:10.1029/95JD00240, 1996.

2432 Schumann, U.: A contrail cirrus prediction model. *Geosci. Model Dev.*, 5, 543–580,
2433 doi:10.5194/gmd-5-543-2012, 2012.

2434 Schumann, U.: On conditions for contrail formation from aircraft exhausts. *Meteorol. Z.*, 5, 4–23,
2435 doi:10.1127/metz/5/1996/4, 1996.

2436 Schumann, U., Konopka, P., Baumann, R., Busen, B., Gerz, T., Schlager, H., ... & Volkert, H.:
2437 Estimate of diffusion parameters of aircraft exhaust plumes near the tropopause from nitric
2438 oxide and turbulence measurements. *J. Geophys. Res.*, 100, 147–162, doi:10.1029/94JD01508,
2439 1995.

2440 Schumann, U., Schlager, H., Arnold, F., Baumann, R., Haschberger, P., and Klemm, O.: Dilution
2441 of aircraft exhaust plumes at cruise altitudes, *Atmos. Environ.*, 32, 3097–3103, 1998.

2442 Schumann, U., Jeßberger, P., and Voigt, C.: Contrail ice particles in aircraft wakes and their
2443 climatic importance, *Geophys. Res. Lett.*, 40, 2867–2872, 2013.

2444 Schumann, U.: Formation, properties and climatic effects of contrails, *C. R. Phys.*, 6, 549–565,
2445 2005.

2446 Siddiqui, N.: Atmospheric Contrail Detection with a Deep Learning Algorithm, *Scholarly*
2447 *Horizons: Univ. Minnesota Morris Undergraduate Journal*, 7(1), Article 5,
2448 doi:10.26757/sh.v7i1.1334, 2020.

2449 Spangenberg, D. A., Minnis, P., Bedka, S. T., Palikonda, R., Duda, D. P., & Rose, F. G.: Contrail
2450 radiative forcing over the Northern Hemisphere from 2006 Aqua MODIS data. *Geophys. Res.*
2451 *Letts.*, 40, 595–600, doi:10.1002/grl.50119, 2013.

2452 Spinhirne, J. D., Hart, W. D., & Duda, D. P.: Evolution of the morphology and microphysics of
2453 contrail cirrus from airborne remote sensing. *Geophys. Res. Letts.*, 25, 1153–1156,
2454 doi:10.1029/97GL03477, 1998.

2455 Sridhar, B., Ng, H. K., & Chen, N. Y.: Aircraft Trajectory Optimization and Contrails Avoidance
2456 in the Presence of Winds, in: 10th AIAA Aviation Technology, Integration and Operations
2457 Conference (ATIO), Fort Worth, TX, 2010.

2458 Stenke, A., Grewe, V., & Pechtl, S.: Do supersonic aircraft avoid contrails?, *Atmos. Chem. Phys.*,
2459 8, 955–967, doi:10.5194/acp-8-955-2008, 2008.

2460 Stier, P., Feichter, J., Kinne, S., Kloster, S., Vignati, E., Wilson, J., et al.: The aerosol-climate
2461 model ECHAM5-HAM. *Atmos. Chem. Phys.*, 5(4), 1125–1156, 2005.

2462 Stocker, T.F., Qin, D., Plattner, G.K., Tignor, M., Allen, S.K., Boschung, J., ... & Midgley, P. M.
2463 (Eds.): *Climate Change 2013: the Physical Science Basis, Contribution of Working Group I to*
2464 *the Fifth Assessment Report of the Intergovernmental Panel on Climate Change.* Cambridge
2465 University Press, Cambridge, United Kingdom and New York, NY, USA, 2013.

2466 Stuber, N., Sausen, R., & Ponater, M.: Stratosphere adjusted radiative forcing calculations in a
2467 comprehensive climate model. *Theor. Appl. Climatol.*, 68(3–4), 125–135,
2468 doi:10.1007/s007040170048, 2001.

2469 Sun, J., & Roosenbrand, E.: Flight Contrail Segmentation via Augmented Transfer Learning with
2470 Novel SR Loss Function in Hough Space. arXiv preprint arXiv:2307.12032, 2023 Jul 22.

2471 Taylor, K. E., Williamson, D., & Zwiers, F.: The sea surface temperature and sea-ice concentration
2472 boundary conditions for AMIP II simulations, PCMDI report no. 60, program for climate
2473 model diagnostics and intercomparison. The University of California, Lawrence Livermore
2474 National Laboratory, 2000.

2475 Teoh, R., Schumann, U., Majumdar, A., & Stettler, M.E.: Mitigating the climate forcing of aircraft
2476 contrails by small-scale diversions and technology adoption. *Environ. Sci. Technol.*, 54(5),
2477 2941–2950, doi:10.1021/acs.est.9b07102, 2020.

2478 Teoh, R., Engberg, Z., Shapiro, M., Dray, L., & Stettler, M. E. J.: The high-resolution Global
2479 Aviation emissions Inventory based on ADS-B (GAIA) for 2019–2021, *Atmos. Chem. Phys.*,
2480 24, 725–744, doi:10.5194/acp-24-725-2024, 2024.

2481 Tesche, M., Achtert, P., Glantz, P., & Noone, K. J.: Aviation effects on already-existing cirrus
2482 clouds. *Nat. Commun.*, 7(1), 12016, doi:10.1038/ncomms12016, 2016.

2483 Testa, B., Durdina, L., Edebeli, J., Spirig, C., & Kanji, Z. A.: Contrail processed aviation soot
2484 aerosol are poor ice nucleating particles at cirrus temperatures [Preprint]. *EGUsphere*,
2485 doi:10.5194/egusphere-2024-151, 2024.

2486 Unterstrasser, S.: Properties of young contrails-A parametrization based on large-eddy
2487 simulations. *Atmos. Chem. Phys.*, 16(4), 2059–2082, doi:10.5194/acp-16-2059-2016, 2016.

2488 Unterstrasser, S., & Sölch, I.: Numerical modeling of contrail cluster formation. *Proc. Third Int.*
2489 *Conf. on Transport, Atmosphere and Climate (TAC-3).* Prien am Chiemsee, Germany, DLR,
2490 114–119, 2012.

2491 Unterstrasser, S., & Görsch, N.: Aircraft-type dependency of contrail evolution. *J. Geophys. Res.-*
2492 *Atmos.*, 119, 14 015–14 027, doi:10.1002/2014JD022083, 2014.

2493 Unterstrasser, S., Gierens, K., Sölch, I., & Wirth, M.: Numerical simulations of homogeneously
 2494 nucleated natural cirrus and contrail-cirrus. Part 2: Interaction on a local scale. *Meteorol. Z.*,
 2495 26, 643–661, doi:10.1127/metz/2017/0844, 2017.

2496 Vazquez-Navarro, M., Mannstein, H., & Kox, S.: Contrail life cycle and properties from 1 year of
 2497 MSG and SEVIRI rapid scan images. *Atmos. Chem. Phys.*, 15(15), 8739–8749,
 2498 doi:10.5194/acp-15-8739-2015, 2015.

2499 Vázquez-Navarro, M., Mannstein, H., & Mayer, B.: An automatic contrail tracking algorithm.
 2500 *Atmos. Meas. Tech.*, 3, 1089–1101, doi:10.5194/amt-3-1089-2010, 2010.

2501 Vazquez-Navarro, M., Mayer, B., & Mannstein, H.: A fast method for the retrieval of integrated
 2502 longwave and shortwave top-of-atmosphere upwelling irradiances from MSG and SEVIRI
 2503 (RRUMS). *Atmos. Meas. Tech.*, 6(10), 2627–2640, doi:10.5194/acp-6-2627-2013, 2013.

2504 Verma, P., & Burkhardt, U.: Contrail formation within cirrus: ICON-LEM simulations of the
 2505 impact of cirrus cloud properties on contrail formation. *Atmos. Chem. Phys.*, 22(13), 8819–
 2506 8842, doi:10.5194/acp-22-8819-2022, 2022.

2507 Voigt, C., Schumann, U., Jessberger, P., Jurkat, T., Petzold, A., Gayet, J.-F., ... & Fahey, D. W.:
 2508 Extinction and optical depth of contrails. *Geophys. Res. Lett.*, 38, L11806,
 2509 doi:10.1029/2011GL047189, 2011.

2510 Voigt, C., Schumann, U., Minikin, A., Abdelmonem, A., Afchine, A., Borrmann, S., ... & Curtius,
 2511 J.: ML-CIRRUS: The airborne experiment on natural cirrus and contrail cirrus with the high-
 2512 altitude long-range research aircraft HALO. *Bull. Am. Meteorol. Soc.*, 98, 271–288,
 2513 doi:10.1175/BAMS-D-14-00193.1, 2017.

2514 Wang, Z., Bugliaro, L., Jurkat-Witschas, T., Heller, R., Burkhardt, U., Ziereis, H., Dekoutsidis,
 2515 G., Wirth, M., Groß, S., Kirschler, S., and Kaufmann, S.: Observations of microphysical
 2516 properties and radiative effects of a contrail cirrus outbreak over the North Atlantic, *Atmos.*
 2517 *Chem. Phys.*, 23, 1941–1961, 2023.

2518 Weickmann, H.: Formen und Bildung atmosphärischer Eiskristalle. *Beitr. Phys. freien Atmos.*, 28,
 2519 33, 1945.

2520 Wilkerson, J. T., Jacobson, M. Z., Malwitz, A., Balasubramanian, S., Wayson, R., Fleming, G., ...
 2521 & Lele, S.: Analysis of emission data from global commercial aviation: 2004 and 2006. *Atmos.*
 2522 *Chem. Phys.*, 10(13), 6391–6408, doi:10.5194/acp-10-6391-2010, 2010.

2523 Wolf, K., Bellouin, N., & Boucher, O.: Sensitivity of cirrus and contrail radiative effect on cloud
 2524 microphysical and environmental parameters. *Atmos. Chem. Phys.*, 9(21), 14003–14037,
 2525 doi:10.5194/acp-9-14003-2009, 2009.

2526 Wuebbles, D., Gupta, M., & Ko, M.: Evaluating the impacts of aviation on climate change. *Eos*,
 2527 *Trans. AGU*, 88(14), 157–160, doi:10.1029/2007EO140001, 2007.

2528 Wuebbles, D., Forster, P., Rogers, H., & Herman, R.: Issues and uncertainties affecting metrics
 2529 for aviation impacts on climate. *Bull. Amer. Meteor. Soc.*, 91(4), 491–496,
 2530 doi:10.1175/2009BAMS2835.1, 2010.

2531 Xie, Y., Yang, P., Liou, K.N., Minnis, P., & Duda, D. P.: Parameterization of contrail radiative
 2532 properties for climate studies. *Geophys. Res. Lett.*, 39, L00F02, doi:10.1029/2011GL050205,
 2533 2012.

2534 Yi, B., Yang, P., Liou, K.N., Minnis, P., & Penner, J. E.: Simulation of the global contrail radiative
 2535 forcing: A sensitivity analysis. *Geophys. Res. Lett.*, 39, L00F03, doi:10.1029/2011GL050207,
 2536 2012.

2537 Yun, Y., Penner, J. E., & Popovicheva, O.: The effects of hygroscopicity on ice nucleation of fossil
2538 fuel combustion aerosols in mixed-phase clouds. *Atmos. Chem. Phys.*, 13, 4339–4348,
2539 doi:10.5194/acp-13-4339-2013, 2013.

2540 Zängl, G., Reinert, D., Rípodas, P., & Baldauf, M.: The ICON (ICOsahedral Non-hydrostatic)
2541 modelling framework of DWD and MPI-M: Description of the non-hydrostatic dynamical
2542 core. *Q. J. R. Meteorol. Soc.*, 141(687), 563-579, doi:10.1002/qj.2378, 2015.

2543 Zhou, C., & Penner, J. E.: Aircraft soot indirect effect on large-scale cirrus clouds: Is the indirect
2544 forcing by aircraft soot positive or negative? *J. Geophys. Res.: Atmos.*, 119, 11 303–11 320,
2545 doi:10.1002/2014JD021821, 2014.

2546

2547